Università degli Studi di Padova

Department of Industrial Engineering

Master Degree in Chemical and Process Engineering

Fatigue life prediction and performance index evaluation of SEPS block-copolymers and advanced TPU for the design of a trileaflet Prosthetic Heart Valve.

Supervisor:
Prof. Michele Modesti
Cosupervisors:
Dr. Geoff D. Moggridge
Dr. Martina Roso

Student:
Eugenia Biral

Academic Year 2015/2016

Contents

Introduzione

I Materiali Polimerici sono una delle più promettenti categorie di materiali, ma il loro campo di applicazione si è ampliato solo recentemente e si continuano a ricercare nuovi possibili usi. Tutti i prodotti polimerici devono essere adatti per la propria applicazione, affidabili e funzionanti durante tutto il loro ciclo di utilizzo. Infatti, dopo l'installazione, molti di questi prodotti possono essere molto difficili da raggiungere o rimpiazzare e quindi guasti, rotture e danneggiamenti permanenti devono essere evitati. Esempi di questo genere di applicazione sono le Protesi di Valvole Cardiache. Con maggiori avanzamenti nella comprensione dei polimeri saremo capaci di predire efficacemente il loro tempo di vita a fatica e le proprietà meccaniche rilevanti. Tutto questo potrebbe aumentare l'effettivo utilizzo di questi materiali per l'applicazione delle valvole cardiache. Le Protesi di Valvole Cardiache polimeriche devono ancora raggiungere un livello di perfomance che le renda una soluzione clinicamente accettabile. Non ci sono al momento protesi di valvole in commercio che includano l'uso di "leaflet" polimeriche. Le protesi commerciali sono sia meccaniche (composte da materiale rigido) o biologiche (prodotte da tessuti animali di pericardio bovino o suino) e sono solitamente inserite tramite operazione chirurgica di apertura del torace. Entrambe le valvole hanno dei significativi aspetti negativi: le valvole meccaniche necessitano di anticoagulanti a vita mentre quelle biologiche hanno una durata limitata e subiscono inoltre danneggiamenti alle "leaflet" quando vengono impiantate nel paziente. L'uso di materiali polimerici per produrre valvole con "leaflet" flessibili che abbiano le caratteristiche positive delle valvole biologiche e meccaniche senza i loro aspetti negativi è stato oggetto di ricerca sin dal 1950. Recenti sviluppi nella sintesi di polimeri, metodi per processarli e caratterizzazione hanno riattivato la ricerca nel campo. La sfida che rimane è quella di raggiungere una combinazione di durabilità a biocompatibilità nel design della protesi di valvola polimerica e nella formulazione del polimero. La sostituzione della

valvola è l'unica cura efficace nel trattamento della stenosi e rigurgitazione aortica. Il mercato ora ha bisogno di una soluzione sicura e poco costosa per le sostituzione delle valvole cardiache difettose, richiedendo anche un'operazione chirurgica il meno invasiva possibile. Il fatto che i polimeri godano di tecniche di produzione di massa relativamente economiche, riuscire in questo scopo potrebbe essere di beneficio a milioni di pazienti che al momento non possono ricorrere a trattamenti per la cura delle malattie cardiache. Oggigiorno il mercato è dominato da poche grandi compagnie che producono valvole biologiche molto costose prodotte da pericardio di bovino o suino. L'oggetto di questo lavoro è di indagare il potenziale utilizzo di un polimero da essere usato nella produzione di protesi di valvole cardiache e che possa passare i test clinici. Diversi polimeri, in particolare elastomeri, sono stati testati per verificare la loro durabilità. Infatti, tra tutto i modi in cui la valvola può rompersi, la rottura a fatica meccanica è uno dei problemi più rilevanti da superare. La sezione più importante del lavoro è stata la selezione dei materiali: questa selezione ha compreso diversi tipologie di polimeri includendo anche copolimeri a blocchi stirenici e poliuretani termoplastici di tecnologia avanzata. I materiali sono stati selezionati implementando un Indice di Performance realizzato specificatamente per l'applicazione alla valvola cardiaca. I polimeri selezionati sono stati sottoposti a test meccanici tra i quali: test di nucleazione della cricca e test di crescita della cricca. Queste analisi sono richieste per analizzare il comportamento a fatica dei materiali e predire la loro vita a fatica. I polimeri con il migliore indice di Performance sono stati poi impiegati nella produzione di prototipi di valvole cardiache. Le valvole prodotte sono state poi sottoposte a test a impulsi nel Pulse Duplicator per verificare il loro funzionamento e le loro perfomance.

Introduction

Polymers are one of the most promising class of materials, their field of applications has widely broadened in recent years and new applications are continuously being researched. All polymeric products must be suitable for their applications, reliable and well functioning throughout their lifetime. In fact, after installation , some of these products might be difficult to reach or replace and therefore failure should be avoided completely; examples are implanted medical devices such as Prosthetic Heart Valves.

With further advances in the understanding of polymers we will be able to predict effectively their fatigue life and mechanical properties. This could increase the effectiveness of polymer usage in the PHV.

Polymeric Prosthetic Heart Valve has yet to reach a performance level which makes them clinically acceptable. There is no valve including polymer leaflets in the market. Commercial prosthesis are either mechanical (hard materials) or biological (dead pig or cow pericardium tissue) and are usually inserted via open surgery. Both valves have relevant drawbacks: mechanical valves require lifelong anticoagulation; biological valves have limited durability and they undergo further leaflet damage when crimped during implantation. The use of polymers to produce flexible leaflet valves that have the positive attributes of current commercial bioprosthetic and mechanical valves without any of their drawbacks, has been a focus of research since 1950s. However, recent advances in polymer synthesis, processing and characterisation have rekindled the effort in recent years. The remaining challenge is the achievement of a combination of durability and biocompatibility in valve design and polymeric formulation.

Valve replacement is the only effective treatment for aortic valve stenosis or regurgitation. The business need is for safe and inexpensive replacement of defective heart valves, requiring minimal surgical intervention. As polymers are amenable to relatively inexpensive

mass production techniques, attainment of this goal could potentially benefit millions of patients who currently have no access to treatment of Rheumatic heart disease. The market is dominated by few big companies which produce expensive biological valves made from dead bovine pericardium sutured into nitenol stents.

The objective of this work is to investigate polymers with potential to be used in a Prosthetic Heart Valve and could actually pass clinical trials. Different polymers, in particular elastomers, will be tested in order to satisfy the durability issue. In fact, among the long list of failure, mechanical failure has been the highest hurdle to overcome.

The most important section of the work was material selection: this ranged over different kind of polymers, elastomers and composite materials including styrenic block copolymers and advanced thermoplastic polyurethane. The materials were selected with the implementation of a Performance Index realized specifically for the Prosthetic Valve application.

The materials selected were mechanically characterized. The mechanical tests involved crack nucleation and crack growth test, which are typically required for failure analysis and prediction of fatigue life.

The materials with the best Performance Index were then employed in manufacturing of a several prototypes of PHV. The valves produced were tested in the Pulse Duplicator to verify their good functioning and performance.

Chapter 1

The Heart and Heart Valves

Human heart is a specialised muscle that pumps blood through the entire body. The heart is the centre of the circulatory system. This system consists of a network of blood vessels, such as arteries, veins, and capillaries. Blood provides the body with oxygen and nutrients, and also assists in the removal of metabolic wastes. The heart is located in the middle compartment of the mediastinum in the chest. An electrical system controls the heart and uses electrical signals to contract the heart's walls. When the walls contract, blood is pumped into your circulatory system. The heart is cone-shaped, with its base positioned upwards and tapering down to the apex. It is divided into four chambers: upper left and right atria; and lower left and right ventricles. Each ventricle has one valve at its entrance and one at its exit to prevent blood from flowing backwards through the heart. The heart is enclosed in a protective sac, the pericardium, which also contains a small amount of fluid. The wall of the heart is made up of three layers: epicardium, myocardium, and endocardium. All four heart valves lie along the same plane. Between the right atrium and the right ventricle is the tricuspid valve. This consists of three cusps (flaps or leaflets), made of endocardium reinforced with additional connective tissue. Each of the three valve-cusps is attached to several strands of connective tissue, the chordae tendineae , sometimes referred to as the heart strings. They are composed of approximately 80 percent collagenous fibers with the remainder consisting of elastic fibers and endothelium. They connect each of the cusps to a papillary muscle that extends from the lower ventricular surface. These muscles control the opening and closing of the valves. The three papillary muscles in the right ventricle are called the anterior, posterior, and septal muscles, which

correspond to the three positions of the valve cusps. Between the left atrium and left ventricle is the mitral valve, also known as the bicuspid valve due to its having two cusps, an anterior and a posterior medial cusp. These cusps are also attached via chordae tendinae to two papillary muscles projecting from the ventricular wall.

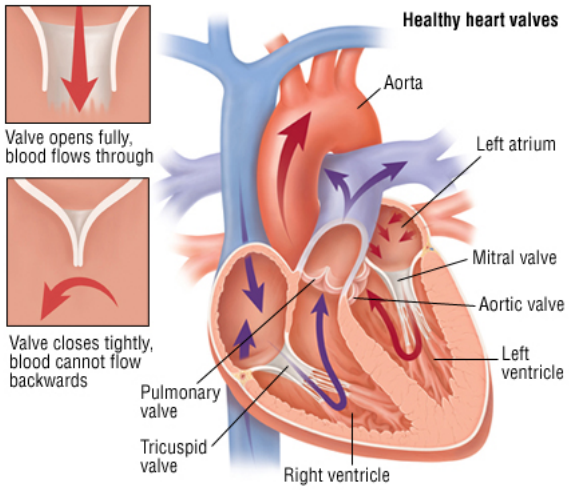

Figure 1.1: Heart section

The tricuspid and the mitral valves are the atrioventricular valves. During the relaxation phase of the cardiac cycle, the papillary muscles are also relaxed and the tension on the chordae tendineae is slight. However, as the ventricle contracts, so do the papillary muscles. This creates tension on the chordae tendineae, helping to hold the cusps of the atrioventricular valves in place and preventing them from being blown back into the atria. The semilunar pulmonary valve is located at the base of the pulmonary artery. This has three cusps which are not attached to any papillary against the cusps which close to seal the valve. The semilunar aortic valve is at the base of the aorta and also is not attached to papillary muscles. This too has three cusps which close with the pressure of the blood flowing back from the aorta. The heart is divided into two pumps which work together. Blood coming back from the organs and tissues of the body enters the right side of the heart which then pumps it to the lungs. The oxygen-rich blood returning from lungs enters the left side of the heart, which then pumps it to all parts of the body, including the heart muscle itself. This process ensures that there is always enough oxygen and nourishment for the body to work efficiently. The atria and ventricles work together by

alternately contracting (systole or systolic phase), to push blood out of the heart, and relaxing (diastole or diastolic phase), to fill with blood. At the start of each heart beat a tiny electrical signal near the top of the heart spreads through the heart muscle making it contract. The atria contract first and the blood returning from the body and lungs fills the atria. The mitral and tricuspid valves are located at the bottom of these chambers. As the blood builds up in the atria, these valves open to allow blood to flow into the ventricles. The electrical impulse then travels into the muscle of the ventricle making it contract. After a brief delay, as the ventricles begin to contract, the mitral and tricuspid valves shut tightly. This prevents blood from flowing back into the atria. As the ventricles contract the atria relax, allowing them to fill with blood and start the next beat. After this last contraction blood is pumped from the ventricle through the pulmonary and aortic valves. The pulmonary valve opens to allow blood to flow from the right ventricle into the pulmonary artery. This artery carries blood to the lungs to get oxygen. At the same time, the aortic valve opens to allow blood to flow from the left ventricle into the aorta. The aorta carries oxygen-rich blood to the body. Normally with each heartbeat the right ventricle pumps the same amount of blood into the lungs as the left ventricle pumps to the body. The heart contracts at a resting rate close to 72 beats per minute.

1.1 Heart Valve Disease

A healthy heart supplies the body with the right amount of blood at the rate needed to work well. If disease or injury weakens the heart, the body's organs won't receive enough blood to work normally.

There are several types of heart disease, in particular some affects heart valves. Heart valve disease occurs if one or more of the heart valves don't work well. There are many changes that can occur to the valves : the chordae tendinea or papillary muscles can stretch or tear, the annulus of the valve can dilate or the valve leaflets can become fibrotic and calcified. This conditions can cause one or more of the heart valves to not open fully or to let blood leak back into the heart chambers. This can make the heart work harder and affect its ability to pump blood.

Heart valves can have three basic kinds of problems: regurgitation, stenosis, and atresia.

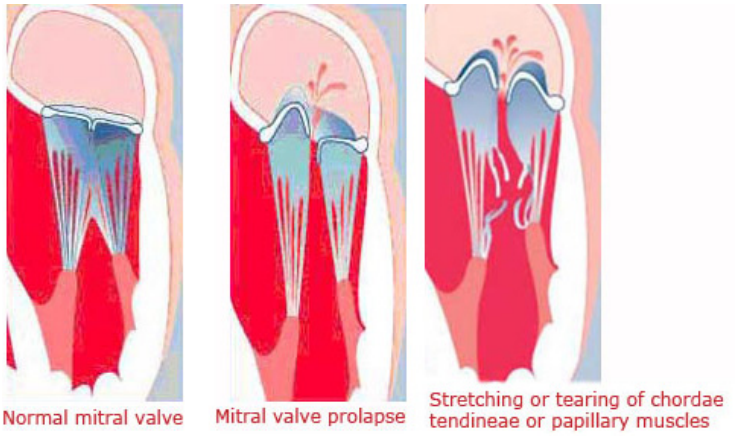

Figure 1.2: Mitral valve diseases

Regurgitation, or backflow, occurs if a valve doesn't close tightly. Blood leaks back into the chambers rather than flowing forward through the heart or into an artery. As the leak worsens, the heart has to work harder to make up for the leaky valve, and less blood may flow to the rest of the body.

Stenosis occurs when a valve opening is smaller than normal due to stiff or fused leaflets. This prevents the heart valve from fully opening. As a result, not enough blood flows through the valve. All four valves can be stenotic and some valves can have both stenosis and backflow problems.

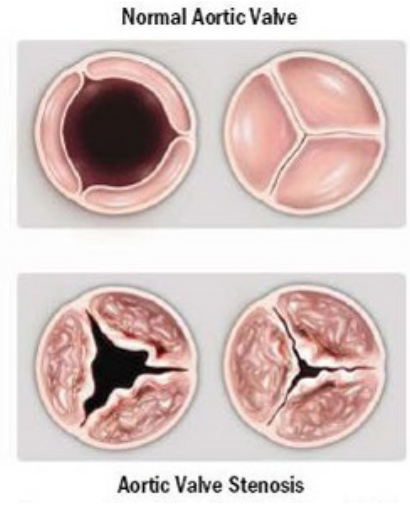

Figure 1.3: Stenotic aortic valve

The last one, Atresia, occurs if a heart valve lacks an opening for blood to pass through. Some people are born with heart valve disease, while others acquire it later in life. Heart valve disease that develops before birth is called congenital heart valve disease. Congenital heart valve disease often involves pulmonary or aortic valves that don't form properly. These valves may not have enough tissue flaps, they may be the wrong size or shape, or they may lack an opening through which blood can flow properly. One example is the Bicuspid aortic valve, which is a congenital valve disease that affects the aortic valve: instead of the normal three leaflets or cusps, the bicuspid aortic valve has only two; without the third leaflet, the valve may be stiff (unable to open or close properly) or leaky (not able to close tightly).

Acquired heart valve disease usually involves aortic or mitral valves. Although the valves are normal at first, problems develop over time. Sometimes the cause is unknown, but it involves changes in the structure of the heart valves as a result of mineral deposits on the valve or surrounding tissue. The causes of acquired heart valve are mainly heart conditions and other disorders, age-related changes, rheumatic fever, or infections .These factors change the shape or flexibility of once-normal heart valves and certain conditions can stretch and distort the heart valves. These conditions include: advanced high blood pressure and heart failure (this can enlarge the heart or the main arteries); Atherosclerosis in the aorta, when plaque (a waxy substance) builds up inside the arteries; damage and scar tissue due to a heart attack or injury to the heart. Damages to heart valves can also be cause by Rheumatic Fever. In particular the valve is damaged or affected.

One more severe condition is represented by the infective endocarditis, which is an infection caused by germs that enter the bloodstream and get carried to the heart. This infection causes growths and holes in the valves and scarring. The process lead to a leaky valve.

If not treated, advanced heart valve disease can cause heart failure, stroke, blood clots, or death due to sudden cardiac arrest .

Currently, no medicines can cure heart valve disease. Eventually, you may need to have your faulty heart valve repaired or replaced.

Some types of congenital heart valve disease are so severe that the valve is repaired or replaced during infancy, childhood, or even before birth.

Chapter 2

Commercial Prosthetic Heart Valve

The introduction of valve replacement surgery in the early 1960s has dramatically improved the outcome of patients with valvular heart disease. Approximately 280 000 valve substitutes are now implanted worldwide each year; approximately half are mechanical valves and half are bioprosthetic valves. Despite the marked improvements in prosthetic valve design and surgical procedures over the past decades, valve replacement does not provide a definitive cure to the patient.

The ideal valve substitute should mimic the characteristics of a normal native valve. In particular, it should have excellent hemodynamics, long durability, high thromboresistance, and excellent implantability. Unfortunately, this ideal valve substitute does not exist, and each of the currently available prosthetic valves has inherent limitations.

2.1 Mechanical Valves

Three basic types of mechanical valve design exist: Bileaflet, Monoleaflet, and Caged Ball valves.

Caged ball valves, which consist of a silastic ball with a circular sewing ring and a cage formed by three metal arches, are no longer implanted. However, several thousands of patients still have caged ball valves, and these patients require follow-up.

Monoleaflet valves are composed of a single graphite disk coated with pyrolytic carbon which tilts between two struts of the housing which is made of stainless steel or titanium. The opening angle of the disk relative to valve annulus ranges from 60° to 80°, resulting

in two distinct orifices of different sizes. This type of valve is no longer manufactured, but more than 360 000 disc valve have been implanted in the past decades.
Bileaflet valves are made of two semicircular leaflets attached to a rigid valve ring by small hinges. The opening angle of the leaflet relative to the annulus plane ranges from 75° to 90°, and the open valve consists of three orifices: a small, slit-like central orifice between the two open leaflets and two larger semicircular orifices laterally. Bileaflet valves and are now the most commonly implanted type of mechanical prosthesis in the world.

Figure 2.1: Mechanical valves : Monoleaflet, Bileaflet and Caged Ball valves

Mechanical valves fail much less frequently, respect to other types of valve in the market, since most of the problems regarding mechanical failure are overcomed.
Mechanical heart valves remain vulnerable to thrombus formation due to high shear stress, flow separation and stagnation, blood damage through the release of pro-coagulant substances.
Given the fact that both the "fluid" flowing through the valves and the "pump" into which these valves are incorporated consist of living cells, problem are likely to be augmented by cascades of biological events. Fluid shear forces and turbulences do not only lead to energy losses but to an activation of the platelet and coagulation system which has the potential to immobilize the entire valve or embolize into vital organs.
As a consequence, anti-coagulation therapy has been until now a sine qua non. In general, thromboembolism is more pronounced in mitral valve replacements. The Bileaflet models have high stress during forward flow and leakage regurgitation as well as adjacent stagnant flow in the hinge area. As it turns out, the hinge area is the most critical part of Bileaflet valves and is where the thrombus formation usually commences.
The necessity for anticoagulation that minimizes, but never completely eliminates the risk

of thromboembolism also exposes patients to the additional risk of major haemorrhagic complications. The most lethal and debilitating of these is intracranial haemorrhage.
One more concern issue is excess tissue growth across the sewing ring, that can lead either to a narrowing of the orifice or to leaflet immobilization. Although widely underestimated, it is likely the primary cause of obstructive prosthetic valve failure in patients on correct anti-coagulation therapy. In the aortic position, pannus formation is mainly in the inflow side while in the mitral position it occurs both on the atrial and the ventricular side. In order to prevent tissue ingrowth into the clearance of leaflets, one contemporary valve design introduced a longer housing cylinder with goal of creating an ingrowth barrier. One of the sources of growth stimulation is the chronic foreign body reaction against the sewing ring material [19].

2.2 Biological Valves

All mechanical prostheses have an absolute requirement for anticoagulant treatment. The potential advantage of avoiding the hazards of anticoagulation has led to the search for a valve replacement of suitable biological material which would not require long term anticoagulant treatment. A number of different approaches to the problem of finding a suitable biological valve have been made.
Biological valvular prostheses are classified into a number of subtypes: autograft, xenograft and homograft.
A human heart valve that is harvested from, and implanted into, the same person is called an autograft: in the Ross procedure, for example, the patient's pulmonic valve is transferred to the aortic position. These pulmonic autografts have excellent hemodynamic properties as well as low rates of thrombosis, degeneration, and endocarditis. The Ross procedure is suitable for children and young adults because it is compatible with further growth of the aortic root. Its long-term success rate is not yet adequately known, however, and a few cases of dilatation of the autograft have been reported [20][21][22].
A homograft, in contrast, is a human heart valve that has been cryopreserved and treated with antibiotics. Homografts are often used in patients with extensive evidence of endocarditis, but their availability is limited and they tend to degenerate.

Xenograft prostheses are made of porcine aortic valves or bovine pericardium. The design of bioprostheses is intended to mimic the anatomy of the native aortic valve. Porcine bioprosthetic valves consist of 3 porcine aortic valve leaflets crosslinked with glutaraldehyde and mounted on a metallic or polymer supporting stent. Pericardial valves are fabricated from sheets of bovine pericardium mounted inside or outside a supporting stent.

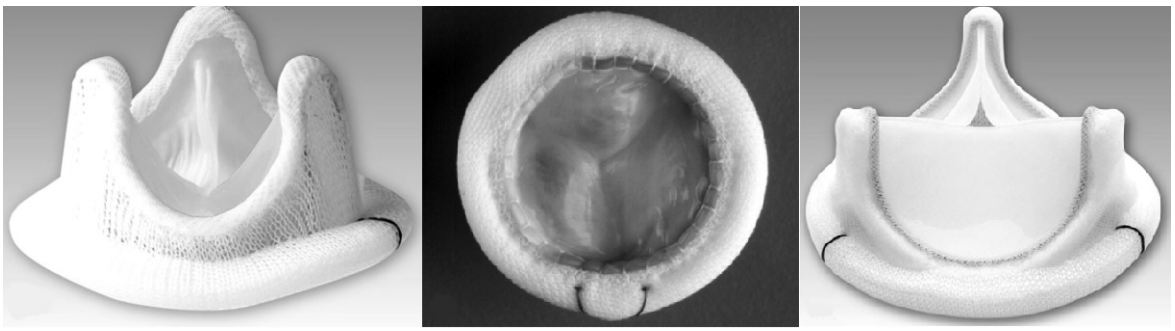

Figure 2.2: Tissue valve

In an effort to improve valve hemodynamics and durability, several types of stentless bioprosthetic valves have been developed. They are manufactured from whole porcine aortic valves or fabricated from bovine pericardium. These prostheses of animal origin do not contain a stabilizing metallic scaffolding and therefore offer a larger opening surface and more favorable hemodynamic properties than stented prostheses. However, the implantation of a stentless valvular prosthesis often requires a more complicated surgical technique than that of a stented one .

The absence of living tissue, as well as the necessity to mask antigenicity, represents the system-inherent problems to contemporary tissue valves. For tissue valves, failure is usually a slow, progressive deterioration of valve function ending in the need to replace the prosthesis. Calcification affects less than half of failed tissue valves while tears, as a consequence of inflammation, collagen degradation and a lack of repair mechanism were the predominant modes of failure.

The preserved tissue of the valve will last a limited number of years, 5-15 years for most patients, potentially less for younger patients. Reoperation requires the chest cavity to be reopened. Certain risks accompany reoperation that were not present for the first operation: tissue may be scarred together and cause excess hemorrhage in certain cases;

operation time is usually extended; recurrence of pain from the operative site and the inconvenience and risks of recovery must be endured again. Furthermore, replacement of valves at an advanvced age carries a higher probability of mortality.

Tissue calcification is an integral component of bioprosthetic degeneration. It is a multifactorial process, of which insufficient immune masking is only one component. Glutaraldehyde is another factor, as this dialdehyde is known to intrinsically elicit calcification.

Tissue valve calcification is initiated primarily within residual cells that have been devitalized, usually by glutaraldehyde pretreatment. The mechanism involves reaction of calcium-containing extracellular fluid with membrane-associated phosphorus to yield calcium phosphate mineral deposits. Calcification is accelerated by young recipient age, valve factors such as glutaraldehyde fixation, and increased mechanical stress.

It has long been known that the low-dose glutaraldehyde treatment used for the fixation of bioprosthetic heart valves reduces immunogenicity but does not abolish it. The low-grade fixation used in commercial valve preparations fails to significantly alter membrane-bound receptors or structural glycoproteins. Therefore the tissue continues to elicit both cellular and humoral immune responses.

In the vast majority of explanted tissue valves, inflammatory cells are either found to cover the surfaces or focally infiltrate into tissue. Given the destructive potential of giant cells to erode even synthetic materials, however, it becomes obvious that these "war-formations" of macrophages are serious culprits of destruction. In bovine pericardial heart valves prostheses, for instance, macrophages are regularly found invading and focally degrading the prosthetic collagen. Conspicuously, dense infiltrates of inflammatory cells are found in valves which had failed due to tissue tearing.

In as much as similar triggers initiate the tissue overgrowth of the sewing ring as in mechanical valves, the process is augmented by the inflammatory potential of the BPT. Amongst other factors, the extent of this inflammation is a reflection of the degree of insufficient immune masking of the tissue.

The most promising preventive strategies have included binding of calcification inhibitors to glutaraldehyde fixed tissue, removal or modification of calcifiable components, modification of glutaraldehyde fixation, and use of tissue cross linking agents other than glutaraldehyde [19].

Chapter 3

Polymeric Heart Valve

3.1 Population needs and obstacles

Unfortunately, socioeconomic circumstances still limit access to valve surgery to a fraction of patients who actually need it. While the bulk of the estimated 275000 to 370000 annual valve replacements benefit predominantly the older patients of the First World, developing countries with their much higher incidence of rheumatic fever often have no access to heart surgery. However, given the fast growing economies of some of these countries, it is predictable that they will soon have a high demand for prosthetic heart valves that are affordable and that address specific needs of their mainly young patients. The fact that 85% of all open-heart procedures are performed in countries representing 11% of the world population emphasize how unrepresentative the current heart valve recipients are with regard to global needs. The fact that the economies of many of these threshold countries are growing fast makes it predictable that cardiac surgery will be increasingly accessible to those millions who are in need of a valve replacement. The promise of synthetic heart valves was to have prostheses available that have the durability of mechanical valves and the haemocompatibility of tissue valves. In reality, most of the valves were the opposite, combining the durablity of tissue valves with the thrombogenicity of mechanical valves. Therefore, years after the first flexible leaflet polymeric heart valves were implantented into patients, they have yet to reach a performance level that makes them clinically acceptable beyond the short-term use in artifical hearts.

Initially, most researchers used the basic trileaflet aortic design for their prototypes

valves. Advances in fluid-dynamic measurements and numerical modelling subsequently allowed for optimization of flow dynamic and leaflet stress. Variations ranged from hemi-cylindrical cusps to leaflets in half-open position; form variable curvatures to elliptical and hyperbolic shapes and from a conical base with spherical upper part to high profile cusps.

Overall, design and material improvements let to a gradually increased durability and fatigue resistance. There still seems to be a high variability in cycle life not only between different valve design and different studies but also between similar valves within the same study [19].

3.2 Polymeric Hearth Valve Background

One of the first used polymer for prosthetic heart valve use was Polyurethanes (PU) and they have continuously been favoured for blood contacting applications in spite of their initially poor long-term chemical stability. However, new generation polyurethanes, such as Elast-Eon™seem to have largely overcome the problem of biodegradation. Similarly, improved fabrication techonologies resulted in even and constant leaflet thickness thereby improving fatigue resistance and durabiity.

Segmented PUs are generally flexible and durable at approx $10\mu m$ leaflet thickness, although there was some concern that a leaflet thickness of less than 150 microns may not be sufficient. Overall, the choice of thickness and material modulus is a trade-off between tensile strength and imparted bending stresses.

The second most widely used polymer family was Silicone rubbers, but disappointing results led to their abbandoning.

Most recently, a novel polyolefin, poly(styrene-b-isobutylene-b-styrene) (SIBS), with excellent chemical stability, has been proposed as alternative to the traditional polymers. The material was found to match PU in platelet deposition tests, and was comparable with PU in terms of tensile and fatigue properties, albeit only after reinforcement with polypropylene fibres.

All together, the promising result with both the latest generation of biostable urethanes and innovative materials such as fibre-reinforced SIBS for the first time after 50 years of

failure a new door may have eventually have opened a small gap.
In fact, until the mid to late 1980s, calcification had almost inevitabily led to leaflet immobilization, rupture and perforation. This seemingly insurmountable limitation briefly resulted in an almost complete discontinuation of polymer valve programs. Over the course of half a century, polymeric valve design have been improved regarding flow characteristics and stress reduction. During the same period of time, degradation-resistant materials were developed, processing methods evolved that allow reproducible high quality manufacturing, and thrombogenicity and calcification have been partly addressed through surface modifications [19].
Bezuidenhout et al. [1] presented an overview of the polymer technology for the application on the PHV ; the following informations and descriptions are taken from their paper.

3.2.1 Polysiloxane Valves

Polysiloxane are polymers of alternating Silicon and Oxygen atoms in backbone and can contain a variety of pendant reactive groups on the silicon $-[Si(R_2) - O]-$, with polydimethylsiloxane (PDMS : $R = CH_3$) comprising the structural chain moiety. Crosslinking through radicals, condensation or addition reactions leads to highly elastic materials which have been used in wide range of implantable devices due to their biostability and flex fatigue resistance.
Benson Roe and collegues in San Francisco developed one of the first flexible trileaflet valves from Silicone material (Silastic 50, Ellay Rubber Company) in the late 1950s. The 380 μm thick leaflet were originally housed in a silicone cylinder, and valve evaluated in acute dog ascending aorta showed satisfactory function, but long term survival could not be achieved in a subsequent subcoronary model.
Later versions were made from different silicone (General Eletric SE-555) and with composite of a steel band/silicone sponge/ Dacron sewing ring that contained slightly thicker leaflets (430-500 μm).
Although some valves were shown to remain intact for 786 million cycles (mc) in accelerated tests (58 Hz; 18 years equivalent at 80 beats per minute) the programme was discontinuos due to high mortality rates in clinical trials with 18 selected patients between

1960 and 1962. Mohri et al. revisited trileaflet silicone valves and tested various Dow Corning silicone formulations and leaflet designs ranging from 225 to 510 μm in thickness with a preferred thickness of 330 μm . Some of the initial combinations exhibited poor durability with tearing at 3.9 years, but the preferred embodiment valves were able to withstand 17.7-23.8 equivalent years in accellerated tests (average 900 mc at 17 or 33 Hz; triangular leaflets; DC-MDX4-4059) experimental polymer).

Another design reported by Gerring et al (the Oxford valve) comprised silicone (DC Silastic 5505) coated Terylene (polyester) fabric and had a thickness of 120 μm. In vivo evaluation in the pulmonary position of calves showed good survival of growing animals up to 30 months, with only 2 out of 7 animals in one series dying of thormboembolic events.

Room temperature vulcanizing silicone (RTV-615; General Electric) was used by Chetta and LLoyd to produce two valve designs with 256 μm leaflets using a cavity molding method and achieved 65 and 280 mc respectively at 21 Hz.

3.2.2 PTFE and ePTFE Valves

Polytetrafluoroethylene (Teflon ®) is a highly crystalline fluorinated polymer that is well known for its inertness, low surface tension (high water contact angle), and low coefficient of friction. Nina Braunwald and Andrew Morrow reported on clinical trials using flexible tricuspid Teflon fabric prosthesis, based on the Muller-Littlefield valve for aortic valve replacement in 23 patients between 1961 and 1963. The prostheses were either of plain Teflon fabric valves, Teflon fabric valve with a Teflon dispersion, or single Bahnson leaflets of jersey-knit Teflon. In most cases valves removed a t reoperation or autopsy were stiffened, with regurgitation through holes in the leaflets and tears of varying sizes from small crack to complete shredding and disruption of the fabric integrity. Nodular calcific deposits were evident but extensive calcification was not observed. Gore-Tex ®trileaflet valves (23-25 mm; WL Gore & Associates) were reinvestigated in an animal study in 1990 (weanling sheep tricuspid up to 34 weeks). Leaflets were all unretracted, but half of the valves had one or more stiffened leaflet, and macroscopic calcification was evident in the commisural areas.

Ando and Takahashi reported the use of hand-made valves comprising Gore-Tex leaflets suspended in Dacron conduits for the tratment of 139 paediatric patients under-going pulmonary reconstruction due to Ross procedures and complex congenital heart disease. The valves showed

functional in vivo durability for up to 10 years and are considered to be a good alternative to homo and xenografts in this position.
The experiences with textile and expanded PTFE thus indicates that the valves made of this material calcify and stiffen, and it seems, apart from hand-made valve mentioned above, that the use of this material for heart valves is limited to employement as chordae tendinae for mitral valve repair.

3.2.3 Polyurethane Valves

Polyurethanes are a broad class of materials with a very wide range of properties depending on the chemistries involved in their manufacture. They can be either thermosets or thermoplastics; in the latter case the polymers may form virtual crosslinks by microphase separation to produce elastomeric materials that are heat and solvent processable and thus relatively easy to form into complex shapes.
The segmented thermoplastic polyurethanes (TPUs) and polyurethanes ureas (TPUUs) are composed of hard and soft segments and have been the most popular materials for use in polymeric heart valves over the history of their development. The polymers have undergone many improvements from first generation materials containing polyestrer soft segments that were hydrolytically degradable, to second generation polyether based materials (polyether urethanes: PEU and polyether urethanes ureas: PEUU) that were susceptible to oxidation , to third generation materials that have greater chemical stability, such as those containing polycarbonate (PCU) and /or polysiloxane soft segments, and polycarbonate based materials that additionally contain polyhedral oligomeric silsequioxanes (POSS) nanoparticles.
Nina Braunwald produced early bileaflet heart valves by impregnating lock-knit Dacron fabric in a mold cast from natural mitral valves from a catalysed liquid prepolymer formulation used to make open-cell foams (American Latex Company) and subsequently attaching woven Teflon cordae. After gaining surgical experience by implanting the valve in dogs, she performed the first succesful mitral valve replacement on a patient that survived for several months after the surgery.
Also in the late 1950s the first three-cusps polyurethane (Estane,a PEU by BF Goodrich) valves (130-180μm thickness) resembling native semilunar valves were made and imolanted in the mitral, tricuspid and aortic position in dogs. Simultaneos development of valves and surgical techniques led to high mortality, and many of the valves showed marked fibrin deposition resulting in stenoses and emboli. A second version of the Oxford valve was produced with segmented

polyurethane urea (Biomer, a PEUU by Ethicon) with leaflet thicknesses from 70 to 80μm, but without the reinforcing fabric used in the silicon version. Three calves receiving these valves in pulmonary position survived for more than 18 months.

Two similar polyurethanes ureas, namely Biomer and DuPont Lycra Spandex-type material, were used in the 1980s to produce trileaflet valves. The Lycra valves had low regurgitation in vitro, and although hte valves were durable for at least a year in adult ovine and caprine models, calcification and subsequent thrombosis was seen in growing calf tricuspid and mitral positions. Earlier work by the group of Helmut Reul in Aachen involved the optimized design Avcothane-51 (a polyether/PDMS based polyurethane) valves for smooth washout, minimum leaflet stress and maximum durability. By October 1976, these valves had operated the equivalent of 10 years in accelerated tests at 12Hz.

The J-3 polyurethane (and aliphatic PCU; ENKA 1025/I; Enka/AZKO) valve was subsequently developed by Josef Jansen et al. forming the leaflets on a stretched stent in the half-open position in ordere to minimize stresses during opening and closing. The valves showed very low energy losses, and reached 400-648 mc (11-17 years equivalent) in accelerated tests. Mitral implants in growing calves (5 months intended duration) showed thrombotic deposits that appeared to be associated with surface roughness on the cusps, and the most extensive deposits contained extrinsic calcification. In the decade thereafter, the company ADIAM developed both bi- and trileaflet polyurethane valves from polycarbonate urethane (PCU, ADIAMat) for the mitral and aortic positions respectively. In vitro durability of the mitral valves ranged from 600 million to 1 billion cycles a 12 Hz while the aortic trileaflet valve showed steady improvement from 300 million to 450 million to 650 million cycles. In vivo comparison of the bileaflet valves with two different bioprosthetic valves by Sabine Daebritz et al. in th egrowing calf mitral model for 20 weeks showed trivial regurgitation, mild leaflet thickening and calcification, and no degeneration of the PCU valves, while the calves receiving bioprostheses had to be sacrificed after 1-4 weeks because of the congestive heart failure due to severe calcification, degeneration and thrombosis . When the trileaflet valves were compared to the same bioprostheses in the aortic position, the synthetic valves had a variable degree of calcification and degeneration was mild, and there was not an increase in thrombogenicity of the valves when compared to the bioprosthesis.

The collaboration of David Wheatley in the United Kingdom concentrated on the valve leaflets originally made from Estane (a PEU, BF Goodrich) and Lycra (a PEUU Du Pont), to later version made from the more advanced Elast-Eon™3 (polysiloxane soft segment based polyurethanes (PSU) and polyurethane ureas (PSUU) with 40% MDI based hard segment, Elastomedic/Aortech).

Durability of more than 300 mc (12Hz) achieved with ellipto-hyperbolic Estane valves could be improved to over 450 million, with some valves achieving 800mc (equivalent to 20 years), when changing to the diamine extended PEUU. Leaflet thicknesses of 60-200 μm.

In vitro dynamic testing (in a fatigue tester)showed some calcification (similar levels for PEU and PEUU) of leaflets associated with tears at the free edge or commissures degradation sites and sometimes with silicone present as additive or lubricant (in the materials or due to frame injection molding). Static in vitro and in vivo calcification assessment highlighted the effect of low molecular mass components in the polymers, as methanol and chloroform extracts and extracted polymers showed differential degrees of calcification. The low molecular mass extractables were generally shown to be accelerating factors in the calcification process. Hydrodynamic function tests in a simulated mitral position of a pulse duplicator demonstrated that the PU valves had similar mean pressure drops to a bioprosthesis , and less reverse flow and energy losses than both the bioprosthetic and mechanical valve controls. In the 6-month duration growing sheep mitral model the PU valves performed as well as the mechanical valve in terms of hemodynamic, while a porcine valve became compromised with time. Calcification of the PU valves was evident, and often associated with surface thrombus and degraded areas on the leaflets.

By the turn of the century, in collaboration between the University of Leeds and Liverpool, the group proposed a new valve design with a conical attachment area and spherical upper/free edge area. Original valves made from Tecothane (a PEU; Young's Modulus: E=10 MPa; Thermedics) with 73-111 /mu m leaflets lasted for at least 360 mc, showed symmetrical opening and closing, and superior EOA, lower regurgitant volume and lower energy losses than the single tilting disk mechanical and porcine bioprosthetic control valves used in the study. Kinematic tests of similar valves with 150 μm leaflets showed the effects of cycle rate in accelerated testing, in that the leaflet kinematics, bending strains, the proportion of time fully open or closed, and strain time integral were all dependent on cycle rate. With valves of this geometry subsequently made from various grade of Elast-Eon™3 (E=5-63.6 MPa and leaflets of 48-230 μm) the hydrodynamic function was not significantly affected by modulus, but significantly influenced by leaflet thickness. PSU and PSUU based valves were implanted in the mitral position of young adult sheep for 6 months, after which the leaflets contained a fine surface proteinaceous layer, with no evidence of thrombus formation, fibrin deposition, calcification or thromboembolism. Although there was some evidence of surface enrichment of siloxane functional groups, the explanted leaflet materials differed little in appearance from their implant state , were structurally intact, showed no degradation and exhibited retained mechanical properties. There is some

evidence, however, of degradation of PDMS soft segment polyurethanes with extended exposure to water, albeit at elevated temperature, with possible site of hydrolysis being the carbamate groups adjacent to the PH(T)MO or PDMS chains.

Yoganathan's group in Atlanta studied three design of Elast-Eon™valves (Aortech Europe), namely ones with closed commissural design with those that had semi-open and open design in detail regarding the flow structure and its potential effect on thrombogenicity. High shear and high velocities and thrombotic potential were identified at the leakage jet diastole, the trailing edge during peak forward flow, and the centre orifice downstream of the value during peak forward flow.

In the interim, the Leeds group led by John Fisher also developed the alpharabola design valve made from thermoformed low modulus Eurothane 2003 (E=6Mpa) to a leaflet thickness of 150-200 4 μm. The valves showed short term durability (100mc), improved opening characteristics over spherical leaflets, as well as a clear effect of increasing opening pressure with thicker leaflets. This design was used to compare two manufacturing methods, namely thermoforming and dip-casting using IT C34 polyurethane (E=7-10 MPa; both types 200 /mu m leaflets thickness). There was only a small difference in hemodynamic properties, but dip casting proved far superior in terms of durability, with at least 160 mc achieved compared to 100 million or less for thermoformed valves. Finite element modelling of the alpharabola design showed reduction in principal tensile stress to 60% of that o spherical leaflet geometry.

Nanocomposite POSS-PCU materials recently developed by group of Alex Seifalian at University College London showed improved mechanical properties and resistance to platelet adhesion. In vitro assessment of a semi-stented surgical aortic valve (SSAV), 100, 150 and 200 μm leaflet valves based on this technology was performed and compared o control valves of similar size. The SSAV design was shown to have improved performance over a conico-spherical design using finite element modelling and pulse duplication tests and had lower transvalvular pressure drops, regurgitation and energy losses and a significantly increased calculated EOA than that control bioprosthetic valves.

3.2.4 Other Polymer Valve

A number of alternate polymers had been evaluated for use in flexible leaflet valves. During the late 1950s Roe et al. switched to silicone only after unsuccessful trials with polyvinyl alcohol, polyethylene and plasticized polyvinyl chloride (PVC, that lost flexibility after relatively short periods in the bloodstream due to loss of plasticizer in the case of PVC).

Poly(styrene-b-isobutylene-b-styrene) (SIBS; Quatromer™, Innovia LLC), either as is or with polypropylene reinforcement fibres, has been proposed as a polymeric leaflet material due to its mechanical properties between that of silicone and polyurethane, and its superior inertness due to its oxidation resistant Carbon-Carbon backbone. In addition to the percutaneous valve, the group also worked on surgically implantable valves. Early SIBS impregnated Dacron mesh valves (240 μm thickness) showed no significant difference to mechanical and bioprosthetic controls regarding thrombogenicity using a platelet activation state (PAS) assay in a VAD device. Valves, with and without precoating with dimyristoyl phosphatidylcholine (DMPC), implanted for 20w in the sheep aortic position, failed due to stent deformation and cracks in the leaflets due to creep, with accompanying exposure of the PET fabric, with severe blood and tissue interactions, including extrinsic calcification. A new SIBS valve design subsequently evaluated in vitro for thrombogenicity and platelet activation rates (PAR) was multiples lower than control bioprosthetic valves using the PAS assay and flow cytometry. Innovia has also developed a thermoset crosslinked version of the material, dubbed xSIBS, to overcome creep problems associated with the non- crosslinked material, and to potentially make leaflets without the need for Dacron reiforcent. The devices were recently optimised by the group at Stony Brook University (in collaboration with groups in Aachen and Arizona) for reduced stress, improved hemodynamics and reduced thrombogenicity using device thrombogenicity evaluation (DTE).

The group of Frank Baaijens in Eindhoven has been working another olefinic material, namely crosslinked ethylene-propylene-diene- monomer rubbers (EPDM; K520 from DSM), for the construction of heart valves. The valve compromises multiple layers of EPDM reinforced with wound fibres in a design that allows for the molding of the leaflet (200 μm) as well as sinuses and part of the aortic root.

Prototype heart valves have also been made from polyvinyl alcohol (PVA, a water soluble polymer) rendered insoluble by a one piece cavity molding/freeze thawing procedure (to form a so called cryogel using well-defined geometries discussed in Sect. 5). Devices were also fabricated from combination of PVA with bacterial cellulose reinforcement to mimic the anisotropic mechanics of natural valve.

3.2.5 Manufacturing Techniques

Various techniques have been used to process the polymers into complex 3-dimensional leaflet shapes required. The first determinant of the technique available is the nature of the polymer used. Thermoplastic materials may be processed using heat and solvent processing (if the

polymer is sufficiently soluble), whereas molding technique are required if the materials are thermosets.

Dipcasting is technologically one of the simplest techniques as it involves dipping a mold into a solution of the polymer, removing the mold such that a film of polymer solution adheres to the mold, and then evaporating the solvent to yield the desired structure. In practice, repeatability in obtaining the desired thicknesses and quality is not trivial. Solvent volatility, polymer concentration/viscosity, dipping number (single vs. multiple), technique and speed, drying position (upright, upside down, rotating), atmospheric conditions (pressure, temperature, gasses), and mold shape and surface properties all affect the distribution of material (leaflet thickness) and quality (surface morphology, uniformity, bubble formation/imperfections, durability and function).

Polyurethane Valves The J-3 polyurethane valve is interesting as it is manufactured in half-open configuration. In order to achieve this, the top of the metal mold was flared so that the arms of the stent would be expanded between the minimal surface area leaflet surfaces. Dipcoating of leaflets and stent integration occurred in one step, using cleanroom conditions within a dry glove box, and the valve is tumbled in a controlled motion during drying to ensure even leaflet thicknesses . This method also avoids shape-memory effects, which can occur when leaflets are made in a precurved closed position.

ADIAM later improved the manufacturing technique by employing a combination of dipcoating and dropping technique of polymers of different hardness (soft outer layers and medium hardness core), whereby the polymer is applied in a controlled dropwise fashion in order to achieve accurate control over leaflet thickness (which is varied between 80 and 200 μm depending on position), the use of flexile stent posts to ensure proper closing, and the use of a precision laser to separate the leaflets. The company also produced a scalloped bileaflet valve with large anterior and small posterior leaflets (varies between 100 and 300 μm thickness) specifically for the mitral position, using sewing rings made from fleece-like sprayed PCU. The Fraunhofer Institute in collaboration with Helmholtz Institute for Biomedical Engineering of RWTH Aachen University has recently also announced the very accurate production of small venous valves using the precise dropping techniques.

Dip-coating onto injection molded PU or machined PEEK frames fitted to metal forming mandrels (35-45% Estane Lycra in DMAc) was used by David Wheatley et al. to produce their ellipto-hyperbolic valves, with the solvent evaporated under slight positive pressure at 70-80 °C.

vented into a water trap to ensure solvent evacuation. Variations of this method when using Elast-Eon involved dipping and drying under inert atmosphere, and using single (1x27% PSUU in DMAc) and multiple (3x15% PSU in DMCAc) coatings on pre-warmed steel former containing the PEEK frame.

The alpharabola and spherical designs of the Leeds group were made by a combination of techniques. It comprised the solvent bonding (8% PU in DMF) of leaflets cut from solvent cast film of PU to PU-dip-coated ($250\mu m$ layer) PEEK frames, and subsequent thermal forming of the leaflet geometries in custom-made metal molds. These valves were later compared to dipcoated valves, whereby stented mandrels were successively dipped in 25, 25 and 12% (twice consecutively in 25% then in 12%) PU solutions in DMF followed by drying respectively in the upright, inverted (upside down) and upright position (12 mm/min dipping ; 75 °C drying for 1 h) . Removal from molds was facilitated by extended immersion in water (12h), and leaflets were cut using a sharp blade.

Alex Seifalian's group originally explored electro-hydrodynamic atomization (electrospraying) to make valves from their POSS-PCU material, but is now using a more established dip coating process . The process comprises the repeated controlled dipping of a metal mandrel containing a contoured stent wire (0,5 mm titanium alloy) into the polyurethane solution (18% w/v in DMAc) followed by drying (60 °C for 1 h) and trimming of the free edges.

Silicone Valves Early silicone valves were cast in one piece (with a tubular root structure surrounding the leaflets) by compression molding, heating the mold to 180°C under high pressure and curing after removal from the die at 200 °C for 4 h. A similar process was followed 15 years later, using highly polished three-piece metal molds into which the silicone was injected, from which excess air was removed via a bleed screw, but in the latter case the valve was made on a three-posted metal stent to yield and integrated scalloped design. With room temperature curing materials, the process can be simpler, as hand-made molds from plaster and silicone can be used to form the desired shape by using centrifugation and/or evacuation to fill the cavity and allow sufficient time for the silicone cure.

ePTFE Valves Due to high melt viscosity, PTFE requires different processing techniques than those used for conventional thermoplastics, and methods akin to those used for metals are often employed . In terms of medical devices the material is often used in a expanded form (expanded or ePTFE, e.g. Gore-Tex®) for the production of vascular grafts, although processing into fibres and subsequently into textile prostheses is also possible. Early ePTFE

valves were constructed from multiple layers o 3 μm thick (original thickness), 1 μm pore size (Gore-Tex®) sheets bonded together in diverse directions to achieve tensile strengths of conventional PTFE. Composites containing various numbers of layers (4-15 layers, ranging from 8-31 4μm total thickness) were then sewn to support stents after reinforcing the attachment zones with additional 5-7 layers of material. More recently, Nistal et al. reported on valves comprised compact PTFE leaflets in a valve frame covered with ePTFE (and using ePTFE sutures) made by WL Gore & Associates. The manufacturing technique, exact nature of the compact PTFE and whether it is similar to the composite used in the previously described valves are not clear. The manufacturing approach of the paediatric surgeon in Tokyo shows how innovative and simple designs can be very successful, albeit in the less demanding pulmonary position. The leaflets were hand made by folding sheet of 100 μm in half, suturing the folded membrane to form three pockets, and then looping the ends around to form cylinder. The cylinders were then sewn into regular 12-28mm Dacron (Haemashield , Boston Scientific Corp) vascular conduits and used with great success.

SIBS and EPDM Valves SIBS percutaneous valves were made by impregnating Dacron fabric with the polymer dissolved in Toluene (15% m/m) and air drying, forming a cylinder by stitching, stitching the cylinder to the Nitinol stent, and then annealing the leaflets into shape using three ball-bearings (9.5 mm) and a 19mm aluminium cylinder. DTE optimised, surgically implantable valves were produced by filling 5-axis machined aluminium alloy molds (made by the collaborating Helmholtz Institute in Aachen) with raw 23% styrene zSIBS, compressing to 1 ton of force and heating to 260°C to effect the Diels-Alder crosslinking.
Valves made from EPDM were manufactured by dipping rotating two piece molds (one for leaflets, one that fits over the leaflet mold to produce the sinuses) into a 7.5% solution of the material xylene, combined and a fibre-winding machine that can be programmed to produce a variety of fibre orientations and patterns.

PVA Valves Dipcoating and film-fabricating technologies were, however, not considered suitable for the production of polyvinyl alcohol cryogel valves, as more constant dimensions and properties were expected from a cavity molding process. Complex 4-axis-machine metal molds comprising 9 parts were filled with hot PVA solutions by injection and pouring, and after closing of the mold, the whole assembly was subjected to freeze/thaw cycles in a water bath (-20 to +20 °C). The Ontario group subsequently developed anisotropic PVA cryogel valves by inclusion of a small percentage of bacterial cellulose, and straining the samples between cycles.

3.2.6 Surface and Bulk Treatments

A variety of surface and bulk treatments/composition have been proposed for the reduction of thrombogenicity and calcification of polymeric valve leaflets, and for the maximization of durability. The main challenges facing these approaches are the limited surface area and volume of the leaflets and the sustained stability and activity of the treatments. This is especially demanding considering that about 6,000 litres of blood washes over the leaflets daily, so that active agents are readily depleted/overwhelmed even if they act in a catalytic manner.

Benson Roe was one of the first to attempt augmentation of the anticlotting properties of flexible leaflet valves by the surface bonding of graphite-benzalkonium-heparin, but the contribution of the coating was unclear due to the confounding factors, as valves failed for a variety of reasons, including thrombosis. Heparin, as well as taurine, aminosilane and polyethylene oxide (PEO) modification of PEU and PEUU valves did not affects leaflet thickness or hydrodynamic properties. When subjected to in vitro calcification in an accelerated tester, the PEO modification was detrimental to calcification and durability (155-200 down to 63-73 mc). The other three surface resulted in increased fatigue life; moderate in the case of the PEUU (155 to 180-320 mc) and marked in the case of the PEU (220 to 418-437 mc). In contrast, sulfonated PEO coupled to polyurethane heart valves and vascular grafts was shown in animal models to improve not only blood compatibility in terms of platelet adhesion and thrombus formation, but also to improve biostability and decrease calcification.

Calcification is of course not only related to the surface of the leaflet, but also its composition. The mechanism of calcification of polyurethanes is not clear, but various have been proposed, including cation complexation by the polyether soft segment and chelation, or deposition of thrombi and cellular debris, although calcification has been shown without the need for thrombus formation. Calcification has often also been shown to be associated with cracks or abrasions on leaflet surface, but it is not clear which causes which, while others have implicated the stresses and strains that leaflets undergo during cycling.

Striking examples of treatments of formulations that result in reduced calcification are the extraction of low molecular mass components from polyurethanes on calcification of leaflets in vitro, the potential of nanocomposite formulations of PCA to decrease calcification, and the lack of degradation, calcification and thrombosis in leaflets made from Elast-Eon™.

Bisphosphonates are well known for their effect on mineralization, and derivation of the hard segment of medical grade polyurethanes have been shown to decrease calcification in the rat subcutaneous model, as well as in the circulating sheep pulmonary valve cusp model without

adverse effects on the polymers.

Cholesterol modification of polyurethanes seems a very promising approach, as endothelial cell attachment and retention could be shown not only in vitro, but also in vivo , employing pulmonary leaflet replacement with autologous endothelium-seeded polyurethane cusps.

Treatment of SIBS with dimyristoyl phosphatidylcholine (DMPC) did show promise in terms of decreased platelet adhesion, but calcification and degradation meant that the coatings did not have much effects when in a full-scale sheep valve model.

Chapter 4

Material Selection and Performance Index

Flexible leaflet polymeric prosthetic heart valves (PHVs) have been proposed as a potential solution able to provide good long term durability and function without the need for anticoagulation, however, no valve has been clinically successful, and in the past 40 years of development no valve has reached clinical trials [1].As such, the process by which a polymeric valves is designed should be seriously considered. The design of polymeric valves may be split into a structural valve design and material selection problem. The use of material selection indices to aid the quantitative design of engineering components was formalized by Ashby et al. [3], and in this work, a novel material performance index (PI) to evaluate potential polymer materials for PHVs, ideated by Brubert et al [2], has been used . The leaflets has been identified as the critical component for the valves, and this report is focused on material selection for leaflets. The remaining challenge is the achievement of combination of durability and biocompability in valve design and polymer formulation. This would allow polymeric valves to become a clinical reality for surgical implantation. In this work the materials considered has already passed the biocompability test, so it could be easier to focus only on the long term fatigue life prediction. In fact among the long list of failures, mechanical failure (which is synergic with calcification) has been the highest hurdle to overcome. In fact durability and calcification are the two failure routes which have plagued all flexible leaflet polymeric valves tested in vitro or in vivo. Durability is a function of material and valve design. Although various leaflet forms and dimensions can result in reduced leaflet stresses, the first order determinant of the stresses induced in a leaflet when loaded during diastole is a function of the leaflet's thickness; thicker leaflets have lower stresses.

Concurrently, the hemodynamics of the valve has to be taken into consideration. In general, the reduction in leaflet thickness leads to a lower mean pressure gradient [4]. Given these conflicting criteria regarding leaflet thickness, we must seek a compromise, leading to the use of a material PI [3]. We must define a relationship for hemodynamics and durability using leaflet thickness and appropriate material parameters. Furthermore viscoelastic polymer exhibit frequency dependent transitions in mechanical properties which makes high frequency testing a poor model for predicting low frequency behaviour. In particular, the use of crack growth models to predict long term behaviour has been successfully employed in the cyclic straining of various rubber components[34].

Brubert and Moggridge proposed a novel material index based on cyclic fatigue theory for the improved design of a Prosthetic Heart valve. The opening of a valve requires bending of leaflets. For a trileaflet valve to successfully function the curvature of each leaflet must be reversed, in theory, $TPG_{max} \propto Et^3$, where TPG_{max} is the maximum transvalvular pressure gradient, E is the Young's Modulus (or flexural modulus), and t is the leaflet thickness.

As such the most relevant material property is the flexural modulus. Furthermore independent of leaflet thickness a load must be supported during diastole, $F_d \leq tW_{max}$, where W_{max} is the maximum strain energy density and σ_{max} is the equivalent maximum stress . Minimising the force required to open the valve, and substituting the thickness using stress constrains, yields the performance index:

$$PI = F_{open,min} = min\left(\frac{E_{flex}}{\sigma_{max}^3}\right) \tag{4.1}$$

Using the minimization of a PI constructed from the flexural modulus and the maximum strain energy density, allows us to select an optimal material from a given shortlist. The model is validated by the cyclic straining of thin, uncracked tensile bar samples where crack growth rapidly leads to sample failure. This theory suggests a way to estimate the size of natural occurring flaws in rubber, by using the initial flaw size as a curve fit parameter to obtain agreement between crack nucleation and crack growth experiments. The resulting flaw size is actually an effective flaw size, reflecting both the size and shape of flaws. The crack growth approach could be used as a total life approach, based on growth of pre-existing flaws to failure. Correlation between crack nucleation life obtained from simple tension specimen and crack growth life obtained from planar tension specimen was studied by Mars and Fatemi [8].

Using the CES Edupack material selection software (Granta Design, UK), the relation between the fatigue strength and modulus has been investigated across the complete space of polymeric materials. All the materials are plotted on log-log axes of Young's Modulus and Fatigue Strength

at 10^7 cycles, as shown in the graph in Figure 4.1 The line has a gradient of 1/3 and materials line upon that line have the equivalent Performance Index value. Materials on the top left of the graph have optimum PI.

Some of the materials are already listed in the graph in figure, in general different classes of materials refer to different colors. The green circles represent foam and they are authomatically excluded from the selection. To the red circles belong: thermoplastic elastomers such as TPV, TPU, TPO, POE and also SEBS (Styrene-Ethylene-Butylene-Styrene), SIS (Styrene-Isoprene-Styrene) and SBS (Styrene-Butadiene-Styrene).

The light blue class represents: EPDM, ECO, Silicone rubbers and Natural rubbers , both filled/reinforced and unfilled/unreinforced, Nitrile and Butyle rubber. Finally to the Blue class belong PE, PP,PTFE, EMA, PA66, but they are all too stiff to be used in a Prosthetic Heart Valve leaflet. In the end, it is possible to see that the best materials on the top left are Natural Rubber and different types of Thermoplastic Polyurethane.

From the investigation carried out for polymeric material, different elastomers have been choosen for further mechanical testing and determination of Performance Index. The selection in particular includes: Elasteon®, Latex, SEPS22, HG252 and SEEPS.

The first material has been chosen because is nowadays one of the most promising polymer for long-term implantation application.

Latex, which represents Natural Rubber, has been selected as the best elastomer according to the PI graph; a sample of this material was requested to an English Rubber Company, so the sheet of rubber was not manufactured during the experiment.

The last three polymers mentioned are all thermoplastic elastomer, in particular they are styrenic block-copolymer. SEPS22 has already been tested by Brubert et al. [2] in a material selection for the same application: the material looked promising, it was manufactured with compression molding technique, hence the internal structure was anisotropic. However random cracks nucleated during mechanical testing, this was related to stress concentrations accumulated in the compression molding process. In this work the idea was to try the same material manufactured with a solvent casting technique and investigate if this could improve the distribution of stresses inside the polymer sheet. The main drawback is that the polymer processed with solvent casting has a isotropic orientation of the internal structure, this could lead to a drop in mechanical properties.

All the materials tested were processed with a solvent casting technique for the reason mentioned above and also to have a better comparison among the polymers.

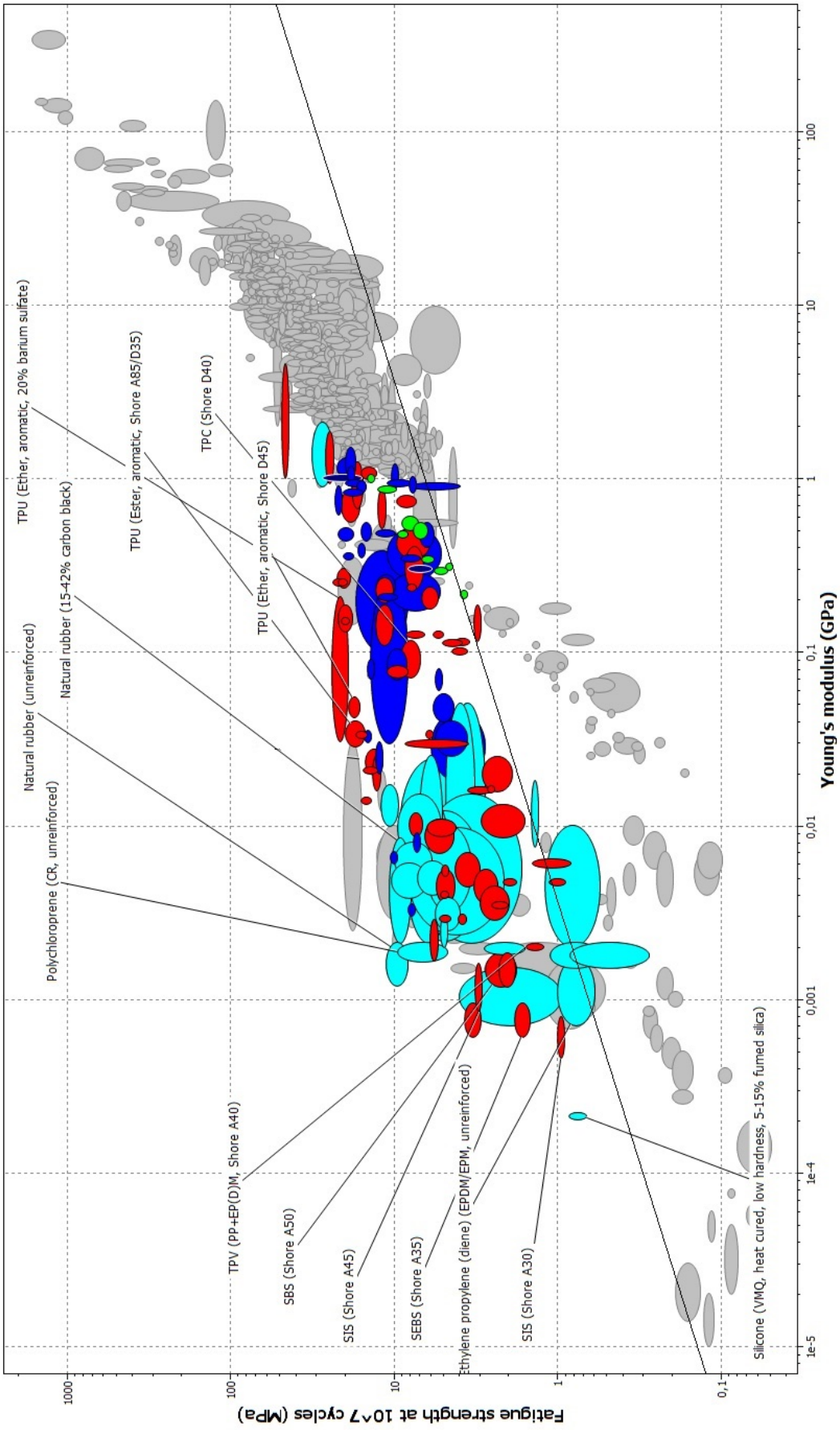

Figure 4.1: Material Selection Graph

The materials are described in the following paragraphs.

Elast-Eon ™ Elast-Eon™belongs to the advanced thermoplastic polyurethane class of materials. Thermoplastic polyurethane (TPU) is the material of choice for many biomedical applications due to the relative ease of its fabrication into devices, its flexibility, biocompatibility, biostability and electrical insulation properties.
The poly(dimethylsiloxane)(PDMS)/poly(hexamethylene oxide)(PHMO)-based TPU based on an optimized formulation from AorTech International Pty Ltd exhibits properties comparable to those of medical grade polyether-based TPU materials [29]. The introduction of nonpolar macrodiols such as polydimethylsiloxane into the polyurethane backbone has been demonstrated to be difficult, due to the difference in solubility with conventional urethane components (i.e., diisocynates, diol, and diamine chain extenders).

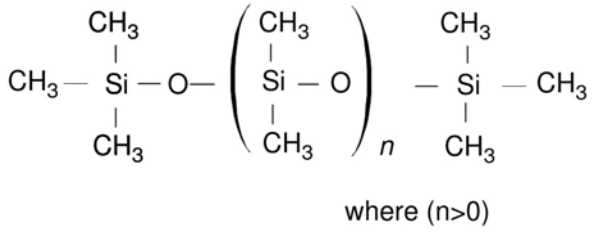

Figure 4.2: PDMS chimical structure

The first attempts in synthesizing PDMS-based polyurethanes resulted in materials with poor mechanical properties, attributed to the resulting low molecular weight and also to the absence of intersegment hydrogen bonding between PDMS and the hard segments. In order to overcome this, a second soft segment macrodiol can be added to interject an intermediate polarity chemical species between the hard and PDMS soft segments. Studies carried out on such segmented copolymers synthesized from amino-terminated PDMS and poly(tetramethylene oxide) (PTMO) reported a multiphase structure: the PDMS was found to microphase separate from both the PTMO and the hard segments [23][29][30]. These materials exhibit physical and mechanical performance equivalent to conventional polyurethanes and biological stability that surpasses rigid biostable polyurethanes. In fact, incorporation of a high level of siloxane segments into the back bone of polyurethanes significantly improves their biostability. These materials are also readily thermally processed using conventional equipment and technologies.

The FTIR analysis has given this result:

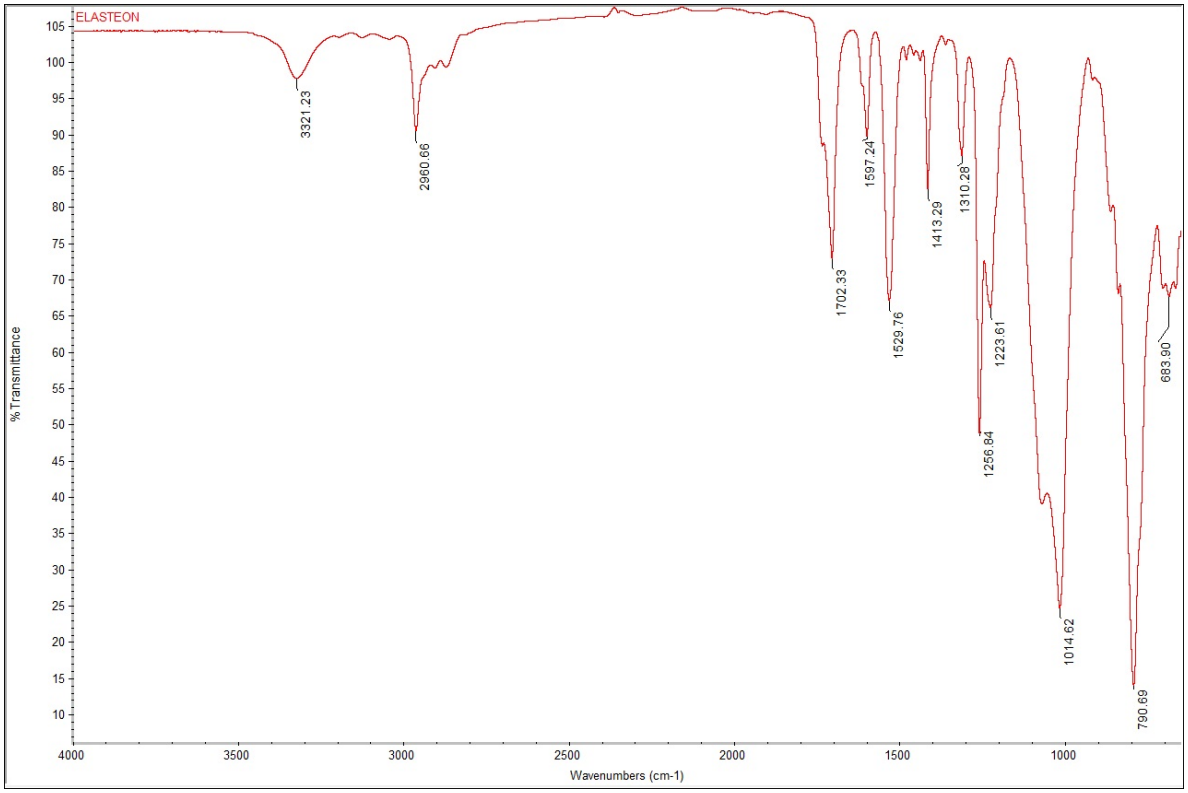

Figure 4.3: Spectrum of Elast-Eon™.

The Spectrum obtained for Elast-Eon™shows the typical peack of a polyurthane with the addition of the Silicon bound stretching. In the high-energy spectral range of CH2 and CH3 stretching modes ($3000 - 2800\ cm^{-1}$) there is a peack at 2960.66 cm^{-1}, while the peack at $3321.23cm^{-1}$ refers to the N-H stretch. The peaks at $1597cm^{-1}$ and $1529cm^{-1}$represents bending of N-H and streatching of C-N, while at $1702cm^{-1}$ the C=O stretching occurs. In the spectral range $1340 - 1250cm^{-1}$ the amine stretch takes place. Finally, in the low energy spectral range, Si-O-Si stretching and Si-C stretching peaks appear, respectively at 1014 cm^{-1} and $790cm^{-1}$. Elast-Eon™is now widely accepted as being the most biostable of all the TPUs, and as such is imminently suitable for long-term implantation. As it has been mentioned in Chapter 3, Elast-Eon™has been already tested for prosthetic heart valve application and it is one of the novel more promising material. In these circumstances it was quite important to test the material mechanically and identify a specific Performance Index.

SEPS 22 SEPS 22 (Polystyrene-b-poly(ethylene/propylene)-b-polystyrene) is a styrenic-based thermoplastic rubber from the SEPTON™series developed by Kurari Co.,Ltd.
It is a block copolymer that consists of a hard cylindrical styrenic segments (22%wt of styrene) and a soft domain. The sinergic combination of the different properties of the two domains are the leading aspect that draw the attention on this polymer.
This kind of material exhibit rubber-like properties since polystyrene blocks act as physical crosslink points below the glass transition temperature (Tg) while it flows and is processable over Tg. It has been shown that the deformation mechanism of block copolymers differs from those of homopolymers and strongly depends on the morphological pattern and microdomain orientation. High tensile strength, high elongation and rapid and almost complete recovery after elongation in addition to good biocompatibility make SEPS22 a promising material for cardiac grafts and prostheses. The molecular structure is represented in Figure 4.4 [51].

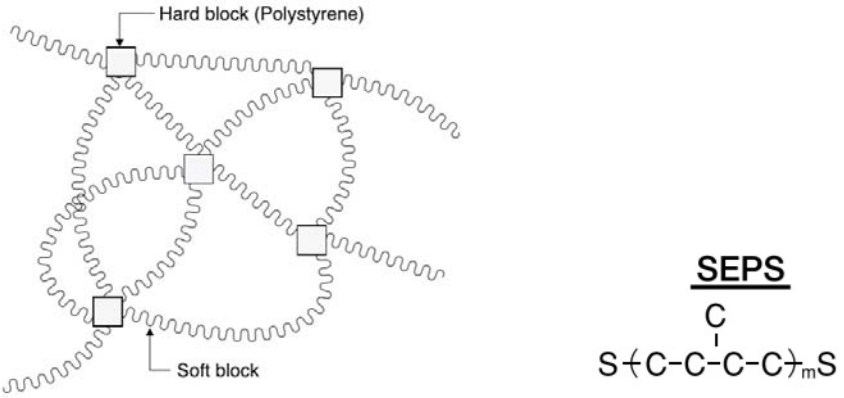

Figure 4.4: SEPS22 chimical and molecular structure

The FTIR analysis has given the result in Figure 4.5.The spectrum obtained for SEPS22 clearly reveals the presence of Styrene. Three distinct peacks are present in the spectrale range of CH2 and CH3 stretching modes ($3000 - 2800 cm^{-1}$). In the $1615 - 1550/1510 - 1450\ cm^{-1}$ range the peacks refer to aromatic ring stretching, while the rest of the peacks in the lower energy band ($1225 - 950/900 - 670\ cm^{-1}$) represent the in plane and out of plane C-H aromatic bending. The peack at $756\ cm^{-1}$ could also refers to the $-(CH2)_n-$ rocking.

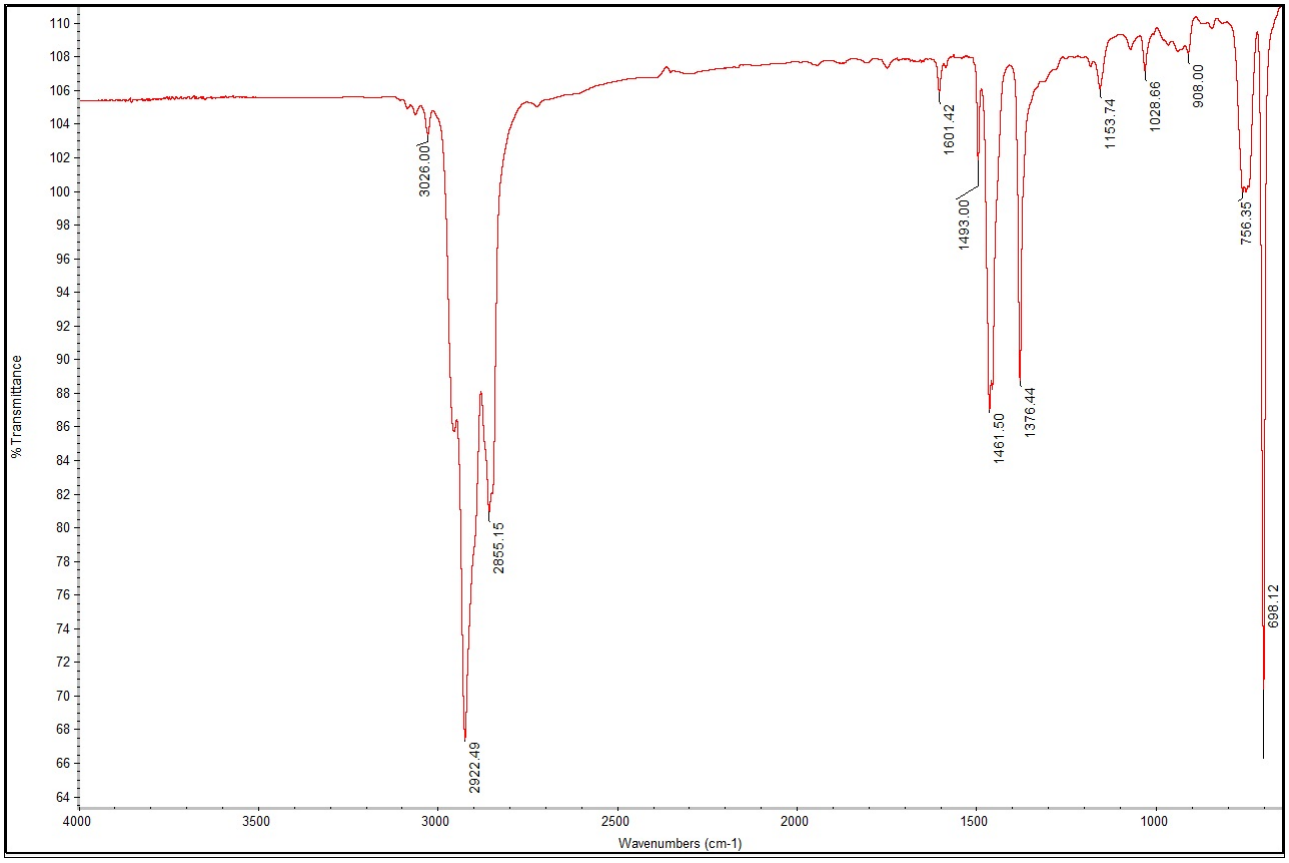

Figure 4.5: Spectrum of SEPS22.

HG252 This thermoplastic elastomer belongs to the SEPTON™series of styrenic block-copolymer. In specific HG252 is polystyrene-poly(isoprenebutadien)-polystyrene-hydroxy hydrogenated.
Its styrenic content is 28%wt so 6% more respect to SEPS22; hence, this polymer is expected to be stiffer and the objective is to see if and how much can this improve the mechanical performance and durability.
HG252 is in pellet form and it has the same general structure and properties of SEEPS. The FTIR analysis has given the result in Figure 4.6; the spectrum for HG252 has the same peacks distribution as SEPS22 and SEEPS so the consideration are identical.

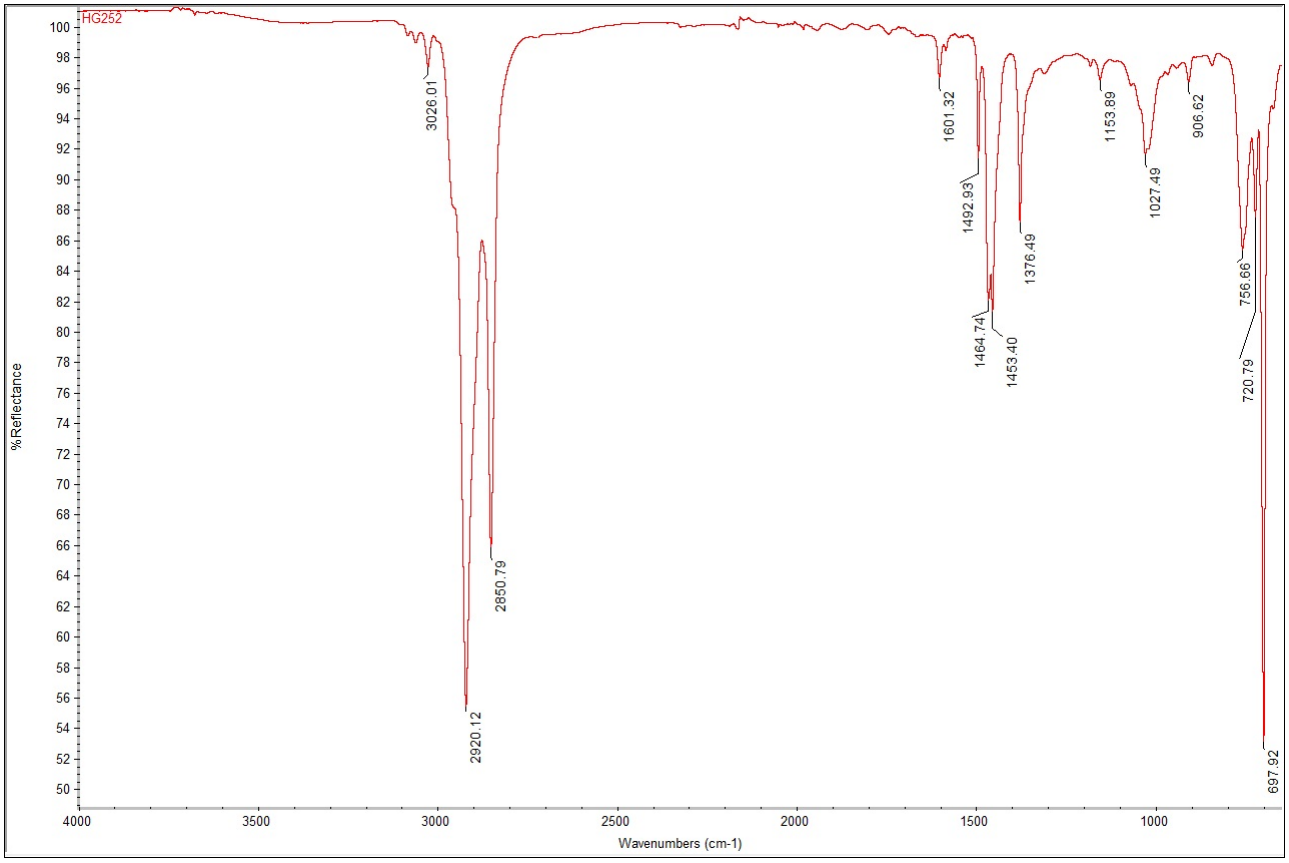

Figure 4.6: Spectrum of HG252.

SEEPS SEEPS (grade 4055) is Polystyrene-b-poly(ethylene-ethylene/propylene)-b-polystyrene and it belongs to the SEPTON™block-copolymer series. It has 30% wt styrene content and it is in powder form. Its chemical structure is described in Figure 4.7.

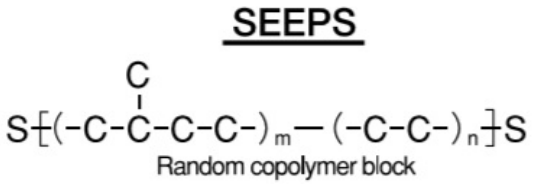

Figure 4.7: SEEPS 4055 chimical structure

The FTIR analysis has given the result in Figure 4.8; the SEEPS spectrum has the same features of the one obtained for SEPS22 and HG252.

This material was not tested, since it was not possible to manufacture a flat and uniform polymer sheet. The result of the experiment are explained in Annex A.

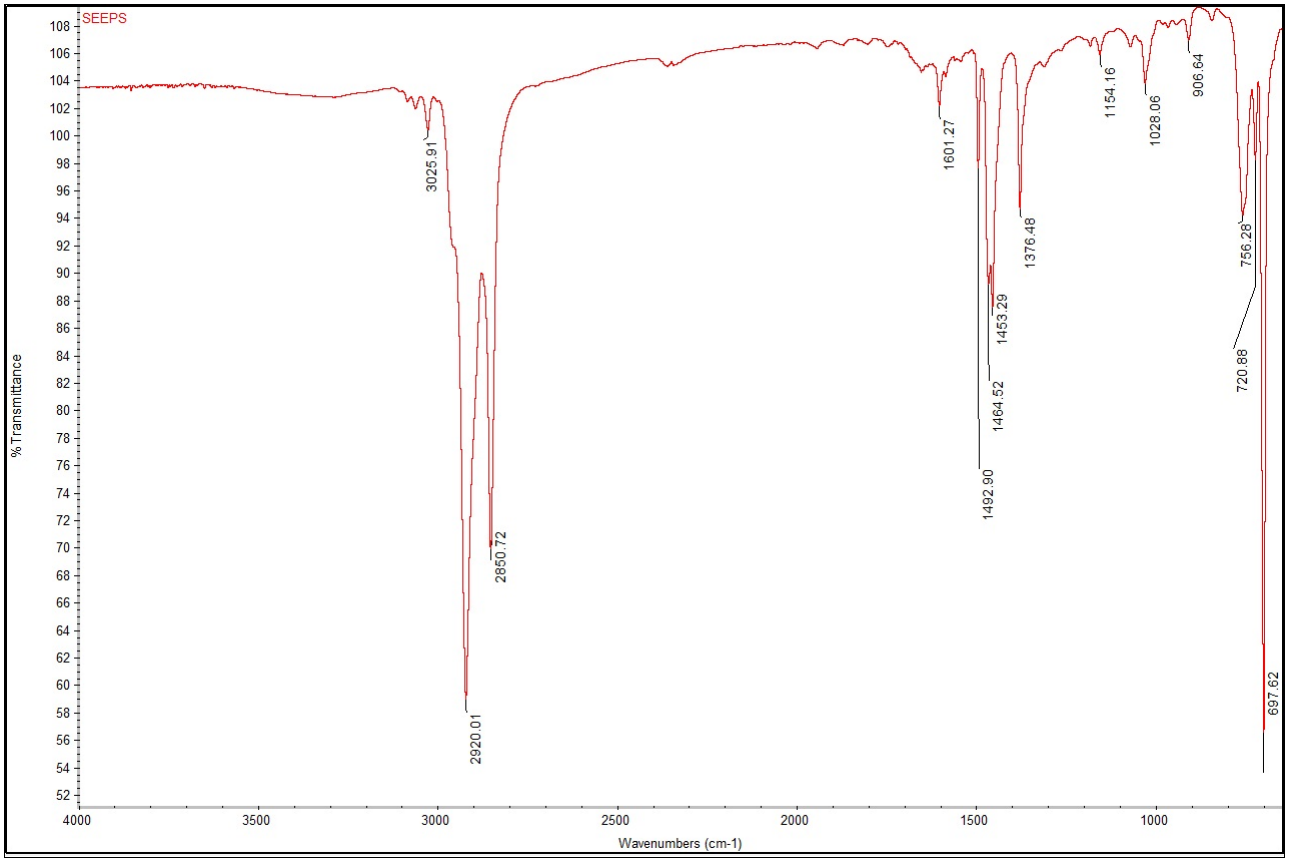

Figure 4.8: Spectrum of SEEPS.

Latex Latex rubber, or Isoprene (2-methyl-1,3-butadiene) is the purest form of rubber. It has a smooth finish on both sides, high tensile strength and elasticity. Latex rubber can be supplied in food compliant, anti-static and high temperature grades. It is commonly used for bakery release films, diaphragms, seals gaskets and vacuum blankets. Natural rubber is a milky fluid found in 10% of all flowering plants (angiosperms) [53]. It is a complex emulsion consisting of proteins, alkaloids, starches, sugars, oils, tannins, resins, and gums that coagulate on exposure to air. Synthetic latexes can be also made by polymerizing a monomer such as styrene that has been emulsified with surfactants. This rubber has been chosen for the material analysis because in the CES graph it occupies the best position respect to the PI, in fact it is the last one on the top left of the graph. For this reason further durability test resulted to be appropriate for the investigation on material selection for PHV application. The Latex sheet tested was a sample received from an English Rubber Company, the sample was added with carbon black and the specific vulcanization grade was unknown. The FTIR analysis produced the result in Figure 4.9.

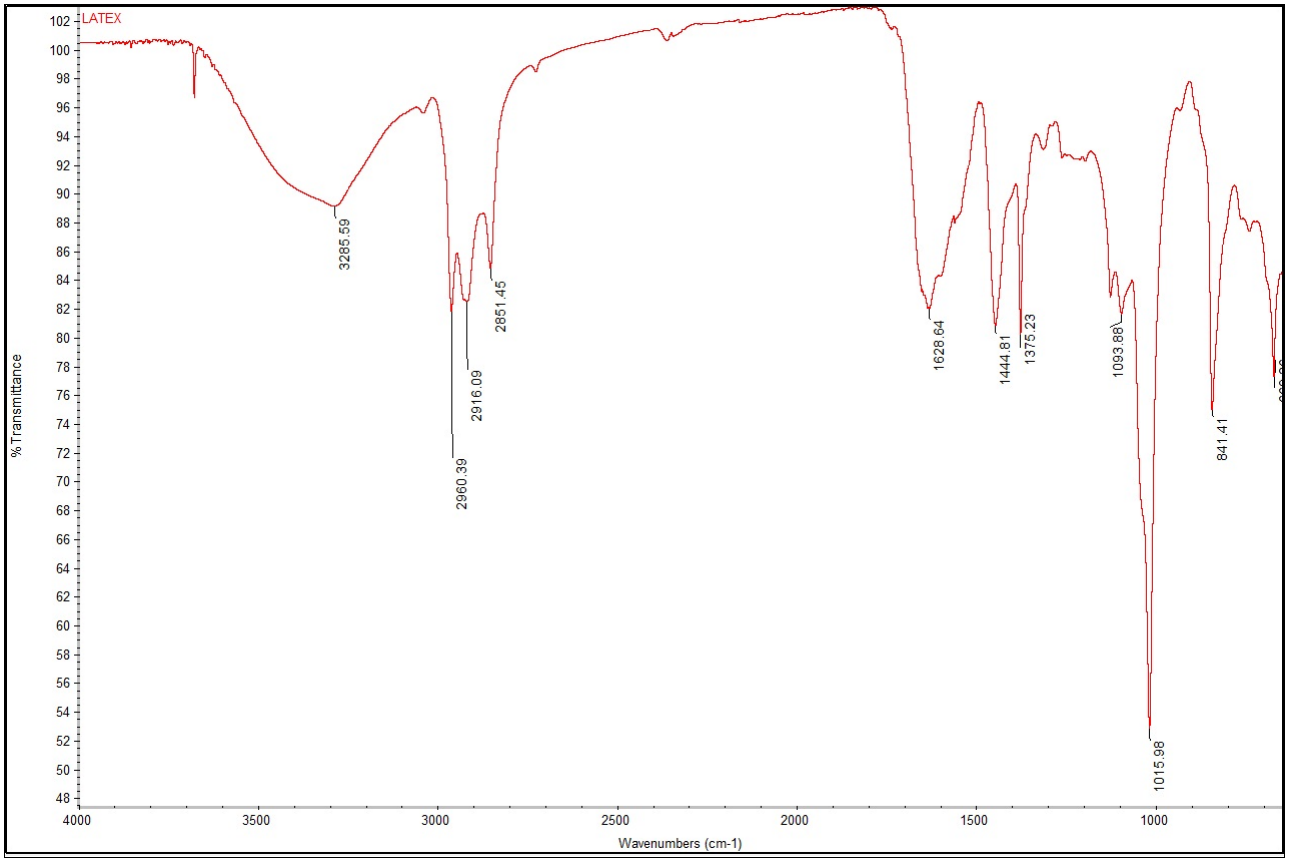

Figure 4.9: Spectrum of Latex.

At $3285cm^{-1}$ it is the O-H stretching, which represent the presence of Carbon Black filler inside the polymer. The three peacks in the spectral range of $3000 - 2800cm^{-1}$) refer to CH3 and CH2 stretching. The peack at $1628cm^{-1}$ can represent C=C stretching. At $1093cm^{-1}$ there is the peack for C-CH2 stretching and at $1015cm^{-1}$ for CH3 rocking, in the end the lower energy peack represents C-H vibration.

The presence of carbon black and the vulcanization grade are two relevant aspects for what concern the mechanical properties of the material, in fact:

1. The addition of carbon black to rubber compound could strengthen the material against fatigue failure and drastically change its mechanical properties. Filled rubbers show more dissipative mechanical responses at both high strains because of network chain breakage and strain crystallization, and at small or moderate strains under alternating loading. Kim and Jeong [8] investigated natural rubber compound with three different filler types to examine the effect of carbon black on fatigue life. They concluded that for larger carbon black agglomerates, separation of fillers from rubber matrix could relatively easily occur resulting in shorter fatigue life, compared to smaller size fillers.

2. Vulcanization is used in thermosetting elastomers to create covalent bonds or crosslinks between adjacent polymer chains. Crosslink density determines the physical properties of rubber, with higher crosslink density resulting in increased stiffness and reduced hysteresis. Compound stiffness has a direct effect on energy release rate, Santangelo and Roland [8] verified that double network of natural rubber (NR) has a higher modulus than single network of equal crosslink density. Fatigue life of double networks NR was also found to be as much as a factor of 10 higher than conventionally crosslinked NR, although tensile strength was slightly lower.

Even though it was not possible to vary and optimise those properties, the Latex sheet was tested in order to have a first result to compare with the other materials PI.

Chapter 5

Fatigue Life Prediction

Rubber's ability to withstand very large strain without permanent deformation of fracture make it ideal for PHV application. This application imposes time-varying strains over a long time, as a result long-term durability is a critical issue. Elastomers are highly nonlinear elastic materials with large deformations. Therefore, linear elastic and small strain assumptions typically used for metals do not apply to elastomers. Continuum mechanics parameters, such as deformation ratio and stretch ratio, better represent the rubber mechanics.

Rubber component subjected to fluctuating loads often fail due to the nucleation and growth of defects or cracks. Material deformation and fatigue characterization including both crack nucleation and crack growth are typically required for failure analysis and prediction of fatigue life. Strain energy release rate is the most appropriate way to describe the energy absorbed by a material which may be used to generate a new surface, and is used for crack growth predictions. Fatigue failure is a typical service failure mode resulting from alternating and repeated loads over a period of time. In particular it is divided into two distinct phases: the first one is the crack nucleation phase during which crack nucleates in regions that were initially free of observable crack; the second one is the crack growth phase when the nucleated cracks grow to the point of failure. These two phases identify maximum principal strain (or stretch) and strain energy density as two broadly used damage quantification parameters.

In rubber the potential energy released from surrounding material is spent on both reversible and irreversible changes to create the new surfaces. In any case, the energy release rate is simply the change in the stored mechanical energy dU, per unit change in crack surface area dA. In the rubber literature this quantity is often called the tearing energy T.

$$T = -\frac{dU}{dA} \tag{5.1}$$

In case of cyclic loading, it was found that the maximum energy release rate achieved during a cycle determined the crack growth rate, for R=0 cycles. Where R is the loading ratio.
Rivlin and Thomas [55] showed that static crack growth occurs above a critical value of the energy release rate, independent of the type of test specimen they used, suggesting that the critical energy release rate may be considered a true material property.
The planar tension specimen, shown in Figure 6.1, is quite practical for use in fatigue crack growth characterization of elastomers. Its geometry is short and wide such that lateral contraction is prevented by grips, while an axial strain is introduced in the direction of the short dimension. In the single edge cut, planar tension specimen, the energy release rate T has an especially simple form, provided that the cut is sufficiently deep and that the growth of the cut results only in translation of the crack tip fields. The expression depend only on the strain energy density W remote from crack and from specimen edges, and specimen height h. In particular the strain energy density (W) is the area under the loading stress–strain curve for a stable cycle for each peak strain level.

$$T = Wh \tag{5.2}$$

Note that, in displacement control, the energy release rate for this specimen is independent of the crack size.
In single edge cut, simple tensions specimen, the energy release rate T depends on the gauge section strain energy density W, the size of the crack a, and a strain dependent parameter k.

$$T = 2kWa \tag{5.3}$$

The parameter k is strain dependent , a practical approximation of the data is given in terms of the engineering strain ϵ by:

$$k = \frac{2.95 - 0.08\epsilon}{(1+\epsilon)^{\frac{1}{2}}} \tag{5.4}$$

Lake and Lindley [56] identified four distinct regimes of fatigue crack growth behaviour, based on the maximum energy release rate per cycle, T, per R=0 cycles in rubber. They are represented in Fig.5.1. So long as the peak energy release rate T remains below a threshold, denoted as To, crack growth rate da/dN below To is independent of the mechanical loading, and is denoted Regime 1.

$$\frac{da}{dN} = r \qquad T < T_0 \tag{5.5}$$

Regime 2 is denoted between a range of To and Tt (where t means transition), over which there is a transition. The transition is described by the following relationship, in which A is a material

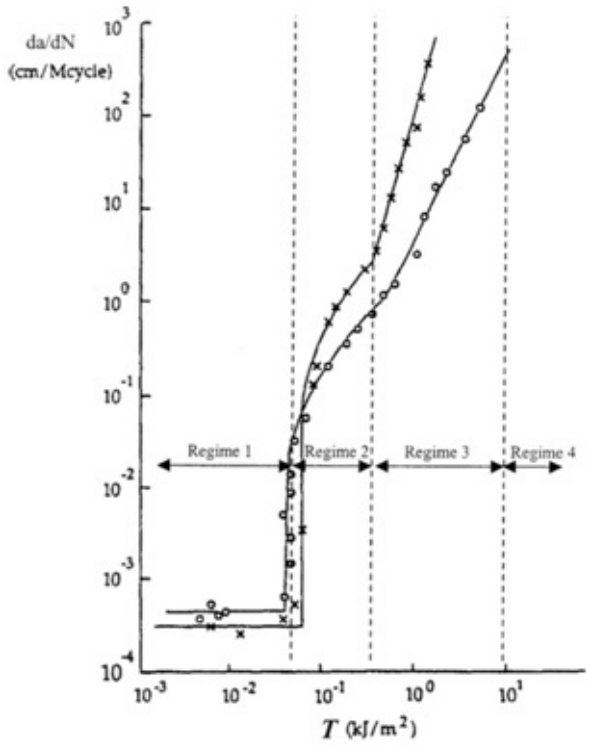

Figure 5.1: Regimes of crack growth behaviour.

property.

$$\frac{da}{dN} = A(T - T_0) \qquad T_0 \leq T \leq T_t \tag{5.6}$$

After the transition, there is a range between Tt and Tc (Critical Tearing energy), over which the relationship between the fatigue crack growth rate and the energy release rate obeys a power-law. This is denoted Regime 3.

$$\frac{da}{dN} = BT^F \qquad T_t \leq T \leq T_c \tag{5.7}$$

where B and F are the fatigue power-law coefficient and exponent for R =0 condition, respectively.

Finally, beyond Tc, unstable crack growth ensues. In this regime, the crack growth rate is essentially infinite. This is denoted Regime 4.

$$\frac{da}{dN} = \infty \qquad T = T_c \tag{5.8}$$

Fatigue life is ultimately determined by a pre-existing flaw that is the first to grow to a critical size. The life is obtained by integrating the growth rate of the fastest growing flaw, from its initial size to its critical or final size. For the purposes of integration, it is assumed that the flaw

growth is planar and self-similar. A practical shortcut assumes power-law behaviour over the entire life of the flaw. This results in a closed-form relationship between the fatigue life and the fatigue crack growth properties.

Combining equations 5.2 and 5.7 the following relationship is obtained :

$$\frac{da}{dN} = f[T(a,W)] = BT^F = B(2kWa)^F \tag{5.9}$$

Then integrating:

$$N_f = \int_0^{N_f} dN = \int_{a_0}^{a_f} \frac{1}{f[T(a,W)]} da = \int_{a_0}^{a_f} \frac{1}{B(2kW)^F} a^{-F} da \tag{5.10}$$

$$N_f = \frac{1}{F-1} \frac{1}{B(2kW)^F} \left[\frac{1}{a_0^{F-1}} - \frac{1}{a_f^{F-1}} \right] \tag{5.11}$$

From this equation we see that if the initial flaw size a_0 is much smaller than the critical size, a_f, then the life becomes independent of the critical flaw size.

$$N_f = \frac{1}{F-1} \frac{1}{B(2kW)^F} \left[\frac{1}{a_0^{F-1}} \right] \tag{5.12}$$

Integrating expression 5.9 also Wmax ,which is the maximum permitted strain energy density to avoid failure, can be obtained:

$$W_{max} = \left[\frac{1}{F-1} \frac{1}{BN_f} \left(\frac{1}{a_0^{F-1}} - \frac{1}{a_f^{F-1}} \right) \right]^{\frac{1}{F}} \frac{1}{2k} \tag{5.13}$$

The maximum strain energy density is then calculated considering $N_f = 10^9$, $c_0 = 0.02\ mm$, $c_f = 0.3\ mm$ (native leaflet thichness) and $k = 2$.

Effective flaw sizes in the range of 0.02–0.06 mm were observed in a study by Lake and Lindley [56], which covered different polymer types, and various fillers, curatives and other compounding variables. In order to compare the relationship between crack initiation and crack growth approaches, Eq 5.12 was used to obtain fatigue life based on the crack growth approach and to compare with the fatigue life based on the crack initiation approach.

By assuming $c_0 = 0.02\ mm$, utilizing $B = 4 * 10^5$ and $F = 2$ as crack growth rate coefficient and exponent, respectively, in Eq 5.12, and by assuming $k = 2$ (in the stretch range studied), relatively good agreement (i.e., about a factor of two in fatigue life) between the $R = 0$ crack initiation life and crack growth life is obtained, as shown in Figure 5.2

Therefore, the crack growth approach could be used as a total life approach, based on growth of preexisting flaws to failure. Correlation between crack nucleation life obtained from simple tension specimen and crack growth life obtained from planar tension specimen was studied by

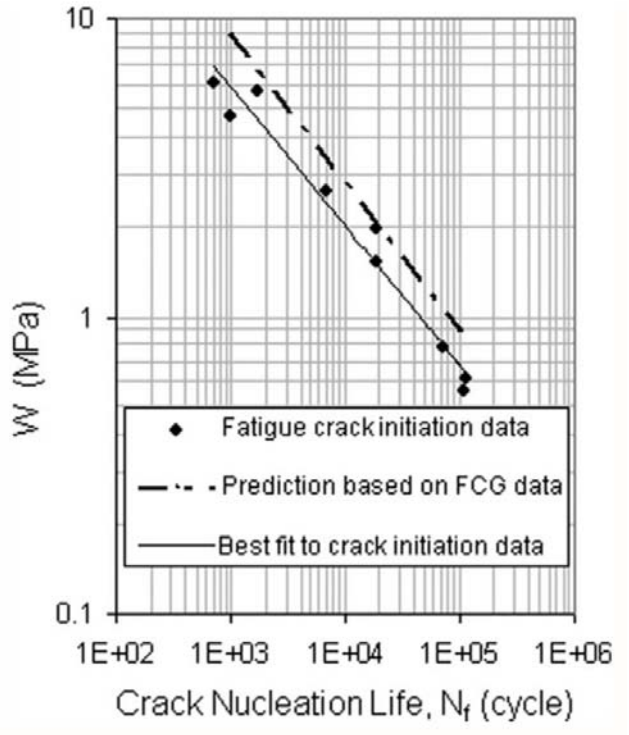

Figure 5.2: Comparison of fatigue lives obtained from crack initiation and crack growth approaches.

Mars and Fatemi [7] and they also found good agreement between the results. It should be mentioned that a change of initial assumed crack length from 0.02 mm to 0.04 mm resulted in very small change in the obtained results.

In conclusion it is possible to state that a key ingredient of fatigue analysis and life prediction of elastomeric components is relevant to material properties. These properties include deformation behavior under different stress states, crack initiation life, and crack growth rate properties. Specific experimental procedures and data analysis techniques will be presented and discussed in the next chapter to obtain each of these material characterizations.

Chapter 6

Experimental Procedure

Two simple specimen geometries can be used for deformation and fatigue behavior characterizations of elastomers: simple tension and planar tension specimens. In the simple tension specimen a uniaxial state of stress with a multiaxial stretch state is present, while the planar tension specimen is under plane stress condition with longitudinal and transverse stresses.
The two types of specimen are illustrated in Figure 6.1.

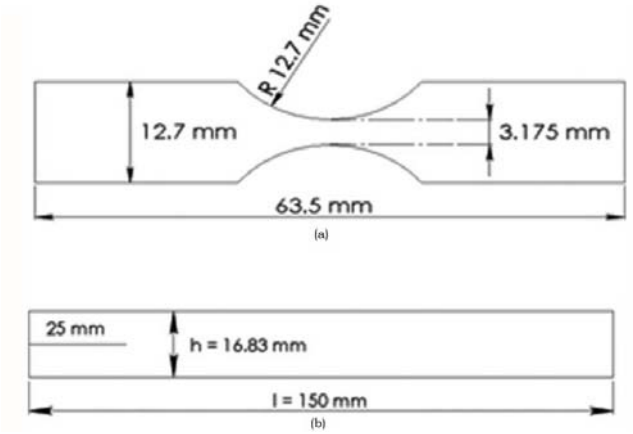

Figure 6.1: Simple tension and Planar Tension Specimen.

As monotonic and cyclic deformation behaviors can be vastly different, it is important to obtain and use cyclic deformation properties in fatigue life analysis and applications. Cyclic incremental tests on simple tension and/or planar tension specimen can be performed to obtain the stabilized cyclic stress–strain curve.
The different tests were performed using a Stable Microsystems Texture Analyser shown in Figure 6.2. The polymeric samples were fixed between the two clamps and the TA was programmed

by a computer. With this instrument it has been possible to performe cyclic test at different strain rate. The machine has been programmed in displacement control: the bottom clamp was fixed on the base of the instrument and the upper clamp was moving according to the instruction given by the computer.

Figure 6.2: TA instrument.

All the experiments have been conduceted at 37°C in order to better represent the condition inside human body. The instrument, in fact, has been positioned inside a heated cupboard.
In the next sections the different experiment procedures and the preparation of the sample sheet are described.

6.1 Preparation of the samples

The samples used for the different tests were all cut from a sheet of solvent cast polymer for what concern Elast-Eon™, SEPS22 and HG252, while Latex was simply cut from the company sample received. The dogbone specimen (fig 6.1) were cut with the specific die. The solvent casting were conducted with different solvents: Elast-Eon™was dissolved in Tetrahydrofuran, SEPS22 and HG252 in Toluene. In order to reach the optimal solution composition 10%w/v of polymer was added to the solvent. The solution then was stirred on a magnetic plate and the beker was covered,otherwise the solvent would have evaporated too quickly.

When the polymer was completely dissolved the solution was carefully pured into a flat tray to let the solvent evaporate. After several hours the solvent was evaporated and it was possible to remove the polymer sheet from the tray.
With this techinque, the most difficult features to obtain in the polymer sheet was uniform thickness . In fact, in order to predict a desired thickeness the factors to be considered were: the area of the tray, the quantity of the solution, a flat surface to position the tray and the rate of evaporation related to the condition inside the fume cupboard. Even if the first two factors were easy to control, the latter two were more unpredictable.
Taking this factor into account, the samples were cutted in order to have the most uniform thickness.

6.2 Planar Mechanical Test

Cyclic deformation curves properties are typically needed for stress–strain relations for fatigue analysis. Extension ratio or stretch ratio (λ) is commonly used for finite strain analysis and is defined as the ratio of the extended length (L) to the original length (L_0):

$$\lambda = \frac{L}{L_0} \tag{6.1}$$

The relationship between engineering strain (ε) and stretch ratio is given by:

$$\lambda = \varepsilon + 1 \tag{6.2}$$

As the rubber is an incompressible material, there is no change in volume under deformation ($\Delta V = 0$). This results in the determination of the deformation gradient to be one, which in turn results in the following relation for principal stretch ratio:

$$\lambda_1 \lambda_2 \lambda_3 = 1 \tag{6.3}$$

The stress states of simple tension and planar tension are often used to characterize the deformation behaviour; in these experiments only the planar tension specimen has been used. From a planar deformation test it will be possible to obtain the stress-strain relation and the Strain Energy Density equation.
For planar tension deformation and crack growth tests, a wide rectangular of average 0.4mm thickness with dimensions shown in Figure 6.1 is used. For crack growth specimen, a precrack is cut at midlength, but for cyclic deformation test no precrack is cut.

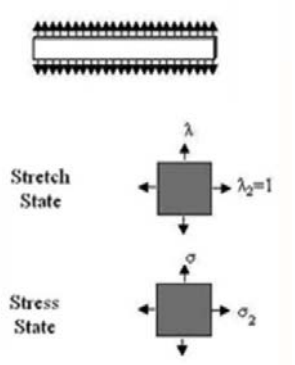

Figure 6.3: Planar tension specimens with the corresponding stretch and stress states.

Figure 6.3 shows the stretch and stress states for the planar tension specimen condition under uniaxial loading. Planar tension specimen is under plane stress condition with longitudinal and transverse stresses. The stretch in the width dimension is 1, indicating there is no strain in this direction. A stretch of λ in loading direction and λ^{-1} exist in the out of plane direction. It should also be mentioned that due to the incompressibility condition, Poisson's ratio is 0.5 and the initial modulus of elasticity (E) is approximately equal to three times the shear modulus (G), $E = 3G$.

A cyclic incremental test on planar tension specimen in displacement control with the sinusoidal waveform was performed to obtain the cyclic stress–strain curve. For each material at least three different samples were tested and they were cut from different batch of polymer solution. Because of the load history dependence associated with the Mullin's effect, peak stress (or strain) should be a key consideration in fatigue analysis of elastomers, in addition to the stress (or strain) amplitude and the mean stress. The initial softening phenomenon, also called the prestretch or preconditioning effect, is widely referred to as the Mullin's effect. Subsequent loadings of equal or lesser magnitude rapidly tend towards a steady state, nonlinear elastic response. This effect is considered to be a consequence of the breakage of links inside the material and both filler-matrix and chain interaction links are involved in the phenomenon. The Mullins effect is transient and is exhibited primarily by filled rubbers.

Because of this initial effect, stabilized cycle data is used for each strain level (i.e., after about 20 applied cycles) and all tests are performed in ascending order of displacement amplitude. The applied displacement was then converted into gauge section strain and the measured load from the load cell,was used for stress calculation. One test consisted in six different strain levels, from 10% to 100% deformation, performed in ascending order with the same number of cycle for each strain level.

Hyperelastic constitutive models are used to represent the nonlinear elastic deformation curve. The resulting stress-strain relation is obtained as :

$$\sigma = a\varepsilon^2 + b\varepsilon + c \tag{6.4}$$

Where parameters a,b,c are calculated using a least squared fit polynomial considering one strain level for each test. Figure 6.4 shows an example of curve fitting.

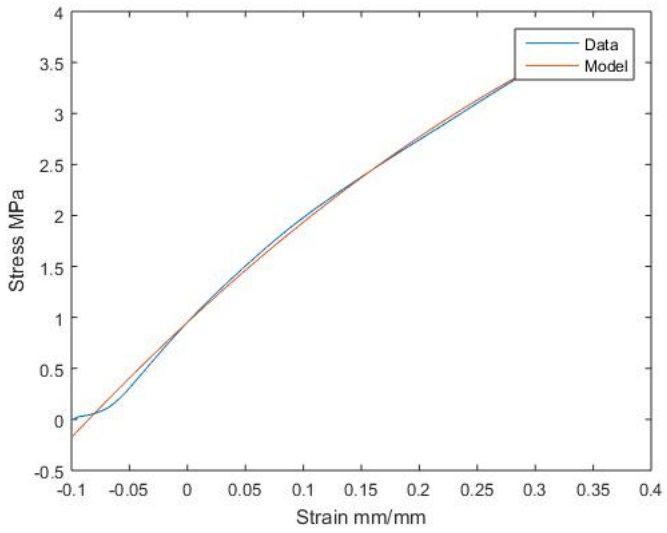

Figure 6.4: Stress-strain relation fitting

For what concern the Strain Energy Density equation, the polynomial fitting was performed considering all the strain levels. The strain energy density is the area under the loading stress–strain curve for a stable cycle for each peak strain level. In fact the data obtained for each strain level are the maximum stress and the maximum SED, all the point collected are fitted with a polynomial relation:

$$SED = a_1\varepsilon^2 + b_1\varepsilon + c_1 \tag{6.5}$$

For every material at least three tests were performed with 1Hz testing frequency and the final values were taken as the mean value of all tests.
The SED-strain relation is also used to calculate the maximum strain energy density for the crack growth model.

6.3 Crack Nucleation Test

Cracks often nucleate from pre-existing flaws in the compound (i.e., such as undispersed carbon black agglomerates), due to processing defects (such as contaminations, voids, and molding flaws), or at stress concentrations. In the context of mechanical design and fatigue analysis, crack initiation life is referred to the life involved in growing a crack from the pre-existing flaw to a small macro-crack typically on the order of 1mm. Strain is commonly used for crack initiation life analysis as an ideal fatigue damage quantification parameter, due to ease of determining displacements in elastomers.

The specimen geometry used in crack initiation tests is the geometry shown in Figure 6.1. This type of specimen is designed in such a way that when a crack grows to a length on the order of 1 mm, there would be little remaining life to fracture. Therefore, these tests characterize fatigue life for a crack on the order of 1 mm, although the criterion for defining fatigue nucleation life in the test is the number of cycles in which the specimen breacks completely according to ASTM standard D 4482 [58].

Multiple specimens can be used for each test, as shown in Figure 6.5. Tests were performed in displacement control and different levels of maximum strain were chosen for testing. The objective of the experiment, in fact, was to lead the sample to rupture. Since each material behaves differently while stressed, different strain levels and number of cycle were chosen for each test. The testing frequency used for all conditions was 1 Hz, except those with higher peak strain values for which testing frequencies of 0.5 Hz was utilized.

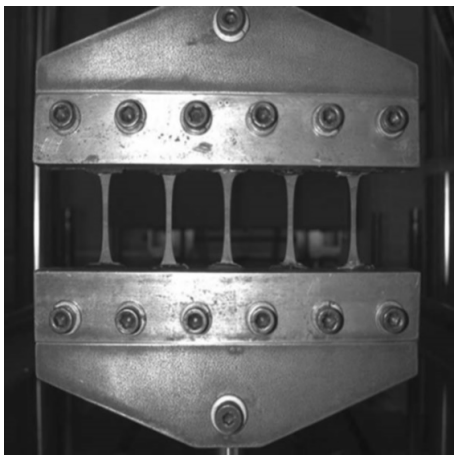

Figure 6.5: Crack Nucleation test set up.

It is importan to verify if there is a good agreement between the results obtained from the crack nucleation test and the crack growth test, as shown in Figure 5.2.

6.4 Crack Growth Test

Energy release rate is often used as the crack driving parameter in characterizing elastomers fatigue crack growth behavior. This parameter relates the global specimen loading to the local stress and strain fields at the crack tip, and is also applicable to finite strain materials, such as elastomers. A precracked planar tension specimen (Fig 6.1) is typically used for fatigue crack growth tests since energy release rate is independent of crack length for this specimen geometry. Therefore, a single specimen can produce results for multiple crack growth tests with different loading conditions. Because of a simple relationship between energy release rate and strain energy density and the fact that energy release rate is independent of crack length in planar tension specimen, this specimen is an ideal choice for fatigue crack growth experiments. In the planar tension specimen energy release rate depends only on the strain energy density remote from the crack and specimen edges, and the specimen height as described in relation 5.2
Stress–strain hysteresis loops from an uncracked test specimen can be used to obtain the test signal parameters for the fatigue crack growth rate.
Numerical integration methods can be used to calculate the area under the stress–strain curve from the experimental data. For a constant displacement or strain, strain energy density is constant and so the crack growth rate would be constant with repeated cycles of the same amplitude.
Control parameters for crack growth test with planar tension specimen are the amplitude and mean values of the applied displacement.
For the cracked specimen 110% of maximum strain was used as preconditioning load for 500 cycles at each strain level used to minimize the transient deformation response as well as to produce a natural crack tip. All the tests have been performed at 1 Hz frequency.
A single test specimen can produce results for multiple crack growth tests as long as the crack length and remaining specimen length are sufficiently longer than the specimen height. Because of the transient softening, however, it is necessary to conduct tests on the same specimen in ascending order of maximum strain level to make sure that the higher levels of load would not affect the lower load level test results. If the crack grew irregularly or at an inclined angle, recutting was performed by a razor blade, followed by some initial cycles to initiate a natural crack tip.
For each materials different strain levels and cycles were used in the experiments, in fact the decision depended on the material behaviour: the general guideline was to apply a number of

cycles able to produce a signigicant crack growth, so for lower stresses a higher number of cycle was applied. Tests were performed at different strain levels for each specimen and a camera was used to measure the growth of the crack tip along the crack line.
Figure 6.5 shows an example of a crack picture taken by the camera.

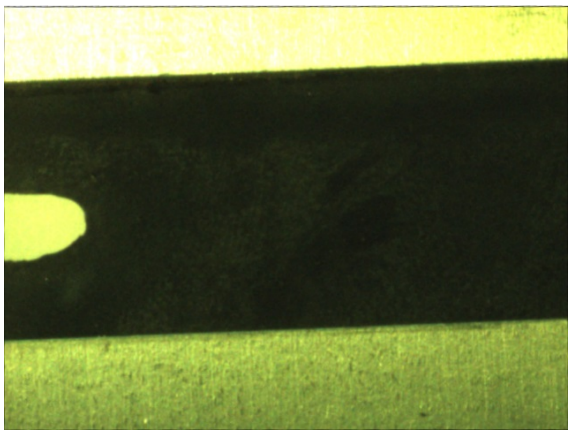

Figure 6.6: Crack growing in the specimen.

Fatigue crack growth rate (da/dN) is obtained by fitting a linear relationship to the crack length versus cycles data and determining the slope of the linear fit. The test conditions used for the constant amplitude fatigue crack growth experiments produces crack growth rates in the region of crack growth that can be characterized by a power-law relation. The crack growth approach could be used as a total life approach, based on growth of pre-existing flaws to failure.

6.5 Tris Buffered Solution Bath

Planar Mechanical test and Crack Growth test have aslo been performed in a Tris Buffered Solution bath. Those experiments have the objective of better represent the enviromental conditions of the polymer manufactured in a PHV. The bath was built aroun the Texture Analyzer instrument as shown in Figure 6.7.

Figure 6.7: Texture Analyzer with solution bath.

The Bath was kept at 37°C and the tests procedure were exactely the same as the experiments performed in air.

The Tris Buffered solution was prepared with distilled water, Tris-base and Hydrocloric Acid. The ammount of each ingredient was measured in order to reach the following properties: Molarity 0.1 M, 7.2 pH.

Chapter 7

Results and Discussion

The results from the Planar Mechanical test, the Crack Growth Test, the Crack Nucleation test and the resulting Performance Index for each material will be discussed in this Chapter.
The Stress-Strain relationship, the SED equation and the graph showing the growth rate of a sharp crack, with a natural tip,as a function of the energy release rate in a planar sample are presented for all the polymer tested.
A power law model is fitted to each crack growth-energy relation, whose parameters B and F are listed in Table 7.13.

$$\frac{da}{dN} = BT^F \tag{7.1}$$

The maximum permitted strain energy density to avoid failure, W_{max}, is then calculated, with $N_f = 10^9$,$c_0 = 0.02\ mm$, $c_f = 0.3\ mm$ (native leaflet thickness), and $k = 2.141$. Given W_{max} and E_{flex}, the PI for each material is calculated as follows:

$$PI = F_{open,min} = min\left(\frac{E_{flex}}{\sigma_{max}^3}\right) \tag{7.2}$$

Where σ_{max}, the maximum equivalent stress, is calculated trough the SED equation and the Stress-Strain relation.
The most important result is the comparison among all the materials tested: using the minimization of a PI constructed from E_{flex} and W_{max} allows us to select an optimal material from a given shortlist; in particular a lower PI indicates a material more suited to use in a Prosthetic Heart Valve leaflet.

7.1 Elast-Eon™

The parameters of the two relations for Stress-Strain and Strain Energy Density are listed in Table 7.1 and 7.2.

Stress-Strain Parameter			Young's Modulus	
a	**b**	**c**	**E (MPa)**	**20% secant**
-7.9223	8.2277	0.5488	8.2277	9.3869

Table 7.1: Stress-Strain parameters and Young Modulus for Elast-Eon™

SED Parameters		
a1	**b1**	**c1**
3.676	0.7828	-0.0575

Table 7.2: SED parameters for Elast-Eon™

The results obtained describe the material as slightly stiffer than a natural rubber or a SBR rubber ($E = 1 - 5\ MPa$).

The graph in Figure 7.1 represents the crack growth rate as a function of the energy release rate.

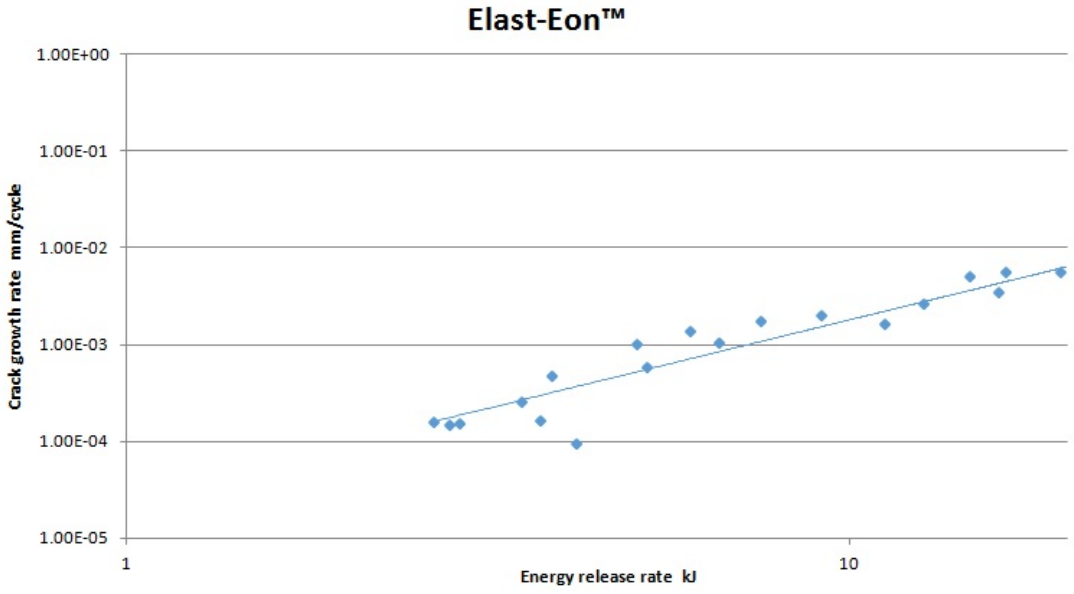

Figure 7.1: Crack growth rate versus Energy release rate for Elast-Eon™.

7.2 SEPS22

The parameters of the two relations for Stress-Strain and Strain Energy Density are listed in Table 7.3 and 7.4.

Stress-Strain Parameter			Young's Modulus	
a	**b**	**c**	**E (MPa)**	**20% secant**
-3.7346	4.1215	0.1707	4.1215	4.2282

Table 7.3: Stress-Strain parameters and Young Modulus for SEPS22.

SED Parameters		
a1	**b1**	**c1**
0.3564	0.8543	-0.0572

Table 7.4: SED parameters for SEPS22.

The Young's Modulus for SEPS22 is half the value obtained for Elast-Eon™, this means that the former polymer is softer.

The graph in Figure 7.2 represents the crack growth rate as a function of the energy release rate.

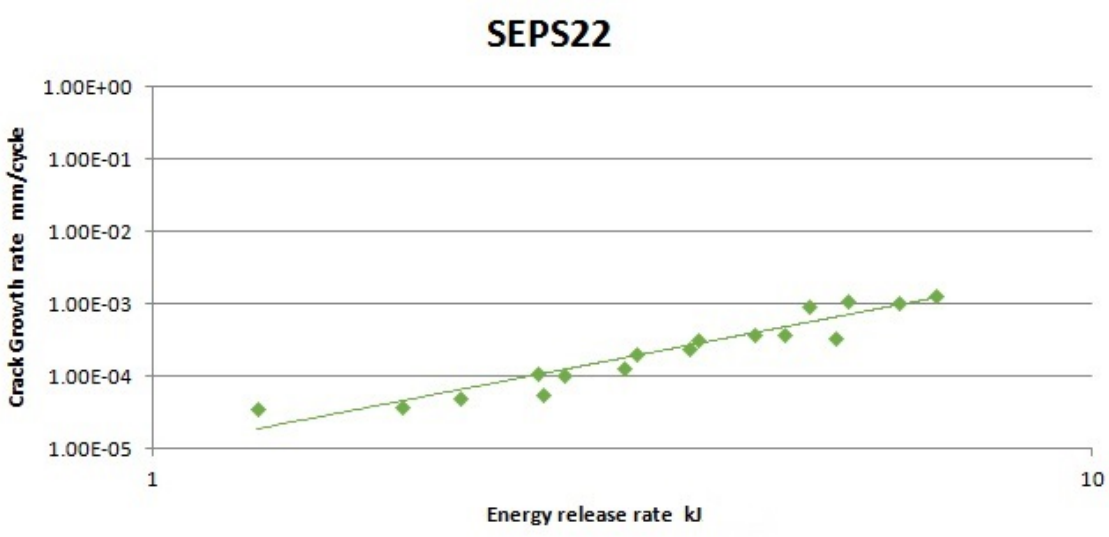

Figure 7.2: Crack growth rate versus Energy release rate for SEPS22.

7.3 Latex

The parameters calculated from the polynomial fitting for the Stress-Strain and SED relations are listed in Table 7.5 and 7.6 .

Stress-Strain Parameter			**Young's Modulus**	
a	**b**	**c**	**E (MPa)**	**20% secant**
-0.8748	1.4546	0.0256	1.4546	1.4076

Table 7.5: Stress-Strain parameters and Young Modulus for Latex.

SED Parameters		
a1	**b1**	**c1**
0.4061	0.123	-0.0056

Table 7.6: SED parameters for Latex

Latex is the softer material tested, in fact its Young's Modulus is ~ 1.5 MPa.
The graph in Figure 7.3 represents the crack growth rate as a function of the energy release rate.

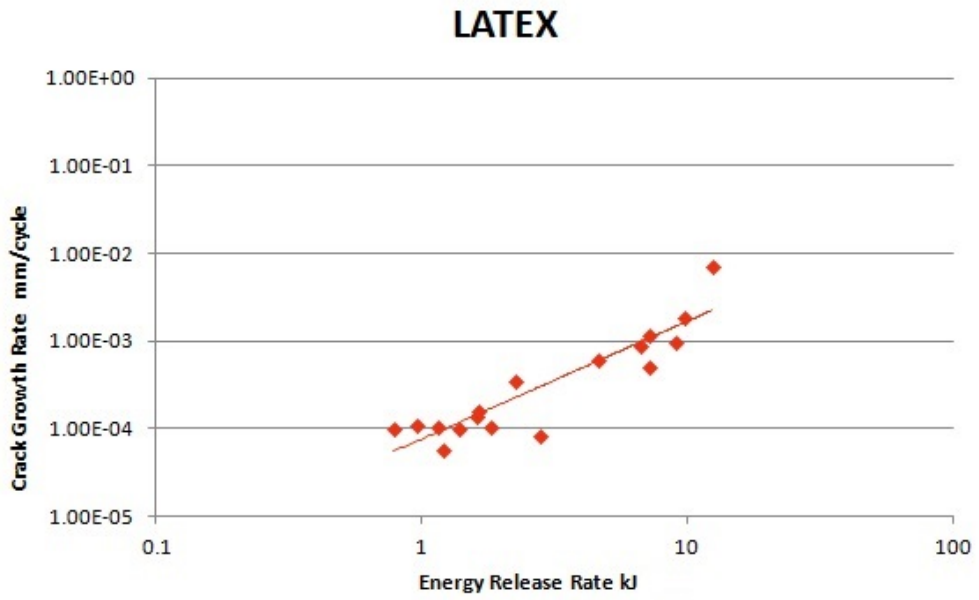

Figure 7.3: Crack growth rate versus Energy release rate for Latex.

7.4 HG252

The parameters of the two relations for Stress-Strain and Strain Energy Density are listed in Table 7.7 and 7.8.

Stress-Strain Parameter			**Young's Modulus**	
a	**b**	**c**	**E (MPa)**	**20% secant**
-9.0464	7.0707	0.5115	7.0707	7.8189

Table 7.7: Stress-Strain parameters and Young Modulus for HG252.

SED Parameters		
a1	**b1**	**c1**
-0.8312	2.0568	-0.0615

Table 7.8: SED parameters for HG252.

HG252 has a Young's Modulus similar to Elast-Eon™rather than SEPS22. This is because of the increased percentage of styrene in the block-copolymer: the material results to be stiffer with an higher percentage.

The graph in Figure 7.4 represents the crack growth rate as a function of the energy release rate.

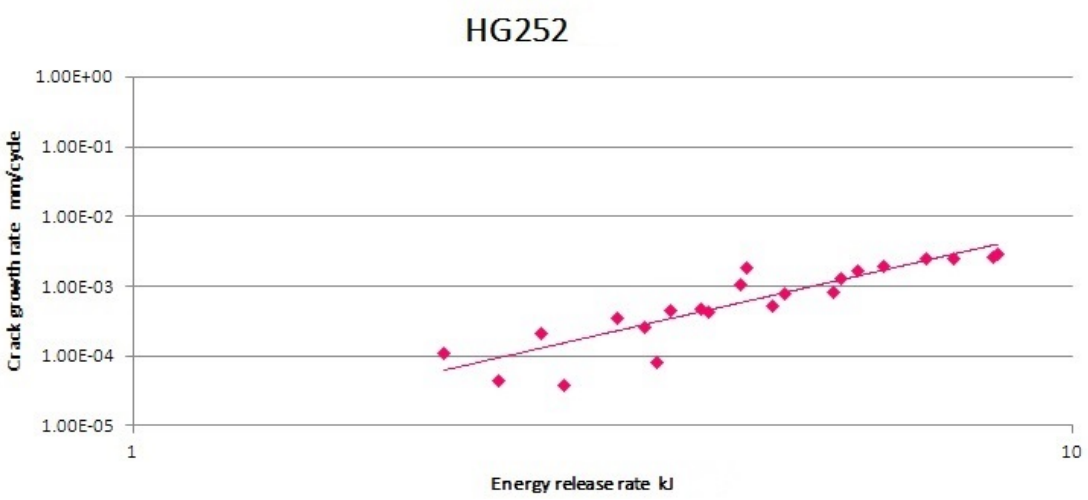

Figure 7.4: Crack growth rate versus Energy release rate for HG252.

7.5 Elast-Eon™and SEPS22 in Tris-Buffered Solution

In Table 7.9 and 7.10 the parameters calculated from the polynomial fitting for the Stress-Strain and SED relations are listed.

Stress-Strain Parameter			**Young's Modulus**	
a	**b**	**c**	**E (MPa)**	**20% secant**
–4.1772	4.6013	0.2484	4.6013	5.0076

Table 7.9: Stress-Strain parameters and Young Modulus for Elast-Eon™in Tris-Buffered solution

SED Parameters		
a1	**b1**	**c1**
1.4795	0.5867	-0.0401

Table 7.10: SED parameters for Elast-Eon™in Tris-Buffered solution

Since the specimens tested were cut from the same polymer sheets of the specimens tested in air, it is evident that Elast-Eon™behaviour changes if tested in physiological solution. In particular it resulted in a better performance, respect to the PHV application, when tested in the solution.

The Young's Modulus for Elast-Eon™, when tested in solution, is half of the result obtained from testing in air, and the same is for the Stress-Strain relation parameters.

From the values of the SED equation parameters it is possible to notice the same reduction that happens for the other relation. This then result in a more vertical trend line from the Crack Growth test (Fig 7.5), which in the end, toghether with the drop of the Young's Modulus, implicates a decresed value of the Performance Index.

The polymer was weighted before and after different periods of soaking in the solution, in this way it was possible to state that the material is hydrophilic and that after aproximately two hours it reaches its maximum level of liquid adsorption (in fact, after that time, its weigh was not increasing anymore). The polymer was tested after this minimum period of time in order to have a better prediction.

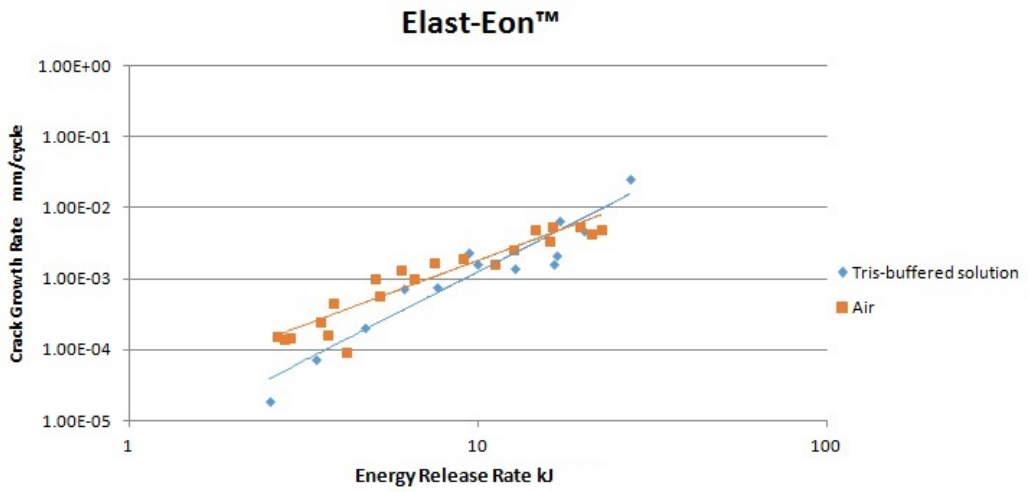

Figure 7.5: Crack growth rate versus Energy release rate for Elast-Eon™ in Air and in Tris-Buffered solution.

The same procedure was followed for SEPS22, but the material resulted to be hydrophobic, in fact its weight did not change over different soaking time. This feature is the reason why the following results were obtained for SEPS22: from table 7.11 and 7.12 it is possible to notice that the parameters and the Young's Modulus are very similar to the results obtained with the test in air; furthermore, the graph in Figure 7.6 shows that there are no evident difference between the two tests. In conclusion it is possible to state that SEPS22 has the same behaviour when stressed in Air or in physiological solution.

Stress-Strain Parameter			**Young's Modulus**	
a	**b**	**c**	**E (MPa)**	**20% secant**
-2.9288	3.3925	0.1482	3.3925	3.5478

Table 7.11: Stress-Strain parameters and Young Modulus for SEPS22 in Tris Buffered solution

SED Parameters		
a1	**b1**	**c1**
0.7473	0.5214	-0.0343

Table 7.12: SED parameters for SEPS22 in Tris-Buffered solution

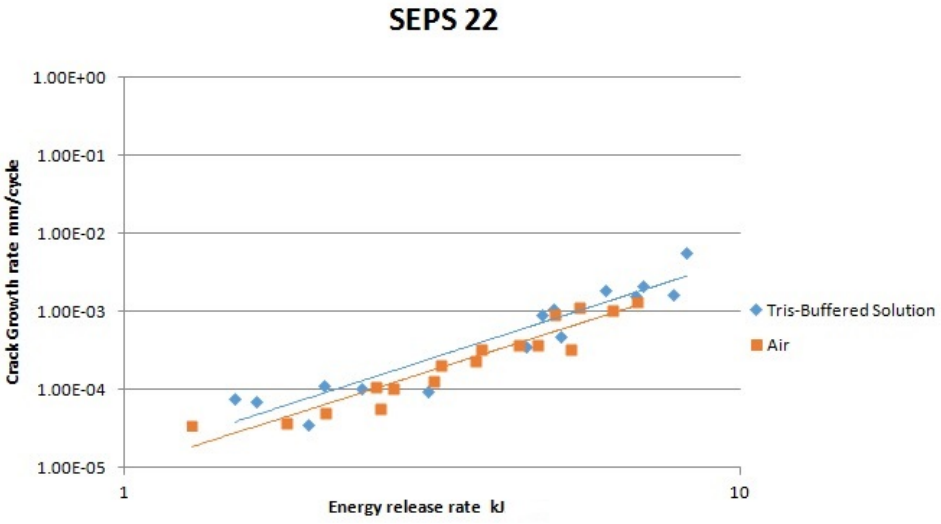

Figure 7.6: Crack growth rate versus Energy release rate for SEPS22 in Air and in Tris-Buffered solution.

7.6 Crack Nucleation Results

The results from the Crack Nucleation test were the most difficult to obtain due to the force and amplitude limits of the machine.

The objective of this test was, as mentioned in Chapter 5, the validation of the crack growth model. This was obtained for SEPS22, as shown in Figure 7.7, the model in fact is validated. It was not possible to obtain a significant number of broken uniaxial samples for HG252 and Elast-Eon™because those materials needed a greater amplitude and an higher force limit to breack in a reasonable number of cycles.

In particular, Elast-Eon™showed a poor creep resistance and thus the TA could not bare an amplitude large enough to breack the sample.

HG252, on the other side, needed an higher force limit and only one sample brokes.

For what concern Latex, the sample riceived from the company was not enough to perform both tests. The conclusion was that the validation for SEPS22 and the material tested by Lake and Lindley [9] and Mars and Fatemi [8] was enough to infer that the model could be valid for all the materials tested.

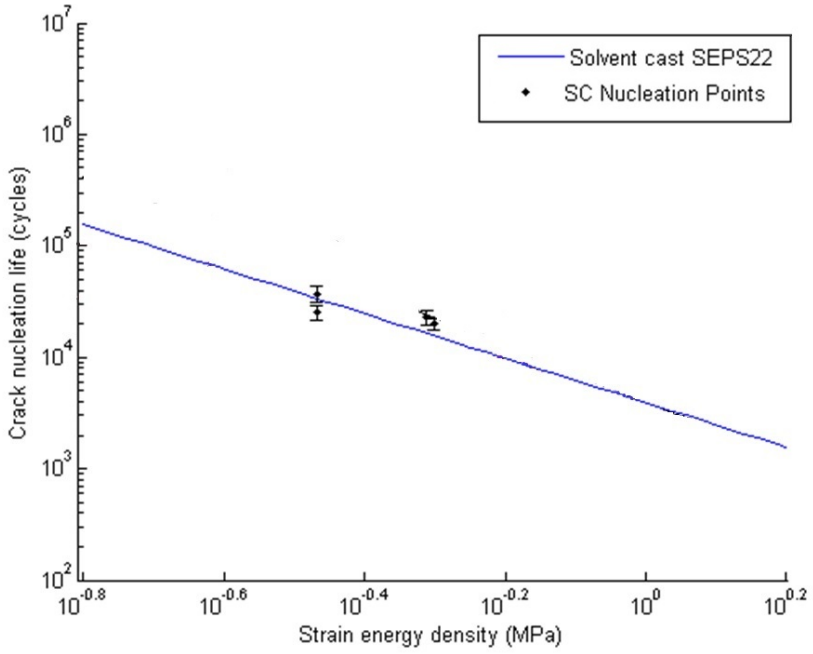

Figure 7.7: Validation of the Crack growth test with the Crack nucleation test.

7.7 Comparison of all the Materials

The selection of the optimal material for the application on a Presthetic Heart Valve has one of the final steps in the comparison of all the Performance Index and relevant properties of the polymer selected.

In general, lower PI indicates a material more suited to use in a Prosthetic Heart Valve leaflets. It is also important to pay attention to the Young's Modulus of the material. In fact, although some materials may appear to have good lifetime properties their stiffness requires thin leaflets and they are less suited to PHV leaflets. It is subsequently possible to estimate an optimal thickness for leaflets. From work performed by Bernacca et al.[4], who varied leaflet modulus and thickness, we determined a maximum value of Et^3. In their instance, this occurred at $1.8 \pm 0.2 * 10^4\ Nm$. Given this information, the maximum leaflet thickness might be estimated given the mechanical properties of the material.

The numerical values for the tested materials are shown in Table 7.13.

B and F represent the parameters obatined from the power law model fitting, W_{max} is the maximum strain energy density permitted to avoid fracture and σ_{max} is the equivalent maximum stress. The Young's Modulus values and the PI are also listed.

Figure 7.8 shows the growth rate of a sharp crack, with a natural tip, for each material as a function of the energy release rate in a planar sample. The more vertical the trend line is the

more optimal the Performance Index will be. This aspect is reflected in the results obtained from the different experiments. In fact the two more leaning line are the ones of HG252 and Elast-Eon™in Tris-Buffered solution and they also have the lowest PI.

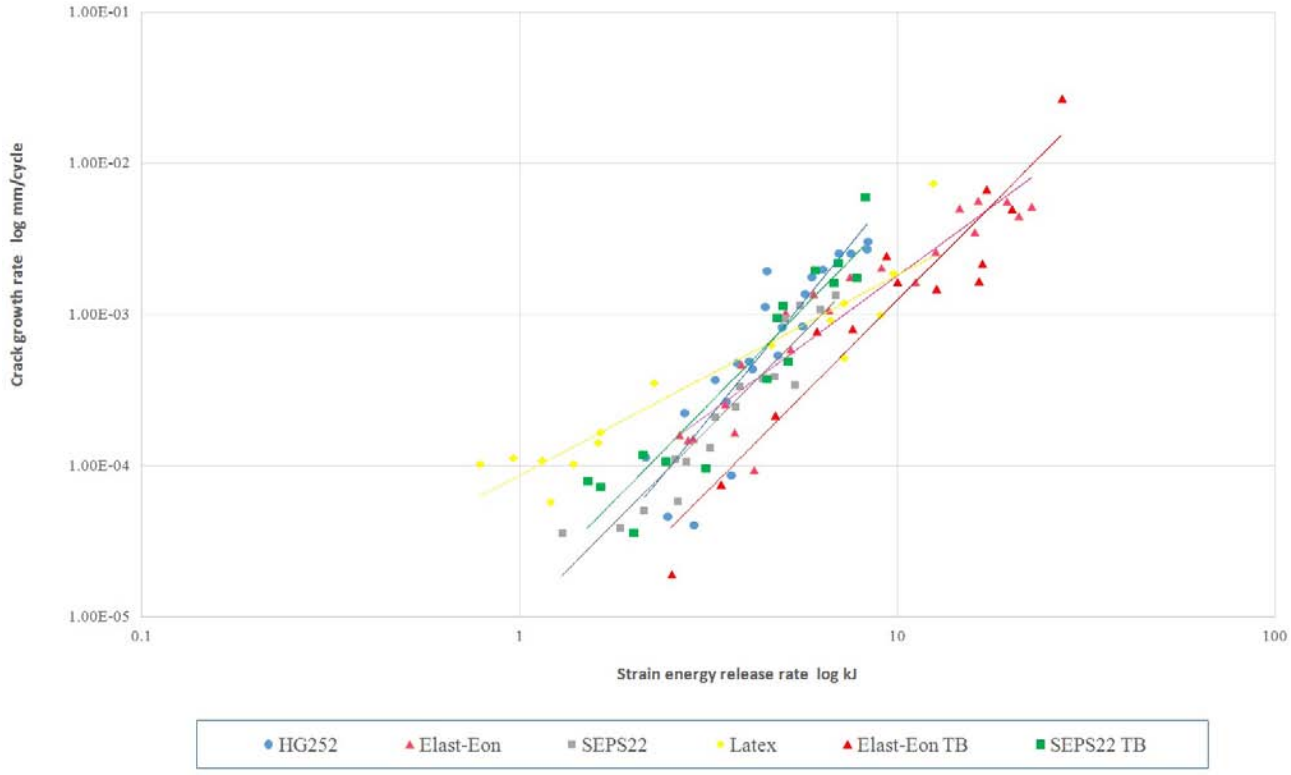

Figure 7.8: Crack growth rate versus Energy release rate for each material tested.

Material	B	F	$W_{max}(MPa)$	$\sigma_{max}(MPa)$	**E (MPa)**	**PI**
Elast-Eon™	2.689E-05	1.826	0.119	0.069	9.39	28797.4
SEPS22	9.866E-06	2.509	0.592	0.155	4.23	1132.9
HG252	5.991E-06	3.068	1.208	0.247	7.819	518.436
Latex	8.652E-05	1.322	0.01	0.0007	1.408	4651674499
Elast-Eon™TB	3.845E-06	2.511	0.865	0.229	5.007	417.615
SEPS22 TB	1.353E-05	2.547	0.547	0.113	3.548	2464.162

Table 7.13: Performance Index for each material based upon its maximum stress and its flaxural stiffness.

It is evident that the best material selected are HG252 and Elast-Eon™. The last one is considered because when tested in solution the PI decreses and when used as a PHV it will be constantly soaking in a physiological solution.
HG252 was not tested in the Tris-Buffered solution because it has the same property of SEPS22 for what concern liquid interaction: the mechanical properties do not change.
Furthermore, the diffrence between the PI of SEPS22 and HG252 means that an increase in the percentage of the styrenic segments improve the material performance. However the incresed Young's Modulus for HG252 could lead to the requirement of thin leaflets and the material could be less suited to PHV leaflets.
A novel method for selecting materials for polymer prosthetic heart valves based upon their mechanical properties has been reported, however it is well ackowledged that biocompability and biostability also play a crucial role in material selection. In fact the materials selected have already passed the cyto- and hemocompatibility tests, as explained in chapter 4.
Even though one or two optimal materials have been selected among the shortilist of polymer, the lowest PI should be smaller than the one obtained in this selection ($10^1 or 10^0$ order of magnitude). Despite that, several valves were manufactured using the materials of the shortlist, in particular Elast-Eon™and SEPS22 (this experiment is described in chapter ...). It was quite importan to test the material in the valve leaflet shape mainly because the geometry of the valve is an important factor in the determination of the maximum strain energy density permitted; a second aspect to investigate was the influence of the Young's Modulus: if the material was to stiff the valve could not close properly.

Chapter 8

In vitro testing of Polymeric PHV

The experiments consisted in the manufacturing and testing of PHV made of the polymers selected. For the experiments Elast-Eon™and SEPS22 were used.
The two materials were chosen because they both have a small PI and a relatively low Young's Modulus.
All the valves were manufactured with a dip casting technique; the intention was to obtain the same isotropic condition that characterized the polymers tested mechanically.
A second aspect to investigate was the hydrodinamic behaviour of the dip casted valve in order to study its adequacy.
A total of 9 PHV prototypes were manufactured by dip casting technique with Elast-Eon™and SEPS22. The test was conducted in pulsatile condition using a Pulse Duplicator showed in Figure 8.4. In addition to this experiment, a finite element simulation was applied to the valve geometry in order to evaluate the distribution of stresses and to compare the result with the pulsatile test. For the simulation an isotropic hyperelastic rubber consistutive law was necessary. In fact, in the case of static deformations, rubber exhibit hyperelastic behaviour, thus a strain energy density function W can be attributed. For isotropic materials, strain energy density function can be represented in terms of right Cauchy-Green tensor $\mathbf{C}$, invariants (I_1, I_2, I_3) or even values of deformation gradient tensor F, called principal stretches $(\lambda_1, \lambda_2, \lambda_3)$, hence the function can be:

$$W = W(I_1, I_2, I_3) \quad or \quad W = W(\lambda_1, \lambda_2, \lambda_3) \tag{8.1}$$

where:

$$I_1 = tr(\mathbf{C}) \quad ; \quad I_2 = \frac{1}{2}\left[I_1^2 - tr(\mathbf{C}^2)\right] \quad ; \quad I_3 = det(\mathbf{C}) \tag{8.2}$$

In the case of rubber material, due to the negligible compressibility under conventional pressures, incompressibility assumptions is often used ; therefore given

$$\mathbf{F} = \begin{bmatrix} \lambda_1 & 0 & 0 \\ 0 & \lambda_2 & 0 \\ 0 & 0 & \lambda_3 \end{bmatrix} \tag{8.3}$$

and

$$\mathbf{C} = \mathbf{F}\mathbf{F}^T \tag{8.4}$$

Incompressibility means that:

$$det(\mathbf{F}) = 1 = \lambda_1\lambda_2\lambda_3 \tag{8.5}$$

With this conditions it results that $I_3 = 1$ and so W is semplified as:

$$W = W(I_1, I_2) \tag{8.6}$$

At this point the true stress tensor σ is interpreted by the differentiation of W with respect to $\mathbf{C}$ or equivalently with respect to the invariants, as described in equation 8.7.

$$\frac{\partial W}{\partial F} = \sigma = \frac{\partial W}{\partial I}\frac{\partial I}{\partial F} \tag{8.7}$$

The Mooney-Rivling model is now considered to obtain the strain energy density function and it is expressed as follow:

$$W = c_1(I_1 - 3) + c_2(I_2 - 3) \tag{8.8}$$

where c_1 and c_2 are constants related to the shear modulus of the material and they have been fitted to experimental data. The model satisfy the condition described before and it is utilised to model the hyperelastic mechanical behaviour of the rubber for the PHV.

8.1 Experimental Procedure

8.1.1 Polymeric PHV manufacturing

The PHVs were manufactured with the dip casting techinique, as explained in the previous section. Dip casting process involves repeatedly dipping a product or part of a product into a solution of polymer.

In this specific procedure the positive mold was manually inserted and removed from the solution bath several times until the desired thickness was reached.

The mold elements (Figure 8.1) were manufactured in aluminum by spark erosion (Cambridge Reactor Design), based on a 3-dimensional geometry replicating the natural configuration of trileaflet heart valves [12].

The Valve geometric profile and dimensions are reported in Figures 8.2.

Figure 8.1: PHV alluminium mold.

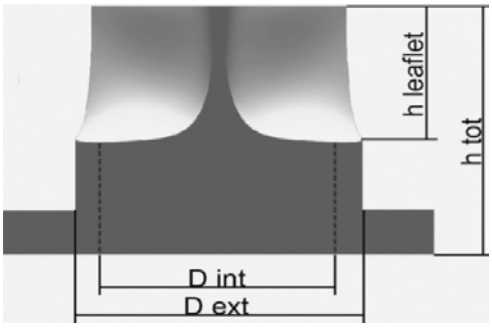

D_{int}	24 mm
D_{ext}	36 mm
$h_{leaflet}$	12 mm
h_{tot}	14 mm

Figure 8.2: Valve geometry dimensions.

Once the solvent was completely evaporated and the thin layer was deposited on the mold, the polymer film was peeled off to form the valve. Two valves example are shown in Figure 8.3: the valve on the left is made of Elast-Eon™, the one on the right is made of SEPS22.

Figure 8.3: Polymeric PHV prototypes

The Elast-Eon™valve has a black rigid polymeric stent which was processed with a MakerBot 3D printing. The stent was used to substain the valve inside the pulse duplicator, it did not reproduce the real medical prosthesis but it was necessary to manufacture and test the valve leaflets. The stent was first positioned on the positive mold and they were dip casted as a one piece.

The main disadvantages were related to the inaccuracy of the procedure, in fact, since it was performed manually, it was not possible to control and repeate the dipping and evaporation steps. Furthermore, the only way to control the leaflet thickness was to measure with a caliber the free edge of the leaflet on the top of the mold; in this way only the thickness on the top of the leaflet was known. Most of the time the thickeness was not uniform in the valve leaflets prototype.

The last drawback to mention is the creation of bubble during the deposition and evaporation steps, this was very difficult to avoid and the only solution was try to keep this bubble under a certain size.

8.1.2 Pulsatile Test

Prosthetic Valve made both of Elast-Eon™and SEPS22 were tested in vitro under pulsatile flow to evaluate pressure drops and an eventual fatigue failure, as recommended by ISO 5840 Standard [15].

Pulsatile flow tests were performed using distilled water at room temperature (25°C).

The experimental test bench used to evaluate Prosthetic Heart Valve pressure drops is shown in Figure 8.4 and the schematic representation in shown in Figure 8.5. The instrument consists of the following elements: a volumetric pumping system, a ventricular chamber, an aortic valve housing (designed according to the guidelines of the ISO 5840 Standard), a systemic impedance simulator and a mitral valve housing.

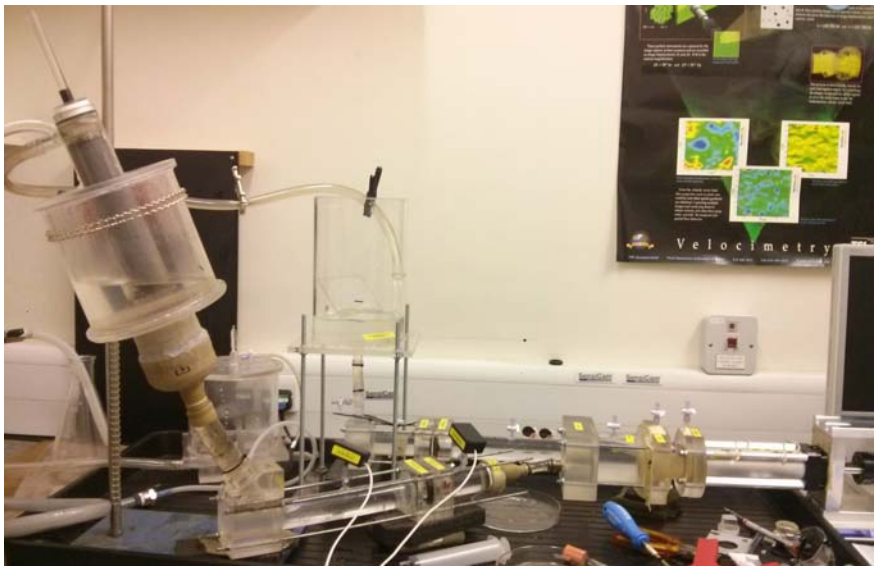

Figure 8.4: Pulse Duplicator set for the experiment.

The pumping system was driven by an electronic controller allowing the setting of different flow rate waveforms and different frequencies. The ventricular chamber allows the simulation of both physiological and pathological stroke volume. The ventricular chamber and the pumping system are divided by a thin silicon membrane (thickness = 0.3 mm). In this way the piston can be isolated and filled with distilled water to prevent damage to the mechanical system, while the other elements of the pulse duplicator can be filled with different fluids (e.g., blood or fluids simulating the blood rheological properties) if required. The aortic and the mitral valve housing are connected with straight tubes to the systemic impedance simulator and to the ventricular element respectively.

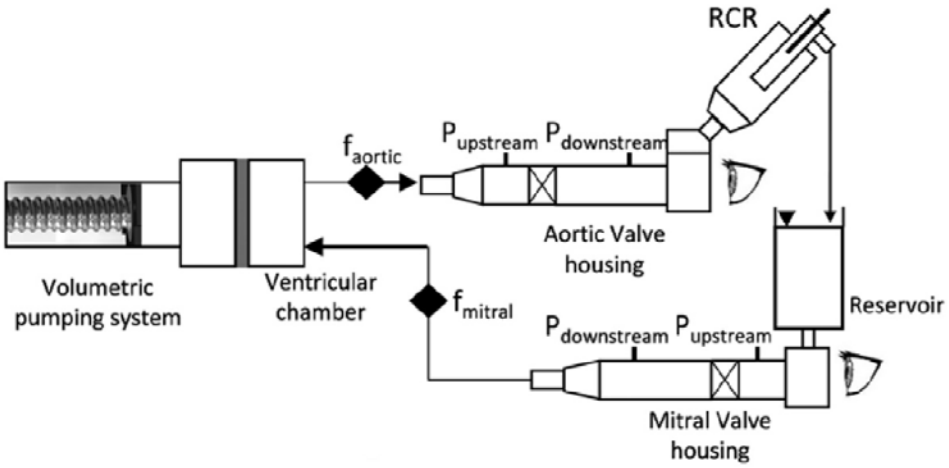

Figure 8.5: Pulse Duplicator scheme.

Furthermore, this setup allows the direct visual observation of both valves at different time steps of the cycle. In Figure 8.6 the two steps of opening and closure are shown, the picture was taken directly during the simulation.

Figure 8.6: Valve opening and closing in the Pulse Duplicator

According to the UNI EN ISO 5840 Standard, the new pulse duplicator reproduces the physiological pressure (Figure 8.7) (i.e., arterial peak systolic pressure ranging from 100 to 130 mmHg, arterial diastolic pressure from 65 to 85 mmHg, differential pressure across closed aortic valve equal to 100 mmHg). Transvalvular pressure drop was measured at a constant frequency of 70 bpm. The valves were sealed with O-rings in the housing unit to avoid any leakage. Transvalvular pressure drop was measured 3 times for each valve by pressure transducers to verify the repeatability of the tests.

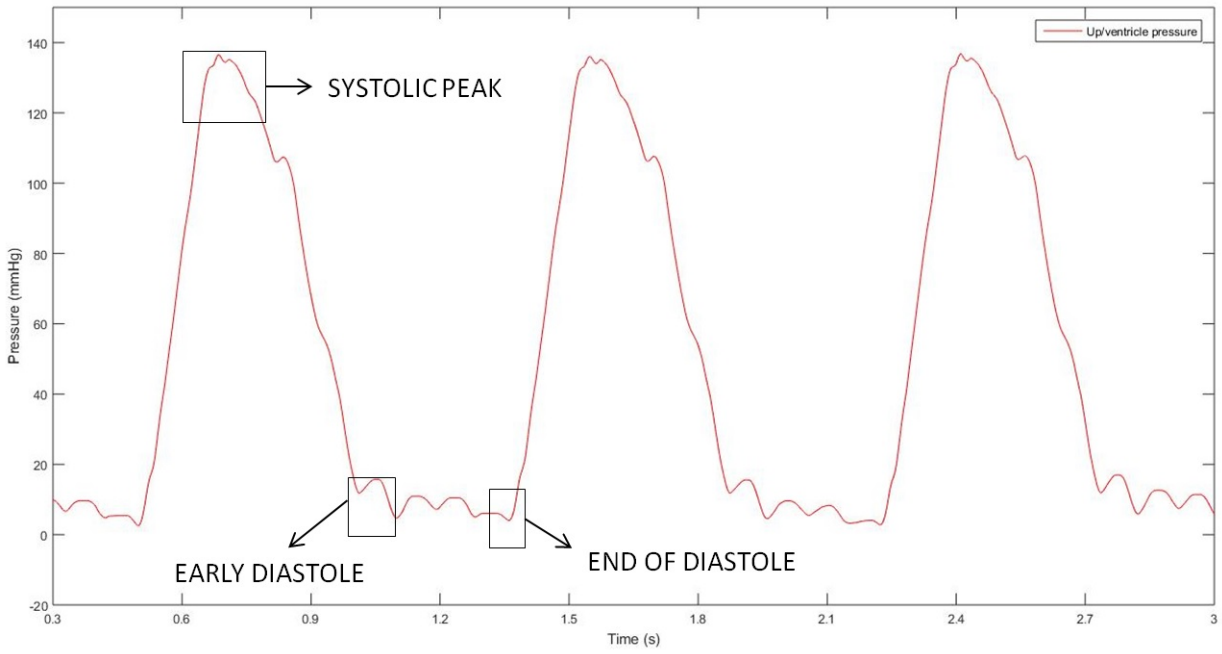

Figure 8.7: Pressure waveform.

The pressure acquisition shown in Figure 8.7 illestrates the systolic peak at around 130mmHg and the early and end of diastole at the bottom part of the wave form; the picture in particulare represents the ventricle pressure, which is the value measured upstream respect to the valve in the Pulse Duplicator.

The mean systolic pressure gradient was obtained by integrating the difference between the simultaneously recorded "aortic" and "ventricular" pressure waves over the systolic time period, defined as the time period during which forward aortic flow occurs. Each set of measurements was obtained by averaging two readings of each of three consecutive beats.

8.1.3 Finite Element Model for the PHV

CAD modeling was used to draw the PHV leaflet shape (Figure 8.8) to fit into the host anatomy with appropriate coaptation of the leaflets when the valve is closed to avoid backward flow.The design of a biomorphic PHV depends on the shape of three critical regions : Commissural Edge (CE), Free-Edge (FE) and leaflet curvature Shape Edge (SE). NURBS-based CAD modeling was chosen to get flexibility in the description of valve geometry.

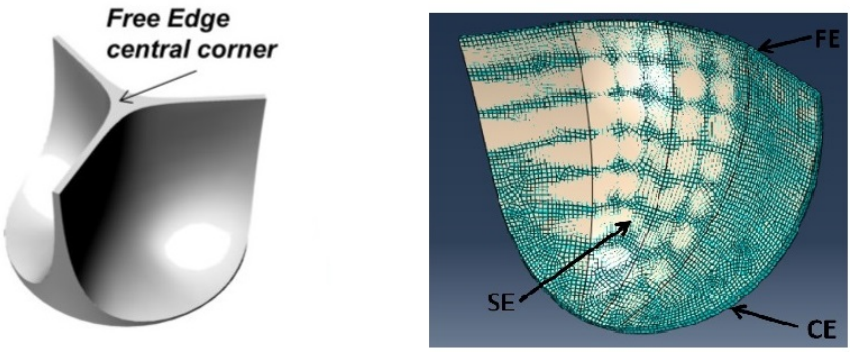

Figure 8.8: PHV Leaflet modelling.

An automatic procedure was developed using the commercial scripting tool RhinoSCRIPT (Rhinoceros, McNeel & Assoc.). After setting the PHV class (i.e., circular, symmetric, trileaflet), the anatomical fitting parameters (i.e.diameter and height) and a constant leaflet thickness, the procedure calculates the NURBS parameterization of CE and FE.

An automatic non rigid registration procedure provides the NURBS surfaces which best fit the boundary curves CE and FE, keeping the thickness constraint. A finite element model (Abaqus®, SIMULIA, Dessault Systèmes) was developed to analyze the mechanical behavior of the valve as a function of the leaflet thickness. Each 3D solid model was discretized with about 3000 linear hexahedral elements . Three leaflets were considered to represent the real mechanical effect on a valve, the complete structrure is shown in Figure 8.9. If only single leaflet was considered, which was a possible solution due to the valve geometry periodicity (120°), the mechanical effect of the omitted leaflets should have been accounted by means of kinematic constraints blocking displacement beyond the plane of symmetry of the PHV.

All the displacements at the CE were avoided to simulate the presence of the valve stent.

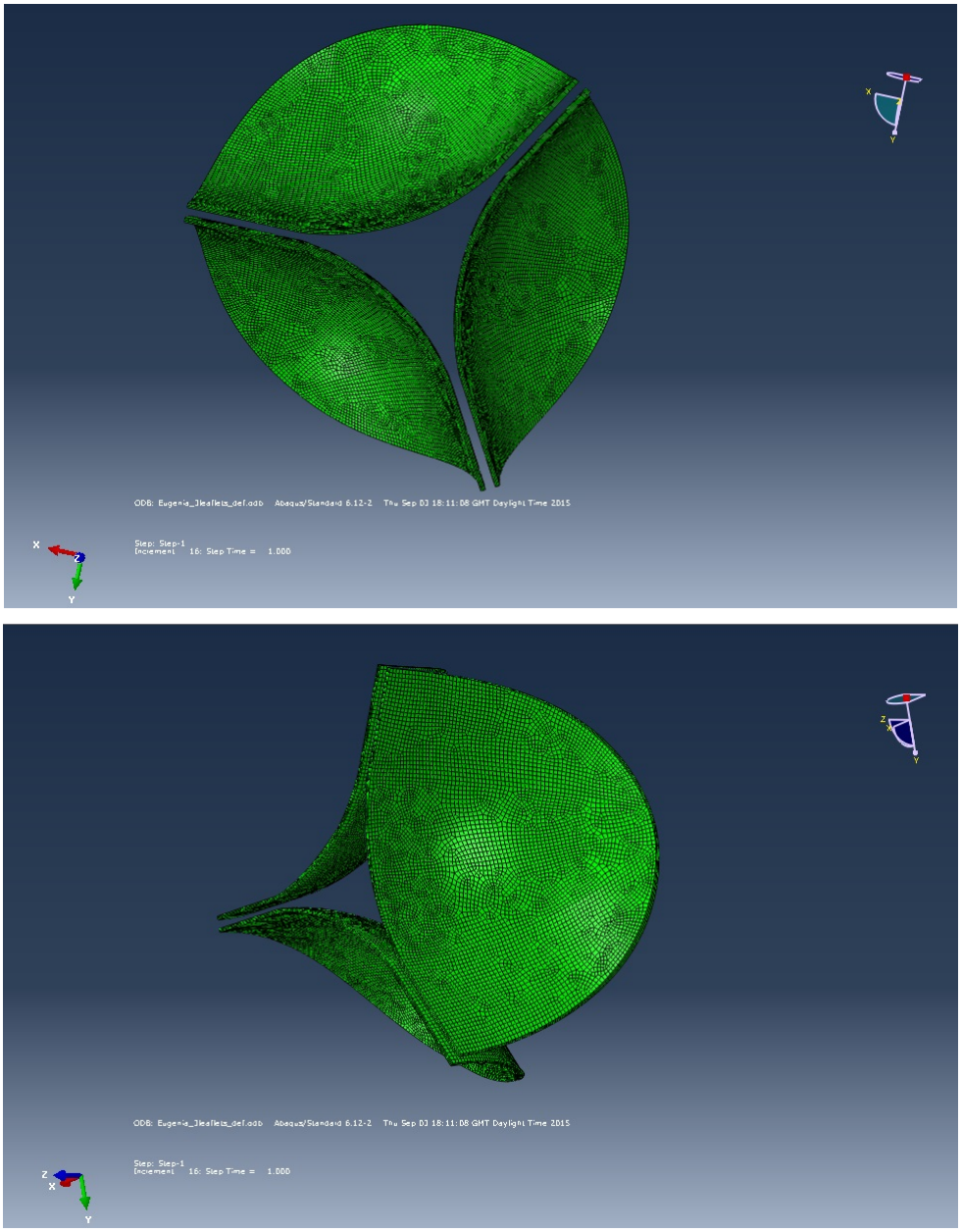

Figure 8.9: PHV geometry and mesh.

Figure 8.9 shows the PHV mesh from two different point of view. Uniform static pressure (120mmHg) was applied over the internal convex face of the leaflet to simulate the opening of the valve.

The polymer mechanical behavior was modeled by a hyperelastic isotropic constitutive law as previously described in equation 8.8.

8.2 Results and Discussion

The results description considers the pressure aquisition for each valve tested. The objects of investigation can be divided in two main problems: the valve functioning, that is wheter it closes and seals or not, and the valve performance, which is the analysis of what happens during systole.

The two values calculated from the test are mean diastolic pressure difference and mean systolic pressure difference. The first one is the mean difference between the pressure downstream and upstream during diastole, while the second one is the mean difference between upstream and downstream pressure during systole.

When the valve is tested in the Pulse Duplicator the mean Diastolic Pressure difference is set to be 100 mmHg, which is the correct value for a normal hearth valve. If the pressure measured reveals that this condition is not met and the pressure gradient is lower than the one set, it means that the heart has to pump more to open and close the valve and thus the prosthesis does not repreduce an acceptable functioning.

For what concern the analysis of the valve performance, the ideal result is zero mean systolic pressure gradient. Since this value is far from reality, the best performance is reached with very small value of MSPD. In general a large pressure gradient during systole is the signal of an unsatisfactury performance.

A reference value for the mean systolic pressure difference is the one of the Perimount-Magna valve [47]: for this bioprosthesis $10.4 \pm 4\ \ mmHg$ pressure gradient has been recorded.

The following resutls are assembled by the material of which they are made of, thus there will be a SEPS22 and a Elast-Eon™section .

SEPS22 valves

Three valves were made out of SEPS22. The first valve was too thin (0.146 mm average thickness on the top of the leaflet) and it brokes after a couple of cycles at 70 bpm. It was possible to observe a sharp horizontal crack in the middle of one of the leaflets. No pressure difference was recorded for this valve.

The second SEPS22 valve was manufactured with thicker leaflets and the performance improved, the results are illustrated in Figure 8.10 and Table 8.1.

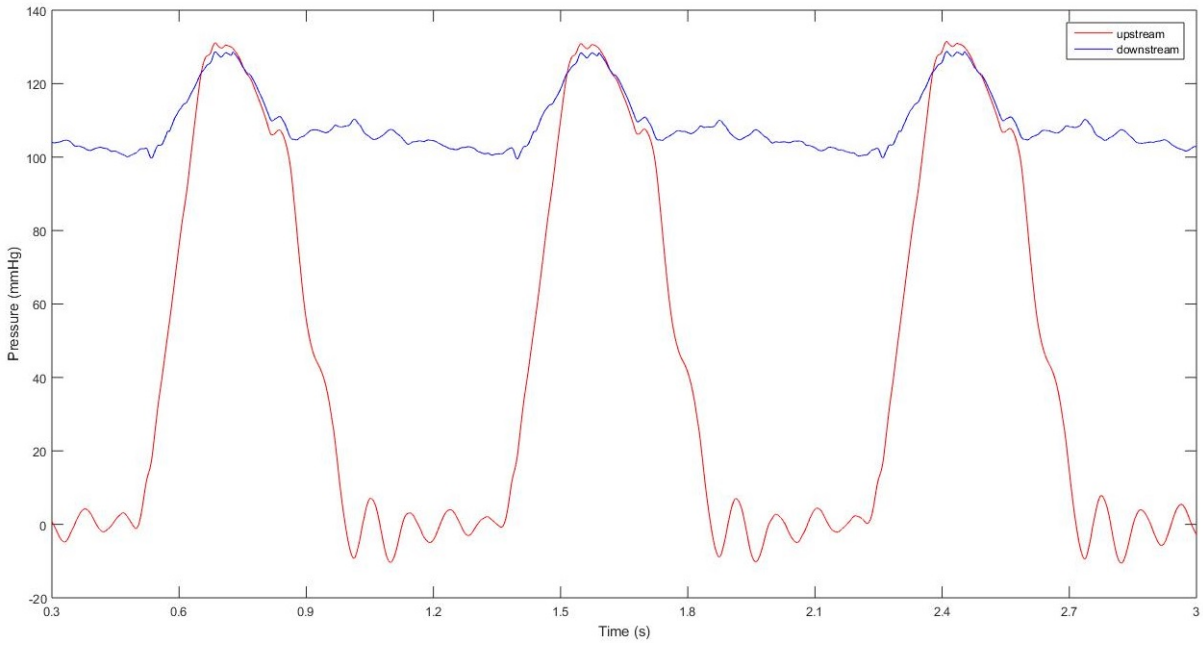

Figure 8.10: Pressure aquisition for the second SEPS22 valve.

Average Thickness	**Mean Systolic Pressure Gradient**	**Mean Diastolic Pressure Gradient**
0.2 mm	0.7 ± 0.005 mmHg	97,6± 0.51 mmHg

Table 8.1: Data for SEPS22 valve.

The mean diastolic pressure gradient reaches the value set in the test, this means that the valve is functioning properly. Furthermore, the mean systolic pressure difference is very small, thus the valve has also a good performance.

Despite this excellent results, the SEPS22 prosthesis brokes after 25 minutes at 70bpm, that means after 1750 cycles. The fact was confirmed by different pressure acquisition results after the valve brokes (Figure 8.11). The crack had the same shape of the one in the previous failed valve, i.e. a sharp cut in the middle of the leaflet as illustrated by the red circle in Figure8.12. Further stress analysis are presented in the modelling section, in fact the opening of the valve with same thickness and material was simulated with a finite element model.

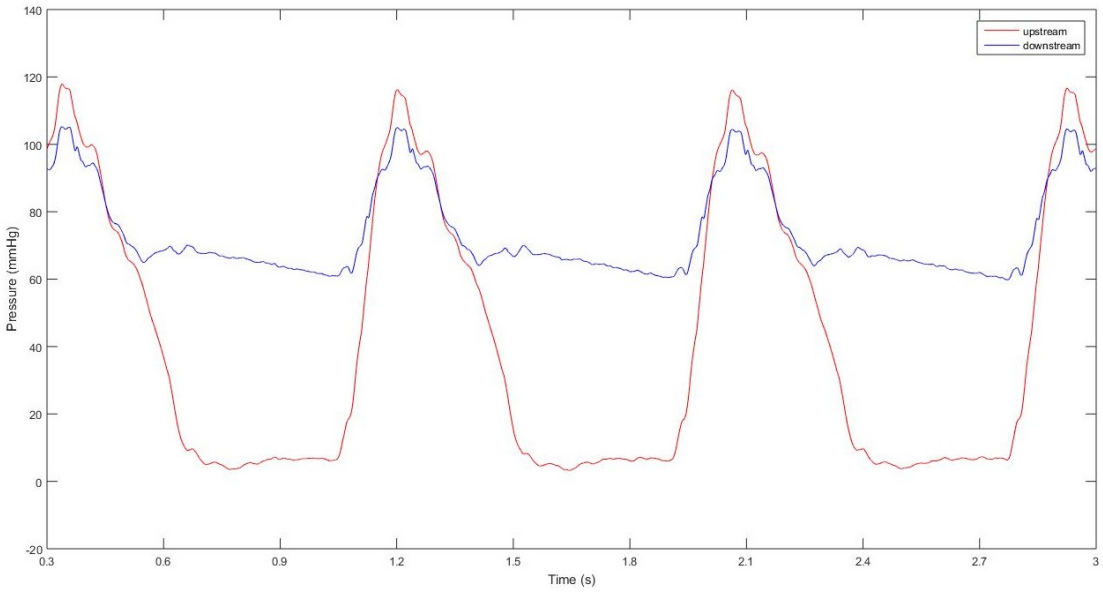

Figure 8.11: Pressure aquisition for the second SEPS22 valve after failure.

Figure 8.12: SESP22 Brocken Valve.

Average Thickness	**Mean Systolic Pressure Gradient**	**Mean Diastolic Pressure Gradient**
0.2 mm	0.92 ± 0.42 mmHg	58.64± 0.95 mmHg

Table 8.2: Data for SEPS22 valve after failure.

After failure there was a drop in the mean diastolic pressure gradient and also an increase in the mean systolic pressure difference.

The structure of the valve could not substain the pressure set by the pump of the Pulse Duplicator. Even if the pressure difference during systole was still adequate, the diastole was the signal of a malfunctioning.

The last SEPS22 valve was thicker than the second one. Pressure acquisition and gradients are shown in Figure 8.13 and Table 8.3.

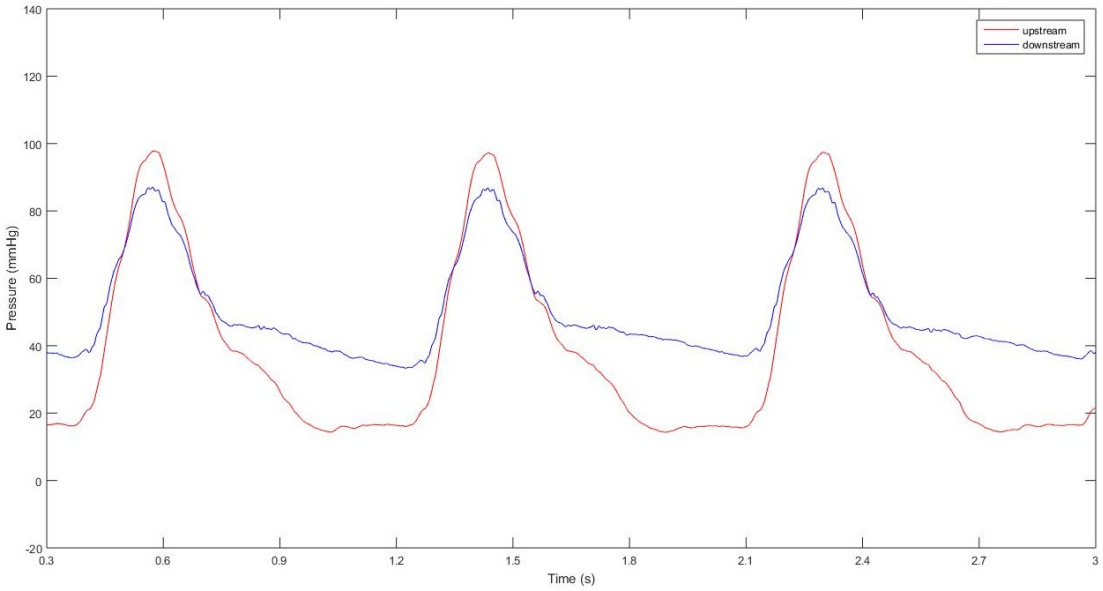

Figure 8.13: Pressure aquisition for the third SEPS22 valve.

Average Thickness	**Mean Systolic Pressure Gradient**	**Mean Diastolic Pressure Gradient**
0.3 mm	2.7 ± 1.9 mmHg	22.2± 0.6 mmHg

Table 8.3: Data for thicker SEPS22 valve.

The valve in this case was too stiff and thus there was constantly a gap between the leaflets, also during diastole. The mean pressure difference during diastole, in fact, is increadibly lower respect to the 100mmHg set in the Pulse Duplicator. A real heart should pump too hard to make this valve work properly. Furthermore, the fact that the valve did not close means that it can not be used in any case, its main function would not be fulfilled.

In conclusion it is possible to state that a valve made of SEPS22 should be thinner than 0.3 mm but then the risk will be a premature failure. A possible correction to the prototypes made for this experiment is a more controlled thickness homogeneity. Probably, the region were the crack propagated was thinner than the average thickeness value indicated for the leaflets. In fact, an efficient dip casting was very difficult to perform manually. Once the mold was dipped in the solution then it was kept both upwards and downwards in order to evenly distribute

the solution allover the surface during solvent evaporation. The result, instead, was a thicker bottom and a thinner top of the leaflets , or the reverse, for the majority of the protoypes. The movements made to distribute the solution and the time during which the mold was kept in both positions were not correct and very difficult to controll, many attempts were made to optimize this two parameters. The best results were obtained with thinner valves, in fact the thickeness homogeneity was more difficult to control with the increse of thickness itself.

Elast-Eon™

Five valves were made of Elast-Eon™. This material was even more difficult to use during dip casting because the solution tended to become very viscous quite quickly. This was related to the properties of the solvent. The first valve tested was very thick and the 100mmHg mean diastolic pressure difference was not respected. In fact the valve did not open and close properly. Figure 8.14 and Table 8.4 describe the data obtained for this valve.

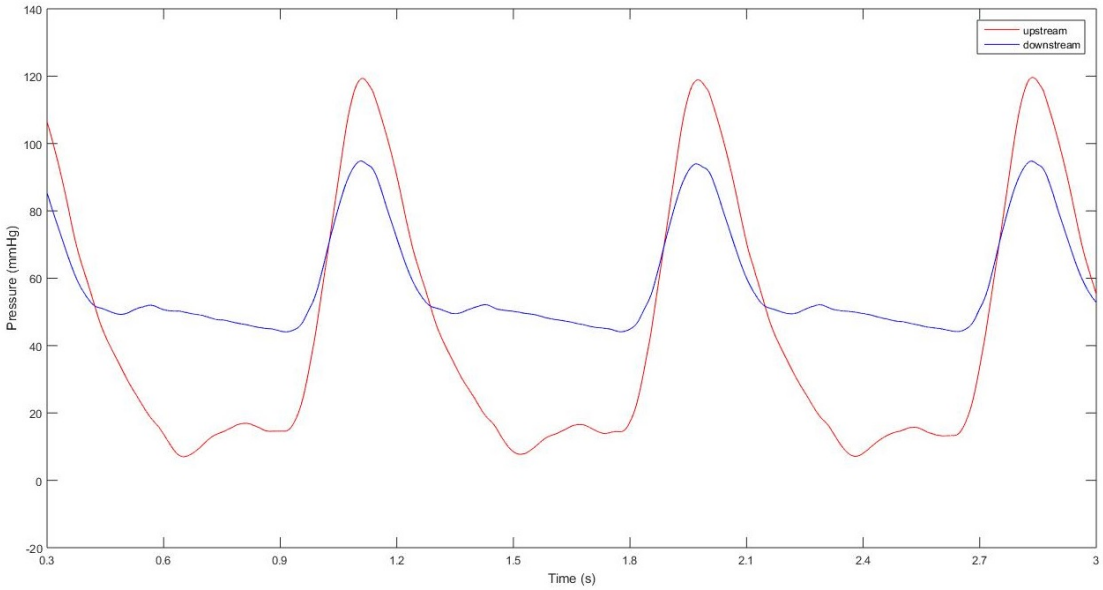

Figure 8.14: Pressure aquisition for the first Elast-Eon™valve.

Average Thickness	Mean Systolic Pressure Gradient	Mean Diastolic Pressure Gradient
0.43 mm	13.22 ± 0.29 mmHg	29.1± 0.31 mmHg

Table 8.4: Data for the first Elast-Eon™valve.

The second valve was thinner than the first one in order to improve its functioning. The results in Figure 8.15 and Table 8.5 actually shows a higher diastolic pressure difference but still it does not reched the minimum requirement. Also for what concern the mean systolic pressure difference it is possible to see a relevant improvement respect to the previous valve.

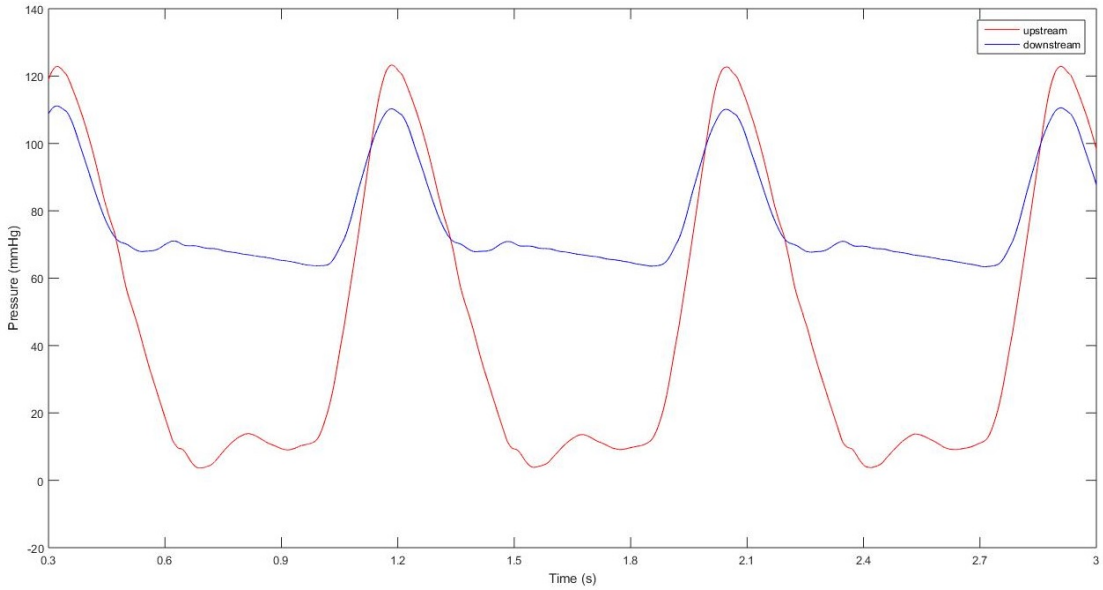

Figure 8.15: Pressure aquisition for the second Elast-Eon™valve.

Average Thickness	Mean Systolic Pressure Gradient	Mean Diastolic Pressure Gradient
0.32 mm	6.95 ± 0.31 mmHg	52.28± 0.16 mmHg

Table 8.5: Data for the second Elast-Eon™valve.

The third valve was made too thick, but probably the distribution of thickness was more optimal for the valve functioning. In fact, as shown in Figure 8.16 and Table 8.6, the mean diastolic pressure gradient is higher than the two previous valves. One of the reason could be also that, even if the average thickness is around 0.5mm, there were two thinner leaflets and a much higher thicker one. Probably the two thin leaflets compensated the stiffnes of the third one.

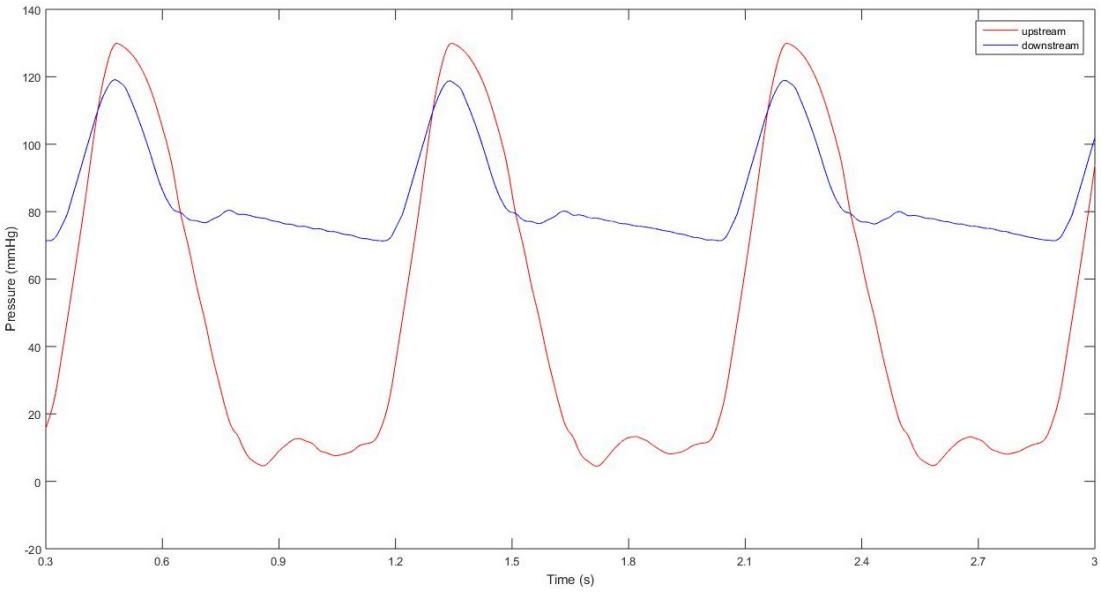

Figure 8.16: Pressure aquisition for the third Elast-Eon™valve.

Average Thickness	Mean Systolic Pressure Gradient	Mean Diastolic Pressure Gradient
0.49 mm	10.41 ± 0.33 mmHg	64.57± 1.95 mmHg

Table 8.6: Data for the third Elast-Eon™valve.

The fourth valve was thinner than the third one and the pressure difference is almost identical for what concern diastole, while is significantly lower during systole. This means that a thinner valve improves the performance of the valve, but still it does not reach the optimal functioning. The main problems was still that the valve did not close completely. The results are resumed in Figure 8.17 and Table 8.7.

Average Thickness	Mean Systolic Pressure Gradient	Mean Diastolic Pressure Gradient
0.27 mm	6.92 ± 0.17 mmHg	63.82± 2.12 mmHg

Table 8.7: Data for the fourth Elast-Eon™valve.

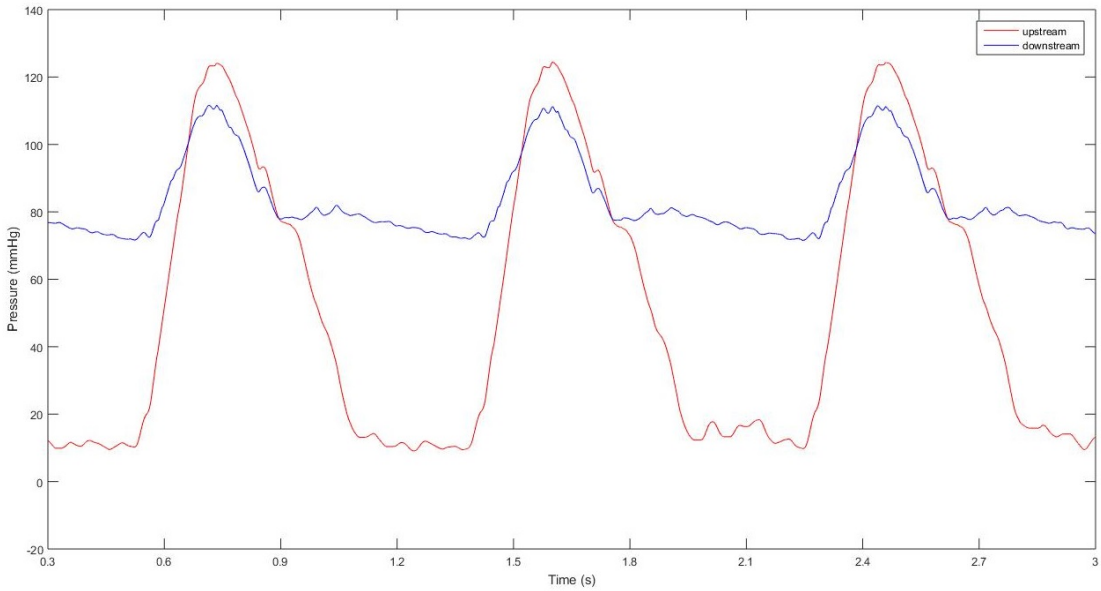

Figure 8.17: Pressure aquisition for the fourth Elast-Eon™valve.

The fifth and last valve did not reached the 100mmHg diastolic pressure difference and also the pressure gradient during systole increase. The performance was more similar to the first Elast-Eon™valve manufactured. The valve did not close, a big gap was constantly present in the centre of the valve. The top of the leaflet was significantly stiffer than the centre and bottom of the leaflet. Figure 8.18 and Table 8.8 shows the results obtained for this valve.

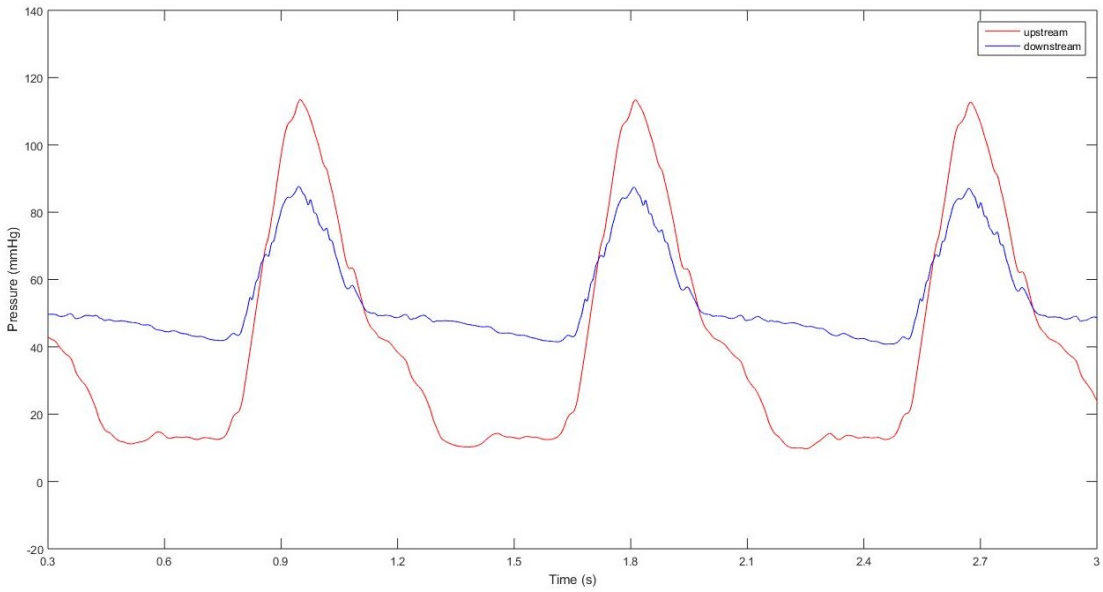

Figure 8.18: Pressure aquisition for the fifth Elast-Eon™valve.

Average Thickness	**Mean Systolic Pressure Gradient**	**Mean Diastolic Pressure Gradient**
0.3 mm	11.99 ± 0.55 mmHg	31.75± 0.31 mmHg

Table 8.8: Data for the fifth Elast-Eon™valve.

The results from pulsatile flow tests demonstrated that the transvalvular pressure drop is related to the stiffness of the polymer, which increases for the Elast-Eon™case respect to the SEPS22 material (see Table 7.13).

As a matter of fact, keeping constant all the other conditions, a higher material stiffness is responsible for a smaller leaflet deformation during the systolic phase, and consequently for a reduced valve opening.

Probably a thinner valve made of Elast-Eon™could have close properly, but it was very difficult with the manual procedure to obtain such valve for the reason mentioned above.

Only one valve made of SEPS22 showed good opening and closing performances mimicking the behavior of natural heart valves, but it failed too early.

The durability of the PHV not only depends on the mechanical properties of the valve materials but also depends on the manufacturing technique and on the stress distribution in the material. As stated before, a better controll on the dip casting procedure could beneficially improved the uniformity of thickness and thus the stress distribution in the leaflets. Nevertheless an isotropic internal structure could still not compete with the orientation achievable with the anisotropic material. In fact a good prediction of the orientation of the different polymeric domains has the potential to produce a more durable material, which is the focus of the research at the moment for what concern polymeric PHV.

Finite Element Simulation

Finite element analyses were performed for the valve made of SEPS22 of 0.2mm average thickness in order to calculate the stress distribution within the leaflet. The standardized finite element model procedure gives information about the mechanical response of the device during opening.

The choice of selecting only the SEPS22 valve for the simulation is related to the fact that it was the only valve that actually closed and opened properly; furtermore it also exhibited a good perfermance for what concern the systolic pressure gradient.

Hence the model was set with a uniform thickness of 0.2mm and the experimental parameters relative to SEPS22: $c_1 = 0.3048MPa$ and $c_2 = 0.3451MPa$.

The results obtained from the simulation are shown in Figure 8.19-8.20-8.21.

Due to the leaflet symmetry, the model shows a symmetrical distribution of stress within the single leaflet. The region of higher stress are the one closer to the pillars of the stent, at the edges of the leaflets (colored in red, orange and yellow in the pictures).

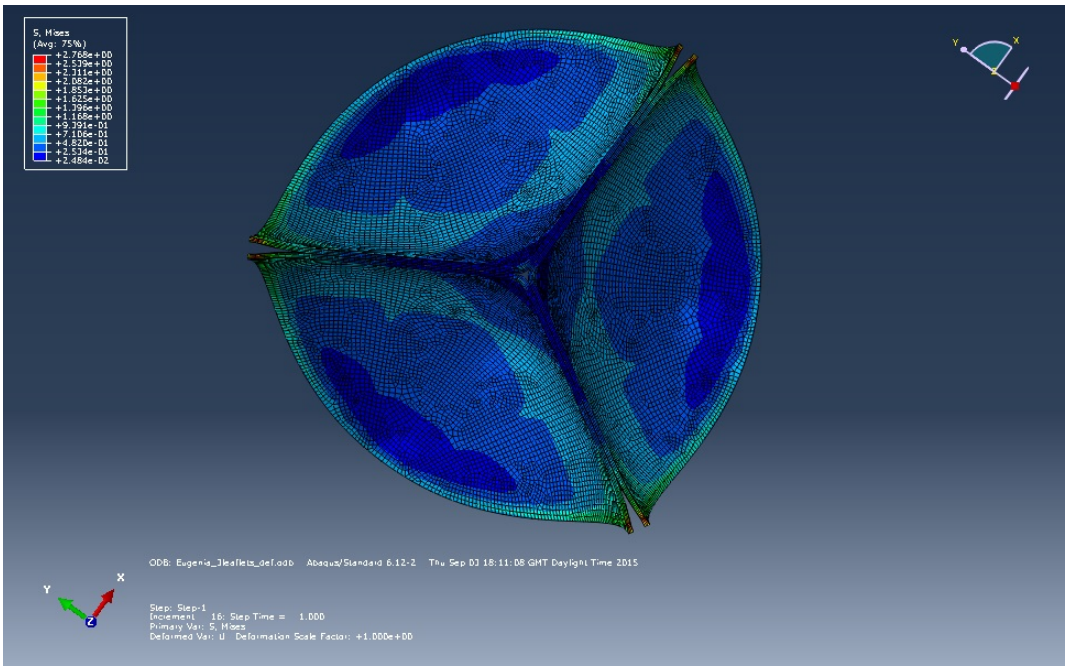

Figure 8.19: Finite element simulation result viewed from the top of the valve.

The maximum energy density calculated by the model is 0.5376 MPa. The maximu strain energy density calculated for the planar specimen at 10^7 cycles was 0.593, this means that the valve potentially could have lasted that time.

What happened in the real valve, instead, is the propagation of the crack in the region highlighted in Figure 8.12. This same region in the simulated geometry correspond to a region of relatively low stresses, as shown in Figure 8.20. This let infer that the thickeness homogeneity is an important factor for the durability of the valve and that probably the leaflet was thinner than 0.2 mm in the region where the crack propagated.

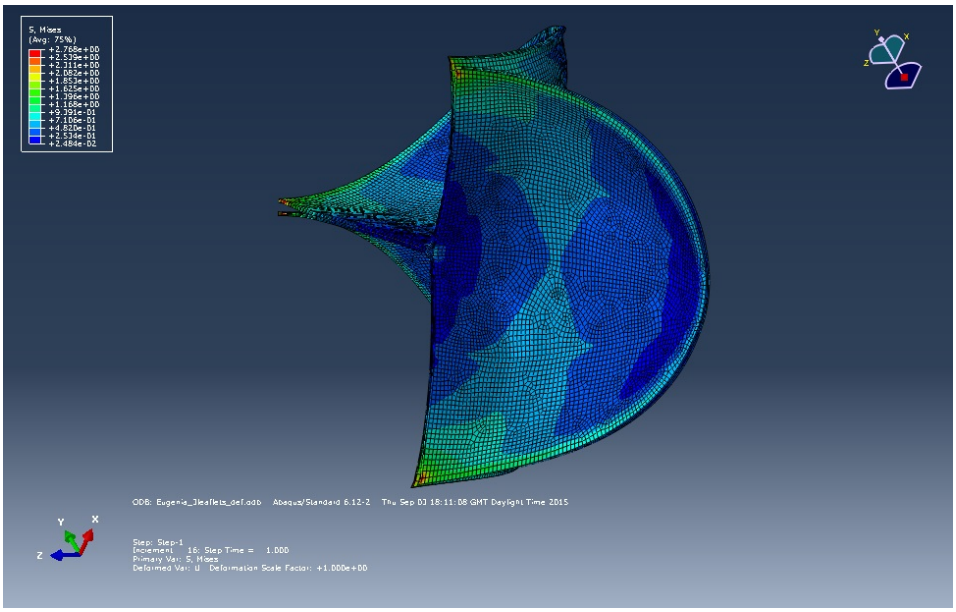

Figure 8.20: Finite element simulation result viewed from the lateral side of the valve.

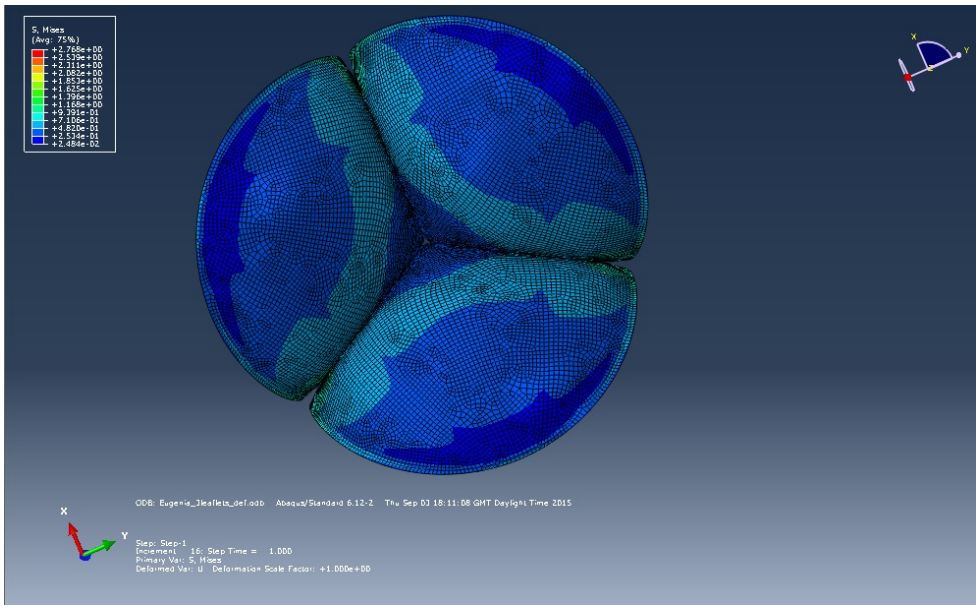

Figure 8.21: Finite element simulation result viewed from the internal side of the valve.

Conclusion

The minimization of the Performance Index, constructed from E (Young's Modulus) and W_{max} (maximum strain energy density), allows to select an optimal material from a given shortilist for the application on a flexible leaflet Prosthetic Heart Valve. The PI obtained from the mechanical testing of the material selection draw the attention to two main category of elastomer: styrenic block-copolymers and advanced thermoplastic polyurethanes. The materials selected are in specific SEPS22 and HG252, which are Polystyrene-b-poly(ethylene/propylene)-b-polystyrene and polystyrene-poly(isoprenebutadien)-polystyrene-hydroxy hydrogenated respectively, and Elast-Eon™which is poly(dimethylsiloxane)(PDMS)/poly(hexamethylene oxide)(PHMO)-based TPU. It is important to specify that the material specimens where cut from a solvent casted sheet of polymers, thus the resulting internal structure was isotropic.

Among the three polymers HG252 had the lowest PI, it has the same structure of SEPS22 but with a higher content of styrene, which implies a larger presence of rigid segments inside the elastomers. Since the increase in styrene weight percentage demonstrated to improve the Performance Index, another polymer of the same family with higher styrene content , SEEPS, was tried to be processed. Unfortunately the material, that appear as a "fluffy powder", could not be processed into a thin sheet.

Latex (natural rubber) resulted to have the worst performance, the material was to soft. In fact, a good compromise between stiffnes and toughness should be the optimal solution for the PHV application. Such features are in part represented by the materials selected, but the real polymers performance was succesively tested into the valve shape during a pulsatile test. In fact several trileaflet heart valves prototypes were manufactured by dip casting, in order to have the same isotropic structure of the speciment tested mechanically. The valves obtained did not have a good thickeness homogeneity within the leaflet and this prevent from giving a definitive judgment on the potential use for the valve application of these materials, the processing technique and the relative internal structure. However it was evident that due to the materials stiffness

it was very important to manufacture the valves with the appropriate leaflet thickness. In fact, most of the valve did not close under the pulsatile test conditions because of thick leaflets.
Even though the results from valve testing were not satisfactory, it would be interesting to perform a more accurate dip casting of the valve and evaluate if the results change respect to the ones obtained in this work.
The optimal solution would be a synergic design of both leaflets geometry and material in order to combine the relevant properties and the stress distributions. This is already a topic of study of different research groups.
Future development are also the studies of a polymeric transcatheter valve. The advantage of using this technology is the less invasive surgery procedure. It would be interesting to test the isotropic polymer selected into the shape of a transcatheter valve.
In conclusion, one more hypothesis is that the anisotropic internal structure of the material could still remain more attractive than the isotropic one.
Despite the fact that since 1950s a polymeric PHV is still to be effectively implanted into a patient, it is a truth universally acknowledged that reserching on the application of polymer in PHV is relevant in order to overcome the limits of the commercial valve and to obtain a new solution for the heart valve disease treatments.

Appendices

Appendix A

SEEPS

SEEPS is a styrenic block copolymer selected for the application on a PHV. It was chosen because of its high content in styrene(30%wt) and the relatively higher stifness of the material compared to SEPS22 and HG52. As it was mentioned in Chapter 4, the material was not tested since the material could not be processed correctly, in fact it was not possible to obtain a uniform polymer sheet.

The first processing attempt was with the solvent casting technique, as the other polymers, but the material was very difficult to dissolve both in Toluene and in THF. To have the polymer completely dissolved the solution was stirred at 30°C on a hot plate. When the polymer was completely dissolved, the solution was poured into the tray. The result, once the solvent was completely evaporated, is shown in Figure A.1.

Figure A.1: SEEPS solvent casted film.

The procedure was ripeated several times but the result remained identical.
The polymer was then processed with the injection molder, but neither with this method a good sheet was obtained to be used in mechanical testing. Figure A.2 represents the injenction molder utilezed. In orderd to have a thin sheet a hot plate die was used.

Figure A.2: Injection molder.

The conditions applied at the injection molder are summarised in Table A.1. Tha main problem was that the polymer was not flowable and needed high temperature to melt.

TEST	**T1 (°C)**	**T2(°C)**	**T3(°C)**	**T4(°C)**	**Tp(°C)**	**v (rpm)**	**P (MPa)**
test 1	150	198	157	113	76	30-35	95
test 2	163	198	157	113	76	30-35	95
test 3	165	203	160	111	76	30-35	95
test 4	165	210	162	125	82	30-35	95

Table A.1: Processing conditions of injection molding.

T1, T2,T3,T4 are the temperature of the screw, where T1 is the last one before the plate. Tp is the plate temperature and v is the screw velocity. The die produced a 0.5 mm thickness film.

After injection, each specimen has been subject to a relaxation stage of 30 minutes during which the temperature slowly decreased. Successively, the samples were water cooled to 30°C.

Figure A.3: SEEPS injected disk.

Figure A.3 shows the samples obtained from the injecion molder. The sample on the bottom left with the most irregular contour is test1, in fact the sheet was not completely melted. The other three samples were processed with a higher plate temperature and the final results were improved. The main problem was that, instead of having a flat film, the samples assumed a conical shape. It was not possible to use these samples for the mechanical testing.

Appendix B

Dynamic Mechanical Analysis

Further characterization for SEPS22 and Elast-Eon™was the Glass transition temperature determination by Dynamic Mechanical Analysis. DMA testing was performed using a TA Instruments Q800 DMA. Specimens were mounted between film tension fixtures. The specimen thickness and width were measured at three points along the specimen length using a micrometer, and the average of these measurements was used for calculation of cross-sectional area. Length of specimens was measured by TA Instruments Q800 DMA.
Elast-Eon™sample was tested under the following parameters:

- Test Mode: Temperature Ramp

- Test Frequency: 1 Hz

- Sample Dimension: 8.9211 mm length, 4.00mm width, 0.3550 mm thickness

- Temperature Program: Equilibrate at -120°C, Isothermal at -120°C for 5 minutes, Ramp 3°C/min from -120°C to 70°C

While SEPS22 sample was tested under these conditions:

- Test Mode: Temperature Ramp

- Test Frequency: 1 Hz

- Sample Dimension: 7.75878 mm length, 6.00mm width, 0.4170 mm thickness

- Temperature Program: Equilibrate at -150°C, Isothermal at -150°C for 5 minutes, Ramp 5°C/min from -150°C to 70°C

The glass transition temperature was calculated using three different methods: as the extrapolated onset of the sigmoidal change in storage modulus (T_s), as the peak of the loss modulus signal (T_l), and as the peak of the tangent delta signal (Tt). In most cases, the order of temperatures for a given material is $T_s < T_l < T_t$. It is expected to see two different glass transition temperatures for both polymers since they are copolymers.

The storage modulus, loss modulus, and tan delta as a function of temperature are shown in Figure B.1 and B.2 and a summary of the measured glass transition temperatures is shown in Table B.2 and B.1.

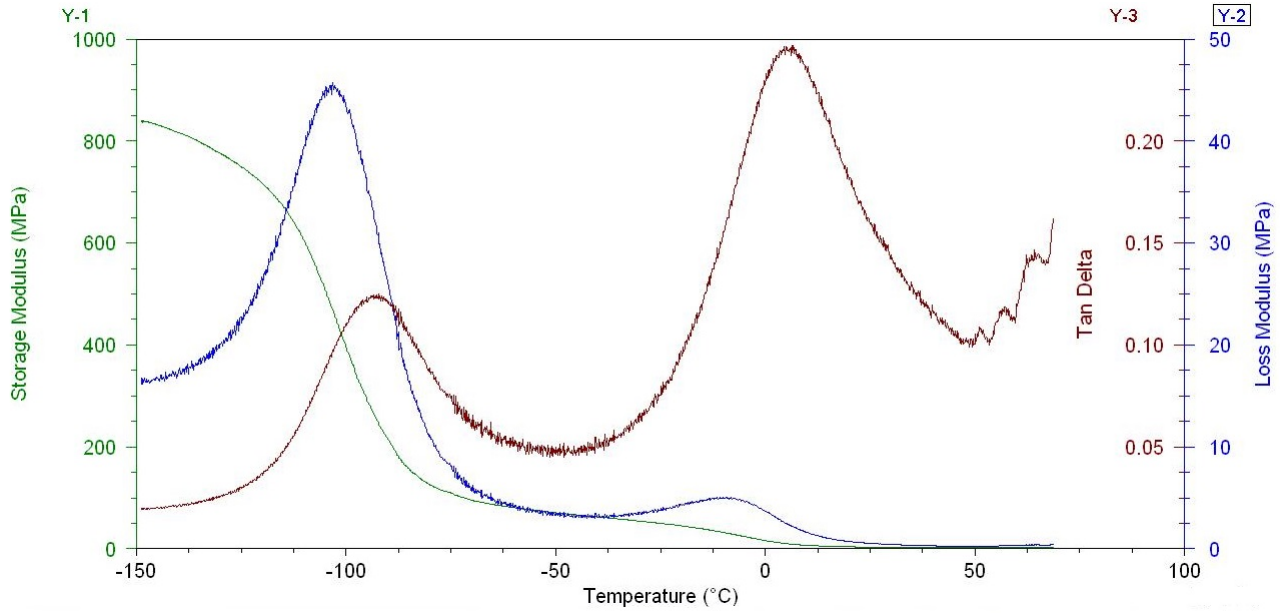

Figure B.1: Storage modulus, loss modulus, and tan delta of Elast-Eon™sample.

T_g	**Storage Modulus Extrapolation**	**Loss Modulus Peak**	**Tan Delta Peak**
T_{g1}(°C)	-116	-102	-93
T_{g2} (°C)	0	-8	6

Table B.1: Measured glass transition temperatures for Elast-Eon™.

In the results it is clear that T_{g1} refers to the silicone presence in the TPU matrix, while the highest T_g (T_{g2}) represent the polyurethane glass transition temperature.

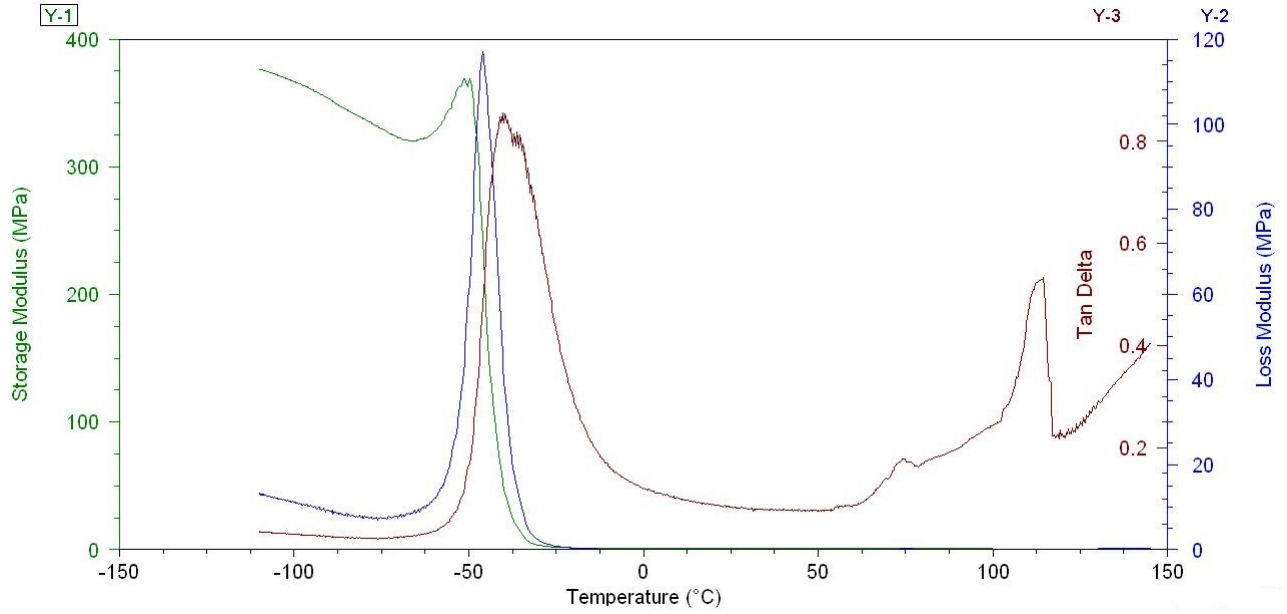

Figure B.2: Storage modulus, loss modulus, and tan delta of SEPS sample.

T_g	**Storage Modulus Extrapolation**	**Loss Modulus Peak**	**Tan Delta Peak**
T_{g1}(°C)	-	-46.5	-40
T_{g2} (°C)	-	-	114

Table B.2: Measured glass transition temperatures for SEPS22.

The graph obtained for SEPS22 is less clear than the one for Elast-Eon™. Only for the Tan Delta results it is possible to obtain the two glass transition temperatures expected: -40°C for the poly(ethylene-propylene) soft domain, 114°C for the styrenic rigid segments. The loss modulus peak registerd only the T_g for the soft domain.

Bibliography

[1] Bezuidenhout, D., and Zilla, P., 2014, "Flexible Leaflet Polymeric Heart Valves," Cardiovascular and Cardiac Therapeutic Devices, Vol. 15, SpringerVerlag, Heidelberg, Germany.

[2] J. Brubert, G. Moggridge "Material Selection and Performance Index for Polymeric Prosthetic Heart Valve Design", Journal of Medical Devices (2015).

[3] Ashby, M. F., Brechet, Y. J. M., Cebon, D., and Salvo, L., 2004, "Selection Strategies for Materials and Processes," Mater. Des., 25(1), pp. 51–67.

[4] Bernacca, G. M., O'Connor, B., Williams, D. F., and Wheatley, D. J., 2002, "Hydrodynamic Function of Polyurethane Prosthetic Heart Valves: Influences of Young's Modulus and Leaflet Thickness," Biomaterials, 23(1), pp. 45–50.

[5] Haworth, W., 1978, "Testing of Materials for Artificial Heart Valves," Br. Polym. J. , 10(4), pp. 297–301.

[6] Parfeev, V. M., Grushetskii, I. V., and Smurova, E. V., 1983, "Mechanical Properties of Elastomers for Artificial Leaflet Heart Valves," Mech. Compos. Mater., 18619 (1), pp. 92–99.

[7] Mars, W., and Fatemi, A., 2003, "Fatigue Crack Nucleation and Growth in Filled 18

[8] W.V. Mars and A. Fatemi,"A litterature survey on fatigue Analysis approaches for Rubber" , Internal Journal of Fatigue, 949-961,2002.

[9] G.J. Lake, Rubber Chem. Technol., 68, 435 (1995).

[10] W.V. Mars, "Multiaxial Fatigue of Rubber," Ph.D. Dissertation, The University of Toledo, Toledo, Ohio (2001).

[11] Zarrin-Ghalam T,. Fatemi A., "Multiaxial Fatigue and life prediction of elastometic components", Int. J.Fatigue, 55, (2013).

[12] De Gaetano F, Bagnoli P, Zaffora A, et al. A newly developed tri-leaflet polymeric heart valve prosthesis. J Mech Med Biol. 2015;15(2):1540009.

[13] P.B. Lindley, "Energy for Crack Growth in Model Rubber Components", Journal of Strain Analysis, Vol 7 no 2, 1972.

[14] T. Zarrin-Ghalami, A. Fatemi "Material Deformation and Fatigue Behavior Characterization for Elastomeric Component Life Predictions", Polymer Engineering and Science,2012.

[15] Cardiovascular implants. Cardiac valve prostheses. ANSI/ AAMI/ISO 5840: 2005;2005.

[16] Grace Huang, MD; Shahbudin H. Rahimtoola, MB, FRCP, DSc (Hon),"Prosthetic Heart Valve",2011;123:2602-2605 Circulation.

[17] Philippe Pibarot and Jean G. Dumesnil , "Prosthetic Heart Valves: Selection of the Optimal Prosthesis and Long-Term Management", 2009;119:1034-1048, Circulation.

[18] Peter Bloomfield, "Choice of heart valve prosthesis", Heart 2002;87:583–589.

[19] Zilla P., Brink J., Human P., Bezuidenhout D., "Prosthetic Heart Valve: Catering for the few", Biomaterials, 29,385-406 (2008).

[20] http://www.onxlti.com/patient-guide/problems-prosthetic-heart-valves

[21] http://www.nhlbi.nih.gov/health/health-topics/topics/hvd

[22] http://www.medicinenet.com/heart-valve-disease/article.htm/how-do-heart-valves-work

[23] Darren J. Martin, Laura A. Poole Warren, Pathiraja A. Gunatillake, Simon J. McCarthy, Gordon F. Meijs, Klaus Schindhelm, "Polydimethylsiloxane/polyether-mixedmacrodiol-basedpolyurethane elastomers: biostability", Biomaterials 21 (2000) 1021-1029

[24] J. R. Rice, "A Path Independent Integral and the Approximate Analysis of Strain Concentration by Notches and Cracks.",Journal of Applied Mechanics, vol. 35, pp. 379-386, 1968

[25] J. Stasiak, S. Nair, G. D. Moggridge, "Mechanical strength of sutured block copolymers films for load bearing medical applications",Bio-Medical Materials and Engineering 24 (2014) 563–569

[26] J. Stasiak, G. D. Moggridge, A. Zaffora, A. Pandolfi, M. L. Costantino, "Engineering Orientation in Block Copolymers for the Application to Prosthetic Heart Valves.", Functional Matierials Letters, Vol. 3, No. 4 (2010).

[27] D.J. Martin, L.A. poole Warren, P. A. Gunatilake, S.J. McCarthy, G. F. Meijs, K. Schindhlem, "New Methods for the assesment in vitro and in vivo stress cracking in biomedical polyurethanes.", Biomaterials 22 (2001) 973-978.

[28] R. Henrnandez, J. Weksler, A. Padsalgicar, J. Runt, "Microstructural Organization of Three-Phase Polydimethylsiloxane-Based Segmented Polyurethanes", Macromolecules, 2007, 40, 5441-5449.

[29] A. F. Osman, Y. Andriani, G.A. Edwards, T. L. Schiller, K.S. Jack, I. C. Morrow, P.J. Halley, D. J. Martin, "Engineered nanofillers: impact on morphology and properties of biomedical thermoplastic polyurethane nanocomposites.", RSC Advances, 2012, 2,9151-9164.

[30] A. Simmons, J. Hyvarinen, R. A. Odell, D.J. Martin, P. A. Gunatillake, K.R. Noble, L.A. Poole-Warren, "Long-Term in vivo biostability of poly(dimethylsiloxane)/poly(hexamethylene oxide) mixed macrodiol-based polyurethane elastomers. "Biomaterials 25, 2004, 4887-4900.

[31] J. Stasiak, J. Brubert, M. Serrani, S. Nair, F. De Gaetano, M. L. Costantino, G. D. Moggridge, "A bio-inspired microstructure induced by slow injection moulding of cylindrical block copolymers. " Soft Matter, 2014, 10, 6077.

[32] J. Stasiak, J. Brubert, M. Serrani, A. Talhat, F. De Gaetano, M. L. Costantino, G. D. Moggridge,"Structural changes of block copolymers with bi-modal orientation under fast cyclical stretching as observed by synchrotron SAXS. ", Soft Matter, 2015, 11, 3271.

[33] F. Cosmi, A. Bernasconi, " Micro-CT investigation on fatigue damage evolution in short fiber reinforced polymers.", Composites Science and Technology 79 (2013), 70-76.

[34] Mars, W., and Fatemi, A., 2003, "Fatigue Crack Nucleation and Growth in Filled Natural Rubber," Fatigue Fract. Eng. Mater. Struct., 26(9), pp. 779–789.

[35] H. Baumgartner, MD, S. Khan, MD, M. DeRobertis, RN, L. Czer, MD, G. Maurer, MD, "Discrepancies Between Doppler and Catheter Gradients in Aortic Prosthetic Valves In

Vitro A Manifestation of Localized Gradients and Pressure Recovery." Circulation, Vol 82 No 4, 1990.

[36] F. De Gaetano, M. Serrani, P. Bagnoli, J. Brubert, J. Stasiak, G. D. Moggridge, M. L. Costantino."Fluid dynamic characterization of a polymeric heart valve prototype (Poli-Valve) tested under continuous and pulsatile flow conditions.",Int J Artif Organs 2015; 38(11): 600-606.

[37] L. Morini, A. Piccolroaz, G. Mishuris, E. Radi, "On Fracture criteria for dynamic crack propagation in elastic materials with couple stresses.", Internal Journal of Engineering Science 71, 2015, 45-61.

[38] G. Arcidiacono, A. Corvi, T. Severi, "Functional analysis pf bioprosthetic heart valves." Journal of Biomechanics 38, 2005, 1483-1490.

[39] Y. Liu, V. Kasyanov, R.T. Schoephoester, "Effect of fiber orientation on the stress distribution within a leaflet of a polymer composite heart valve in the closed position. ", Journal of Biomechanics 40, 2007, 1099-1106.

[40] R. Haj-Ali, L.P. Dasi, H. Kim, J. Choi, H.W. Leo, A.P. Yoganthan, "Structural simulations of prosthetic tri-leaflet aortic heart valves."Journal of Biomechanics 41, 2008, 1510-1519.

[41] C. Martin, W. Sun, "Comparison of thranscatether aortic valve and surgical bioprosthetic valve durability: A fatigue simulation study." Journal of Biomechanics 48, 2015, 3026-3034.

[42] P. B. Zadeh, S.C. Corbett, H. Nayeb-Hashemi, "In-vitro calcification study of polyurethane heart valves." Materials Science and Engineering C35, 2014, 335-340.

[43] T. Beda, "An approach for hyperelastic model-building and parameters estimation a review of constitutive models.", European Polymer Journal 50, 2014 97-108.

[44] H. Khajehsaeid, J. Arghavani, R. Naghdabadi, "A hyperelastic constituive model for rubber-like materials." European Journal of Mechanics A/Solids 38, 2013, 144-151.

[45] H. Bechir, L. Chavalier, M, Chaouche, K. Boufala, "Hyperelastic consitutive model for rubber-like materials based on the first Seth strain measures invariant." European Journal of Mechanics A/Solids 25, 2006, 110-124.

[46] B. Fereidoonnezhad, R. Naghdabadi, J. Arghavani "A hyperelastic constitutive model fro fiber-reinforced rubber-like material.", Internal Journal of Engineering Science 71, (2013) 36-44.

[47] M.A.Borger, MD,PhD, A.F. Nette, MD, M. Maganti, MS, C.M. Feindel, MD," Carpentier-Edwards Perimount Magna Valve versus Medtronic Hancock II: A Matched Haemodynamic Comparison. " The society of Thoracic surgery, 2007.

[48] J.L.Cox, MD, N.Aid, MD, K. Myers, BS, M. Ghabir, PhD, R.C. Quijiano, MD,PhD, "Tubolar Heart Valves: A new tissue prosthesis design-Preclinical evaluation of the 3F aortic bioprosthesis." The Journal of Thoracic and Cardiovascular Surgery, 2005.

[49] C.L. Chow, T.J. Lu, "Fatigue Crack Propagation in Metals and Polymers with Unified formulation.", Tire Science and Techonology, TSTCA, Vol.20,No. 2, April-June,pp.106-129.

[50] B.H. Kim, C.R. Joe, D.M. Otterson, "On the determination of Fracture Toughness in Polymers.", Polymer Testing 8, 1989,119-130.

[51] http://www.septon.info/en/septon/list-septon.html

[52] http://www.aortech.com/technology/elast-eon

[53] https://it.wikipedia.org

[54] D. Bezuidenhout, D.F. Williams, P. Zilla, "Polymer heart valves for surgical implantation, cather-based technology and heart assist device.", Biomaterials 36, 2015,6-25.

[55] R.S. Rivling, A.G. Thomas, "Rupture of rubber. I.Characteristic energy for tearing", Journal of Polymer Science 1953, 10:291-318.

[56] G.J. Lake, P.B. Lindley, "The mechanical fatigue limit for rubber.", Journal of Applied Polymer Science.

[57] T. Zarrin-Ghalami, A. Fatemi "Material Deformation and Fatigue Behavior Characterization for Elastomeric Component Life Predictions",Polym. Eng. Sci., 52:1795–1805, 2012.

[58] ASTM Standard D4482-99, ASTM, West Conshohocken, PA (2002).